TRANSPORTATION RESEARCH

RECORD

No. 1350

Highway and Facility Design

Hydrology and Bridge Scour

A peer-reviewed publication of the Transportation Research Board

TRANSPORTATION RESEARCH BOARD
NATIONAL RESEARCH COUNCIL

NATIONAL ACADEMY PRESS
WASHINGTON, D.C. 1992

Transportation Research Record 1350
Price: $17.00

Subscriber Category
IIA highway and facility design

TRB Publications Staff
Director of Publications: Nancy A. Ackerman
Senior Editor: Naomi C. Kassabian
Associate Editor: Alison G. Tobias
Assistant Editors: Luanne Crayton, Susan E. Gober, Norman Solomon
Office Manager: Phyllis D. Barber
Production Assistant: Betty L. Hawkins

Printed in the United States of America

Library of Congress Cataloging-in-Publication Data
National Research Council. Transportation Research Board.

Hydrology and bridge scour : a peer reviewed publication of the Transportation Research Board.
p. cm.—(Transportation research record, ISSN 0361-1981 ; no. 1350)
ISBN 0-309-05214-9
1. Scour at bridges. I. National Research Council (U.S.). Transportation Research Board. II. Series: Transportation research record ; 1350
TE7.H5 no. 1350
[TG320]
388 s—dc20
[624'.252] 92-28099
CIP

Sponsorship of Transportation Research Record 1350

GROUP 2—DESIGN AND CONSTRUCTION OF TRANSPORTATION FACILITIES
Chairman: Charles T. Edson, New Jersey Department of Transportation

General Design Section
Chairman: Hayes E. Ross, Jr., TTI, Texas A&M University System

Committee on Hydrology, Hydraulics, and Water Quality
Chairman: J. Sterling Jones, Federal Highway Administration, U.S. Department of Transportation
Secretary: Lawrence J. Harrison, Federal Highway Administration, U.S. Department of Transportation
Colby Ardis, Dennis Athayde, Charles W. Boning, Stanley R. Davis, David J. Flavell, Thomas L. Hart, John Owen Hurd, S.Bennett P. John, Kenneth D. Kerri, M. Dean Knighton, Floyd J. Laumann, Norman Miller, Johnny L. Morris, Babak Naghavi, Jerome M. Normann, Glenn A. Pickering, Don L. Potter, Jean Reichert, Everett V. Richardson, Wilbert O. Thomas, Jr., Corwin L. Tracy, E. L. Walker, Jr., Ken Young, Michael E. Zeller

Frank R. McCullagh, Transportation Research Board staff

The organizational units, officers, and members are as of December 31, 1991.

Transportation Research Record 1350

Contents

Foreword

Naghavi et al. investigated four regional flood-frequency analysis methods and determined that the generalized extreme value method is easier to apply and more accurate in terms of descriptive and probably predictive abilities than other feasible methods for Louisiana data. Kilgore and Snodgrass present the program HYCHL, which assists in designing roadside channel linings and riprap lining for irregular channels by analyzing lining stability on the basis of permissible shear stress. Johnson and Jones investigated an indirect method to characterize the vortex strength in terms of shear stress at the base of a bridge pier as a function of pier width and scour depth. The method requires no instrumentation in the scour hole; therefore, it does not interrupt the flow pattern around the pier or within the hole.

Abt et al. report on a laboratory testing program to evaluate the effectiveness and practicality of several devices for monitoring scour. Barbé et al. present a method to evaluate the risk of failure of bridge structures due to pier scour during flood events. Pagán-Ortiz presents the results of research conducted in a flume to determine the stability of rock riprap protecting abutments on flood plains. Thomas summarizes the evolution of current flood-frequency analysis guidelines, describes the activities of an interagency work group, and suggests future directions for federal agencies using the guidelines.

Comparative Evaluation of Four Regional Flood-Frequency Analysis Methods

BABAK NAGHAVI, JAMES F. CRUISE, AND SENARATH EKANAYAKE

Four popular methods for analyzing regional flood frequency were investigated using Louisiana streamflow series. The state was divided into four homogeneous regions and all undistorted, long-term stream gauges were used in the analysis. The generalized extreme value (GEV), two-component extreme value, and regional log Pearson Type III methods were applied to this data base and compared in terms of descriptive capabilities. On the basis of several factors, the GEV method was selected as the overall superior method. The GEV parameters were estimated using the probability-weighted moments (PWMs). Indexing was accomplished using the first PWM (the mean). A procedure to apply this method to ungauged watersheds using regression equations and a regional nondimensional flood distribution was developed. It was found that the procedure performed well when applied to data not used in the calibration of the model. The regional GEV procedure was compared with the method of the U.S. Geological Survey (USGS) and showed significant improvement over the USGS equations in terms of fit to the observed data. This method is easier to apply and more accurate in terms of descriptive and probably predictive ability than other feasible methods for Louisiana data.

Often in hydrologic work, discharges must be estimated for sites at which stream gauge records are unavailable. Several techniques have been developed over the years to do this. Many of these methods are based on some type of regional frequency analysis. The Louisiana Department of Transportation and Development employs the U.S. Geological Survey (USGS) regression technique (*1*) to obtain discharge estimates at ungauged sites in the state. These equations contain a fair degree of error and have not been compared to alternative techniques. The USGS equations are based on regression analysis of at-site frequency estimates, which in turn are based on the regional log Pearson Type III (LP3) distribution. However, this distribution does not lend itself to regionalization techniques because of the variability of the skew coefficient used in LP3 parameter estimation (*2*). Also, LP3 parameters are not easily related to physical watershed characteristics (*3*). Furthermore, the error reported for the USGS equations (typically 40 to 50 percent) represents the standard error of the regression estimates and does not include the error inherent in fitting the LP3 to the samples. This error has been shown to run anywhere from 10 to 30 percent for Louisiana stations (*4*).

Another widely used regional analysis method, recommended by the Interagency Advisory Committee on Water Data (IACWD), is also based on the LP3 distribution but uses a weighted generalized skew coefficient (*5*). The use of a generalized skew coefficient instead of the sample skew coefficient results in a more reliable flood-frequency analysis for streams with short records (*5*).

Alternate regional frequency techniques have been proposed by Dalrymple (*6*) and Stedinger (*7*). Greis and Wood (*8*) recommended an indexing method similar to that of Dalrymple (*6*), but with extreme value Type 1 (EV1) as the base distribution and parameters estimated by probability-weighted moments. This parameter estimation method, first proposed by Greenwood et al. (*9*), has been shown to possess attractive asymptotic characteristics when it is used to estimate the parameters of several distributions, especially when the samples exhibit wide variability (*10*). This characteristic makes the method useful for regional frequency analyses. In support of this, Potter and Lettenmaier tested 10 commonly used frequency methods and found that the GEV index method possessed predictive characteristics superior to the other methods tested (*2*).

Another highly regarded method is the two-component extreme value (TCEV). Rossi et al. (*11*) applied the TCEV with the maximum likelihood method of parameter estimation to regional data series.

The purpose of this study was to formulate two alternative methods of regional frequency analysis using Louisiana annual peak streamflows; compare these methods with the LP3 on the basis of generalized skew coefficients; select the best method based on the basis of statistical comparison indexes of descriptive capabilities and the ease of use (requiring less physical data); and compare the selected regional method to the USGS regression equations. The two regional methods investigated are the TCEV (*11*,*12*) and the GEV (*13*), indexed by the method of PWM (*9*) outlined by Greis and Wood (*8*).

REGIONALIZATION

The state of Louisiana was divided into four hydrologically homogeneous regions that were determined by soil, geologic, topographic, climatic, and streamflow similarities. The purpose of this analysis was to divide the state into regions such that the hydrologic responses of watersheds in each region are comparable. Thus, the regions should have relatively homogeneous soil and topographic characteristics. In addition, the watersheds in each region should be subjected to similar climatic conditions. Information needed to make the determinations was readily available from previously published sources. The *Atlas of Louisiana* (*14*) and the *General Soil Map of Louisiana* (*15*) were used in forming the regional

B. Naghavi, Louisiana Transportation Research Center, 4101 Gourrier Avenue, Baton Rouge, La. 70808. J. F. Cruise, S. Ekanayake, Department of Civil Engineering, Louisiana State University, Baton Rouge, La. 70803.

groupings. The *Geological Map of Louisiana* shows that the state is divided into four general regions by the Mississippi alluvium. The regional groupings were further compared on the basis of climatic and soils information available. A complete description of the methodology used in determining the homogeneous regions is given by Naghavi et al. (*16*).

Once preliminary regions had been identified, the annual peak stream flows of gauged watersheds within each region were analyzed for similarities. This was accomplished by plotting the logarithm of the mean (log Q_M) of the annual flood series (in log space) against the corresponding drainage area (A) for each watershed in the region. A curve through the points was fitted by standard regression techniques. The regression equations for the four regions are as follows:

- *Southeast*:

$$\log Q_M = 2.695\, A^{0.072} \qquad R^2 = .86,\ \text{CV} = 3.1 \tag{1}$$

- *Southwest*:

$$\log Q_M = 2.561\, A^{0.076} \qquad R^2 = .84,\ \text{CV} = 3.22 \tag{2}$$

- *Northwest*:

$$\log Q_M = 2.836\, A^{0.052} \qquad R^2 = .76,\ \text{CV} = 2.509 \tag{3}$$

- *Northeast*:

$$\log Q_M = 2.406\, A^{0.063} \qquad R^2 = .97,\ \text{CV} = 1.36 \tag{4}$$

In analyzing these equations, the coefficient of determination (R^2) represents the percentage of the total variance of the dependent variable (log Q_M) explained by its relationship with the area. The coefficient of variation (CV) represents a dimensionless measure of the error in the regression fit. Thus, the relationship between log mean annual flood values and drainage areas appears to be well confirmed in these cases. Watersheds that fell outside this linear trend (by visual inspection) would not be expected to behave similarly to the other basins within the region. In this way, minor revisions to the regional groupings were determined. These regional boundaries are delineated in Figure 1. The locations of all the stream gauges used in the analysis are also plotted in this figure.

DATA

The data were obtained for all stream gauges in the physiographical regions of the state with a minimum of 20 years of systematic record. A few gauges that fell in the general physiographical regions of Louisiana but that were physically outside state boundaries were included in the analysis. Locations of all gauges are shown in Figure 1. The data set consisted of 110 long-term, continuous stream gauge records. These records were then screened for possible anomalies resulting from flow diversions, interbasin transfers at high discharges, or missing records. The records that passed this screening were further analyzed for consistency within the homogeneous regions previously defined. It was ascertained that gauges with drainage areas of fewer than 10 mi^2 generally did not follow the trend of the rest of the data. Therefore, these records were excluded from the analysis. In the end, 85 gauges passed the screening process and formed the data base for the rest of the analysis. There were 24 gauges in the Southeast region, 32 in the Southwest region, 24 in the Northwest region, and five in the Northeast region. A listing of these gauges, their drainage areas, periods of record, and skews of the log-transformed data are given in Tables 1 through 4.

FLOOD-FREQUENCY ANALYSIS

Regional frequency analyses were performed for each homogeneous region on the basis of all of the screened annual peaks observed in each region. Flood-frequency analysis consists of fitting preselected probability distributions to recorded flood data at individual sites and then estimating the magnitude (quantile) of flood events corresponding to given exceedance probabilities from the distributions. However, using the observed data from only the site under investigation can result in unreliable estimates. This is especially true when the length of record at a single site is relatively short in comparison with the recurrence intervals to be estimated from the data. For instance, it may be necessary to estimate the 100-year flood from only 20 to 30 years of record at an individual site. This is the reason that regional flood-frequency analysis has received much attention in recent engineering literature. Regional frequency analysis consists of using data at other sites considered similar to the site in question to augment the information at an individual site. This reduces the uncertainty inherent in short, systematic records.

Two-Component Extreme Value

TCEV has been derived as a mixture of two exponential marginal distributions from a Poisson counting process (*10*). Thus, its cumulative distribution function can be expressed as the product of two extremal distributions:

$$F(x) = \exp[-\lambda_1 \exp(-x/\theta_1) - \lambda_2 \exp(-x/\theta_2)] \tag{5}$$

where λ and θ are the shape and the scale parameters, respectively, and $F(x)$ is the nonexceedance probability of an event of magnitude x. This distribution attempts to account for the possibility that two distinct subdistributions make up the total annual distribution of flood peaks. In cases in which the marginal distributions can be shown to be exponential or the asymptotic distribution is Gumbel, the TCEV has been shown to give accurate results.

In the original formulation (*11*), TCEV parameter estimation was accomplished by maximum likelihood. However, Arnell and Gabriele (*17*) found that maximum likelihood estimates of TCEV regional parameters sometimes failed to converge and resulted in relatively variable quantile estimates. Therefore, in this study the TCEV was fitted to the regional data series by the method of maximum entropy proposed by Fiorentino et al. (*12*). This method has been shown to require less cumbersome computation and to be more reliable than the maximum likelihood procedure originally proposed by Rossi et al. (*11*).

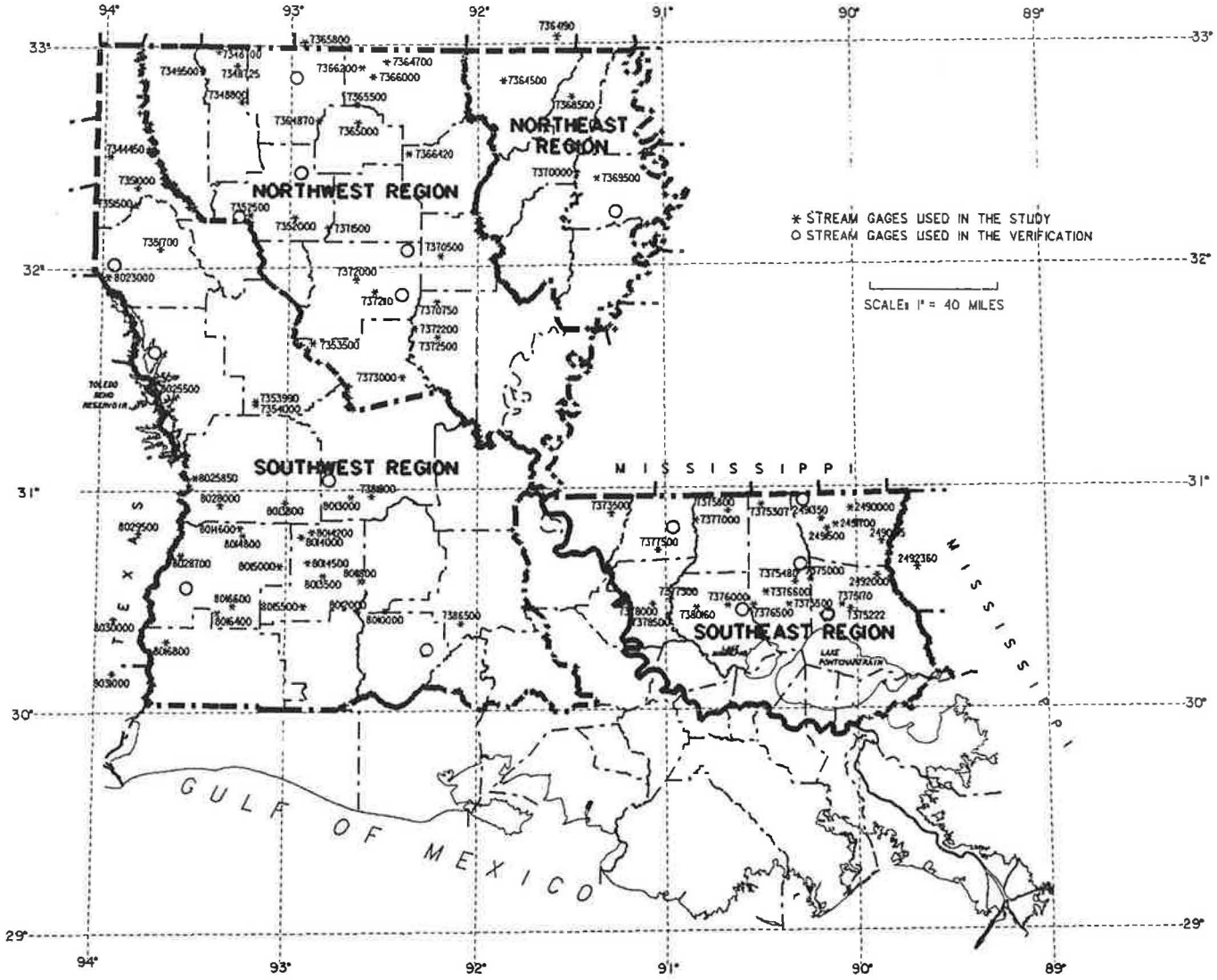

FIGURE 1 Hydrologic regions of Louisiana.

In the regionalization technique, two dimensionless parameters, $\theta = \theta_2/\theta_1$ and $\lambda = \lambda_2/\lambda_1^{1/\theta}$, are assumed to be constant for the homogeneous region; the other two parameters, θ_1 and λ_1, are allowed to vary from site to site. The parameters θ_1 and λ_1 represent the basic component, and θ_2 and λ_2 represent the outlying component of the compound distribution. The parameters θ and λ represent the regional component of the distribution. Conceptually, θ_1 and λ_1 represent the smaller, more frequently occurring events that would be expected to vary from site to site within the region. θ_1 essentially represents the mean flood for this distribution, and λ_1 represents the number of floods per year over the watershed. The parameters θ and λ represent the regional distribution; they are expected to behave similarly within the homogeneous region. As in the previous case, θ represents the mean flood of this distribution and λ represents the number of such events occurring per year. The maximum entropy procedure results in four equations to be solved for the four unknowns described previously.

Generalized Extreme Value Index Method

The index method has been receiving a great deal of attention in recent engineering literature, although its basic premise was outlined by Dalrymple some 30 years ago (*6*). In this procedure, an assumed distribution is fitted to the observed flood series at each site in a hydrologically similar region. The statistics (or parameters) of the distributions at each location are standardized by dividing by the at-site mean in each case. Regional estimates of the parameters are obtained by averaging the parameter estimates for the region. These regional parameters are then used to generate flood quantiles for the site of interest and are subsequently readjusted to account for the differences in scale between watersheds.

The index method has gained popularity since the PWM method of parameter estimation was introduced by Greenwood et al. (*9*). It has recently been used by Greis and Wood (*8*), Landwehr et al. (*10*), and Stedinger (*7*). PWM, which is usually applied only to distributions that can be expressed in

TABLE 1 PERTINENT DATA ON WATERSHEDS IN SOUTHEAST LOUISIANA

STATION No.	AREA IN (sq.mile)	YEARS OF OBS.	SKEW OF LOG TRAN. DATA	SRMSE		
				GEV	TCEV	LP3
02492000	1213	50	-0.08	0.256	0.317	0.327
02492360	175	21	-0.02	0.149	0.107	0.111
02490105	73	22	0.12	0.209	0.222	0.215
02491500	990	66	-0.34	0.171	0.186	0.201
02491700	44	20	-0.69	0.280	0.236	0.188
02491350	42	21	0.70	0.186	0.188	0.179
02490000	12	20	-0.63	0.357	0.319	0.173
07378500	1280	49	-0.12	0.122	0.142	0.130
07375222	46	22	-0.69	0.324	0.227	0.244
07380160	20	33	-0.34	0.298	0.111	0.084
07375170	88	20	0.33	0.144	0.145	0.169
07376000	247	47	-0.20	0.129	0.152	0.108
07376500	80	44	-0.08	0.183	0.097	0.090
07375500	646	49	-0.14	0.157	0.211	0.193
07377300	884	35	0.17	0.159	0.110	0.125
07376600	14	32	-0.89	0.394	0.122	0.081
07375480	91	20	-0.23	0.191	0.200	0.166
07375000	103	44	-0.13	0.266	0.244	0.164
07377000	580	39	-0.44	0.183	0.150	0.198
07375800	90	32	0.24	0.439	0.411	0.379
07375307	52	22	0.20	0.406	0.329	0.262
07378000	284	44	-0.53	0.189	0.069	0.090
07377500	145	45	-0.22	0.215	0.171	0.179
07373500	35	21	-0.32	0.172	0.110	0.104
REGIONAL AVG.			-0.21	0.232	0.191	0.173

TABLE 2 PERTINENT DATA ON WATERSHEDS IN SOUTHWEST LOUISIANA

STATION No.	AREA IN (sq.mile)	YEARS OF OBS.	SKEW OF LOG TRAN. DATA	SRMSE		
				GEV	TCEV	LP3
07386500	19	28	-1.33	0.346	0.100	0.110
07381800	68	33	-0.22	0.169	0.168	0.105
08012000	527	49	0.95	0.188	0.247	0.321
08010000	131	49	-0.96	0.355	0.155	0.087
08011800	44	24	-0.32	0.153	0.110	0.109
08015500	1700	49	0.46	0.215	0.255	0.351
08013500	753	49	-0.17	0.104	0.098	0.165
08014500	510	48	0.16	0.656	0.642	0.720
08014000	171	27	0.29	0.263	0.314	0.323
08014200	94	37	-0.02	0.370	0.387	0.422
08013000	499	44	-0.46	0.139	0.131	0.113
08016800	177	31	0.08	0.186	0.272	0.328
08016400	148	39	0.21	0.161	0.179	0.168
08016600	82	38	0.36	0.278	0.211	0.161
08015000	238	31	0.02	0.262	0.218	0.181
08014800	120	24	-0.30	0.111	0.129	0.121
08014600	26	20	0.13	0.249	0.284	0.270
08013800	10	21	-0.50	0.116	0.150	0.103
08031000	83	34	-0.78	0.221	0.199	0.147
08030000	69	32	-0.17	0.199	0.156	0.145
08028700	13	26	0.68	0.173	0.253	0.332
08029500	128	36	0.84	0.453	0.445	0.514
08028000	365	36	0.38	0.430	0.352	0.301
08025850	10	20	0.80	0.306	0.371	0.437
08025500	148	31	0.72	0.461	0.419	0.457
08023000	97	28	-0.25	0.140	0.136	0.119
07354000	21	30	-0.71	0.353	0.176	0.118
07353990	37	22	-0.02	0.326	0.285	0.219
07351700	20	26	0.36	0.978	0.981	1.050
07351500	66	49	-1.12	0.121	0.095	0.219
07351000	79	43	-1.12	0.192	0.136	0.270
07344450	81	31	0.05	0.354	0.372	0.352
REGIONAL AVG.			-0.06	0.282	0.263	0.273

TABLE 3 PERTINENT DATA ON WATERSHEDS IN NORTHWEST LOUISIANA

STATION No.	AREA IN (sq.mile)	YEARS OF OBS.	SKEW OF LOG TRAN. DATA	SRMSE		
				GEV	TCEV	LP3
07373000	51	46	0.03	0.285	0.295	0.164
07372500	92	31	1.15	0.518	0.566	0.769
07372200	1899	30	-0.31	0.124	0.142	0.208
07370750	48	30	0.53	0.138	0.229	0.318
07372110	24	23	0.72	0.443	0.433	0.517
07372000	654	42	-1.10	0.320	0.254	0.275
07370500	271	30	-1.07	0.194	0.195	0.280
07371500	355	49	-0.44	0.074	0.148	0.123
07366420	113	22	0.16	0.462	0.463	0.533
07365000	355	28	-0.34	0.162	0.185	0.140
07364870	47	22	-1.27	0.173	0.130	0.230
07365500	178	30	0.96	0.547	0.561	0.765
07366000	462	43	0.12	0.385	0.424	0.524
07366200	208	32	-0.13	0.357	0.395	0.431
07364700	141	22	1.28	0.737	0.725	0.875
07362100	385	49	0.04	0.176	0.203	0.327
07365800	180	29	0.39	0.969	0.894	1.044
07352000	154	47	-0.12	0.183	0.240	0.097
07352500	423	43	0.17	0.337	0.289	0.147
07348700	605	30	-0.03	0.173	0.237	0.256
07349500	546	49	-0.36	0.285	0.172	0.122
07348725	33	22	-1.71	0.314	0.213	0.377
07348800	67	24	-0.01	0.094	0.165	0.212
07353500	47	26	-0.17	0.311	0.270	0.180
REGIONAL AVG.			-0.06	0.323	0.328	0.380

TABLE 4 PERTINENT DATA ON WATERSHEDS IN NORTHEAST LOUISIANA

STATION No.	AREA IN (sq.mile)	YEARS OF OBS.	SKEW OF LOG TRAN. DATA	SRMSE		
				GEV	TCEV	LP3
07369500	309	51	-0.58	0.068	0.943	0.038
07370000	782	60	-0.43	0.102	1.270	0.104
07368500	42	28	-0.55	0.048	1.070	0.075
07364500	1645	52	-1.93	0.071	1.103	0.097
07364190	1170	45	-1.92	0.089	1.088	0.101
REGIONAL AVG.			-1.08	0.076	1.095	0.083

inverse form such as Gumbel and GEV, offers a method of parameter estimation that may be more robust and less biased than the traditional methods. The GEV can be expressed in inverse form as (*13*)

$$x(F) = \xi + \alpha[1 - (-\log F)^k]/k \qquad k \neq 0$$

$$x(F) = \xi - \alpha \log(-\log F) \qquad k = 0 \tag{6}$$

where F is the nonexceedance probability corresponding to the quantile x, and ξ, α, and k are the parameters of the distribution. When $k = 0$, the GEV reduces to the EV1. The index procedure is applied by calculating the PWMs from the observed data at each site in the region. The PWMs are standardized at each site by dividing each PWM by the at-site mean. The standardized PWMs are then averaged over all of the sites in the region. These regional average PWMs are used to obtain the parameters of the regional GEV distribution. Regional indexed quantiles can be generated for any exceedance probability $(1 - F)$ from Equation 6. These quantiles are then rescaled for any site of interest by multiplying by the at-site mean. The at-site mean flood can be determined from

the plot of log mean Q versus drainage area for any gauged or ungauged site.

Log Pearson Type III

The regional procedure recommended in the IACWD guidelines (*5*) involves the LP3 distribution. The probability density function of the LP3 is:

$$f(x) = \frac{1}{|a|x\Gamma(b)}\left[\frac{\ln(x) - c}{a}\right]^{b-1} \exp\left[-\frac{\ln(x) - c}{a}\right] \quad (7)$$

where x is the raw (untransformed) flood magnitude, and a, b, and c are the scale, shape, and location parameters, respectively. $\Gamma(b)$ is the gamma function of the parameter b where b is always positive. The LP3 density function is very flexible and can take many forms. Parameters a, b, and c are estimated by the method of logarithmic moments (*4*).

The variability of the skew coefficient of the station record is sensitive to extreme events and sample size, thus making it difficult to obtain accurate skew estimates from small samples. For this reason, the generalized skew values are used in place of at-site skew values, or the at-site skew values are adjusted using the generalized skew when skew estimates are to be obtained from small samples. A generalized skew coefficient for each region was obtained from the arithmetic mean of the station skew values. The generalized skew value was then used to estimate LP3 parameters. To generate regional quantiles at each site of interest, at-site mean and standard deviation of the logarithms of the observed data series, together with the regionalized skew value, are used. In this study, in contrast to Bulletin 17B (*5*), only the generalized skew values were used.

COMPARATIVE ANALYSIS

Each of the three regional frequency methods was fitted to the data by the procedures previously described using the observed annual series at the 85 stream gauges. The purpose of this analysis was to select the most accurate method, on the basis of the comparisons to the observed data, among the three methods. At-site quantiles were generated from the regional distributions for each gauge location in the study. These quantiles were compared to the observed data at each site in terms of standardized root mean square error (SRMSE). The SRMSE between observed and predicted values is given by

$$\text{SRMSE} = \left\{(1/N)\sum_{i=1}^{N}[(\hat{x}_i - x_i)/\bar{x}]^2\right\}^{1/2} \quad (8)$$

where

x_i = observed value of standardized variate x,
$\hat{x}_i$ = predicted value of variate at the same probability point as x_i,
N = sample size, and
$\bar{x}$ = sample mean—used to standardize the root mean square error (RMSE).

$\hat{x}_i$ is calculated as $F^{-1}[p(x_i)]$, where $p(x_i)$ is approximated by the Weibull plotting position formula. The RMSE is standardized by dividing by the sample mean to remove the effects of scale and to make the comparison meaningful. This index only measures the descriptive capability of the methods. That is, SRMSE is an index of the ability of each method to interpolate the observed data at each gauged location.

The SRMSE results for the three methods are given in Tables 1 through 4. As can be seen from these results, no one method gave superior fits for all four regions. The TCEV resulted in the lowest SRMSE for the Southwest region, the LP3 method gave superior results in the Southeast region, and the GEV resulted in superior fits to observed data in both the Northwest and Northeast regions. However, the difference between the methods did not appear to be significant in many cases. The TCEV and LP3 methods performed about equally in the Southeast region and both performed significantly better than the GEV for this region. All three methods performed about the same in the Southwest region, where the average SRMSE difference between the methods were less than 10 percent. In the Northwest region, the GEV and TCEV performed evenly and resulted in significantly better fits to observed data than did the LP3, whereas the LP3 and GEV outperformed the TCEV by a considerable margin in the Northeast region. Thus, each method was clearly inferior to its counterparts in one region, clearly superior in one region each, and about equal elsewhere. It would appear difficult to choose between them on a statistical goodness-of-fit basis.

On the basis of the extreme ease with which the GEV can be extended to ungauged sites when compared with the other methods, it was selected as the superior method. The only geomorphological relationship needed is between the indexing factor (mean flood, Q_M) and basin characteristics. Because past studies have shown that the mean flood is highly correlated to the drainage area (as shown by Equations 1 through 4), a simple Q_m–versus–drainage area relationship is all that is required to apply this method to ungauged sites.

Another important factor in the selection of the GEV is that parameter estimation is done by PWM. It has been shown by Greenwood et al. (*9*) and Hosking et al. (*13*) that PWMs are more robust and less biased than conventional methods. Thus, estimates obtained by this method should be better in these respects than those obtained from other methods. This was confirmed in a study by Potter and Lettenmaier (*2*).

REGIONAL COMPARATIVE ANALYSIS

Regional comparative analysis was performed between the USGS equations and the GEV. The combined records of all the gauges within each region composed the data base for that particular region. The GEV regional procedure was applied by using Equations 1 through 4 to approximate the means at each location in the study. Using the mean values, the at-site quantiles corresponding to recurrent intervals of 2, 5, 10, 25, 50, and 100 years were recalculated from the regional values. These quantiles were then compared to the observed data at each site by the SRMSE. The regional average SRMSE results are given in Table 5. The table shows that the error in the procedure averages about 48 percent for the Southeast, Southwest, and Northwest regions and about

TABLE 5 MODEL COMPARISON BASED ON SRMSE FOR EACH REGION

REGION	NUMBER OF STATIONS	REGIONAL AVG. SRMSE		% DIFF.
		GEV/PWM	USGS/REG	
SE	24	0.468	0.536	+ 15
SW	32	0.491	0.695	+ 42
NW	24	0.532	0.872	+ 64
NE	5	0.132	0.563	+327
WEIGHTED AVERAGE		0.475	0.692	+ 31

13 percent for the Northeast region. However, the error in the quantile estimates from the distribution itself will be greater for the Northeast region because of the small data base.

Table 5 also shows the average SRMSE values obtained by comparing the USGS equations with the observed data at each site in each region. The USGS equations were derived by fitting the LP3 distribution to the data representing 217 gauging stations with more than 10 years of recorded data. On the basis of the results of this analysis, a regression equation was developed for quantile estimation. The general form of this equation is

$$\log Q_x = \log a + w \log A + y \log (P - 35) + z \log S \qquad (9)$$

where

Q_x = peak discharge for a given recurrence interval (x),
a = regression constant,
A = drainage area (mi^2),
P = average annual precipitation (in.),
S = average stream channel slope (ft/mi), and
w,y,z = regression coefficients.

This equation was calibrated for quantiles corresponding to recurrence intervals of 2, 5, 10, 25, 50, and 100 years using the LP3 results. Thus, the comparison of this method with the regional GEV can be based only on the analyses of these quantiles.

The results show, in every case, that the GEV procedure showed a significant improvement (greater than 10 percent) over the USGS equations in terms of fit to the observed data. The overall weighted average for all regions was 31 percent.

It is assumed that if a method accurately describes the data at gauged sites, it will probably describe the ungauged data within a hydrologic homogeneous region. Of course, not only must a frequency method describe the observed data accurately, but it should be capable of extending the data as well. Many times quantiles, which are beyond the systematic record, must be predicted. The SRMSE index does not directly measure this ability. However, studies by Greis and Wood (*8*), Hosking et al. (*13*), Landwehr et al. (*10*), and Potter and Lettenmaier (*2*) have examined the predictive capabilities of various regional and at-site frequency techniques. From the Monte Carlo or Boot Strap sampling methods, the studies concluded that methods based on PWMs possessed asymptotic characteristics in terms of bias and variability of long-term quantile estimates that were superior to other conventional methods.

VERIFICATION OF RESULTS

To verify the GEV regional procedure, the procedure was evaluated using short-term data not used in the development and calibration of the distribution. Five gauges were selected in each region except the Northeast, where only one gauge was available. Because of the lack of adequate data in the Northeast region, verification of results would not be meaningful for this region. The sites from the other three regions were selected in order to gain maximum coverage of each region. The locations of these gauges are shown by the open circles on the regional map in Figure 1.

In performing this analysis, the sites were treated as ungauged areas. The mean floods were estimated from the appropriate drainage area plots and used to scale the respective regional quantiles for each test site. The regional at-site quantiles were then compared with original data for each gauge record by SRMSE. Each gauge used in this phase of the study had between 15 and 20 years of record. Thus, the SRMSE values are based on the number of events in each case.

The SRMSE values shown in Table 6 result from analysis of each site by the GEV regional method, the at-site LP3 and the USGS equations. The LP3 distribution is used for the comparison, considering that the at-site LP3 would give the best possible distributional fit to the observed data. Analysis of the results in the table shows that the average SRMSE value by the GEV regional method was .278 for the Southeast region, .483 for the Southwest region, and .546 for the Northwest region. Comparison of these values with those given in Table 5 reveals that the method performed as well or better with the new data as it did with the data used in its derivation. Furthermore, the GEV method was generally superior by a wide margin to the USGS equations and even compared fairly well with the at-site LP3 in two regions. These results suggest that the method can be used confidently throughout the regions delineated on Figure 1.

TABLE 6 VERIFICATION OF REGIONAL GEV MODEL

REGION	STATION NO.	SRMSE		
		REGIONAL GEV/PWM	USGS REGRESSION	AT-SITE LP3
SE	07375050	0.220	0.433	0.201
	07376520	0.230	0.623	0.140
	07375463	0.314	0.315	0.339
	07377190	0.449	0.407	0.248
	02491200	0.176	0.307	0.169
	AVG.	0.278	0.417	0.219
SW	08010500	0.435	--	0.147
	08012900	0.578	0.824	0.277
	08016700	0.661	0.158	0.356
	08022765	0.515	0.389	0.102
	08024000	0.225	0.530	0.267
	AVG.	0.483	0.475	0.230
NW	07370700	0.402	0.520	0.339
	07370600	0.145	0.113	0.161
	07365300	0.888	1.140	0.682
	07352700	0.638	1.291	0.367
	07351980	0.658	1.151	0.155
	AVG.	0.546	0.843	0.341

LIMITATIONS

The applications of the results of this study are limited by the range of data available. First, the procedure should not be applied outside the physical bounds of the areas for which gauge data were available. These areas are delineated on Figure 1 and should be adhered to strictly. This eliminates the coastal zones and the Mississippi alluvium (except the Northeast region) from applicability. Second, the range of drainage basin sizes and the corresponding land uses available in each region also limit the application of this procedure. Note that the drainage basins represent undeveloped conditions. The drainage areas of each basin used in the study are given in Tables 1 through 4. The method should not be applied to drainage areas smaller than 10 mi^2, because preliminary work clearly showed that these areas respond differently to a storm event than do the larger areas. Not enough of these small gauges were available to perform a separate study.

CONCLUSIONS

The results of this study indicate that the GEV distribution fitted by the PWM method describes the annual flood series of Louisiana streams better than the other methods examined. The overall weighted average improvement of GEV index method over the USGS regional method was 31 percent. Also, verification results revealed that the GEV procedure describes data better than the USGS method in the vast majority of cases. Past Monte Carlo studies have shown that this procedure also possesses superior predictive capability in the cases for which flood estimates are required that may be out of the range of the recorded data. Therefore, on the basis of the results of this analysis as well as previous studies cited in this report, it is concluded that the GEV-PWM procedure results in overall superior flood estimates from both descriptive and predictive points of view and can be used confidently throughout the regions delineated in Figure 1. GEV-PWM is easily extended to the case of ungauged watersheds by using the relationship between the mean of the observed data (indexing factor) and corresponding drainage area of the watershed (Equations 1 through 4) for each region. However, this procedure should not be applied outside the physical bounds of the areas used in its development and verification. Particularly, the method should not be applied to drainage areas smaller than 10 mi^2, because preliminary work clearly showed that these areas respond differently to a storm event than do the larger areas.

ACKNOWLEDGMENTS

The authors wish to express their thanks to Andrea Populus and Karen Jarreau for their assistance in preparation of this document. Funding for this project was made available through FHWA.

REFERENCES

1. *Floods in Louisiana, Magnitude and Frequency*, 4th ed. Water Resources Technical Report 36. Louisiana Department of Transportation and Development, Baton Rouge, 1985.
2. K. W. Potter and D. P. Lettenmaier. A Comparison of Regional Flood Frequency Estimation Methods Using a Resampling Method. *Water Resources Research*, Vol. 26, No. 3, 1990, pp. 415–424.
3. J. R. Stedinger. Design Events with Specified Flood Risks. *Water Resources Research*, Vol. 19, No. 2, 1983, pp. 511–522.
4. B. Naghavi, J. Cruise, and K. Arora. A Comparative Evaluation of Three Estimators of Log Pearson Type 3 Distribution. In *Transportation Research Record 1279*, TRB, National Research Council, Washington, D.C., 1990.
5. Interagency Advisory Committee on Water Data. *Guidelines for Determining Flood Flow Frequency*. Bulletin 17B. U.S. Government Printing Office, Washington, D.C., 1981.
6. T. Dalrymple. Flood Frequency Analyses. *Manual of Hydrology, Part 3*. U.S. Geological Survey Water Supply Paper 1543-A. U.S. Geological Survey, 1960.
7. J. Stedinger. Estimating a Regional Flood Frequency Distribution. *Water Resources Research*, Vol. 19, No. 2, 1983, pp. 503–510.
8. P. Greis and E. Wood. Regional Flood Frequency Estimation and Network Design. *Water Resources Research*, Vol. 17, No. 4, 1981, pp. 1167–1177.
9. J. Greenwood, J. Landwehr, N. Matalas, and J. Wallis. Probability Weighted Moments: Definition and Relation to Parameters of Several Distributions Expressible in Inverse Form. *Water Resources Research*, Vol. 15, No. 5, 1979, pp. 1049–1054.
10. J Landwehr, N. Matalas, and J. Wallis. Probability Weighted Moments Compared with Some Traditional Techniques in Estimating Gumbel Parameters and Quantiles. *Water Resources Research*, Vol. 15, No. 5, 1979, pp. 1055–1064.
11. F. Rossi, M. Fiorentino, and P. Versace. Two-Component Extreme Value Distributions for Flood Frequency Analysis. *Water Resources Research*, Vol. 20, No. 7, 1984, pp. 847–856.
12. F. Rossi, M. Fiorentino, K. Arora, and V. P. Singh. Two-Component Extreme Value Distributions for Flood Frequency Analysis: Derivation of a New Estimation Method. *Journal of Stochastic Hydrology and Hydraulics*, No. 1, 1987, pp. 199–208.
13. J. R. M. Hosking, J. R. Wallis, and E. F. Wood. Estimation of the Generalized Extreme Value Distribution by the Method of Probability Weighted Moments. *Technometrics*, Vol. 27, No. 3, 1985, pp. 251–261.
14. M. B. Newton, Jr. *Atlas of Louisiana*. Miscellaneous Publication 71-2. School of Geosciences, Louisiana State University, Baton Rouge, 1972.
15. S. A. Lytle and M. B. Sturgis. *General Soil Areas and Associated Soil Series Groups of Louisiana*. Agricultural Experiment Station, Louisiana State University, Baton Rouge, 1962.
16. B. Naghavi, J. Cruise, and S. Ekanayake. *Prediction of Flood Quantiles at Ungauged Watersheds in Louisiana*. Report 229. Louisiana Transportation Research Center, Baton Rouge, 1989.
17. N. W. Arnell and S. Gabriele. The Performance of the Two-Component Extreme Value Distribution in Regional Flood Frequency Analysis. *Water Resources Research*, Vol. 24, No. 6, 1988, p. 879–887.

Development and Use of HYCHL for Channel Design

ROGER T. KILGORE AND KENNETH W. SNODGRASS

The HYCHL program is introduced and ways it is an enhanced combination of Hydraulic Engineering Circulars 15 and 11 are described. HYCHL is a program that assists in designing roadside channel linings and riprap lining for irregular channels by analyzing lining stability on the basis of permissible shear stress. Enhancements discussed include (a) flexibility in the calculation of Manning's roughness coefficient by giving a designer both a choice of method and a default method; (b) ability to change Shields' parameter for riprap linings; (c) capability of analyzing irregular channel cross sections for riprap linings; and (d) ability to design riprap size on the basis of stability factors and channel shape. The use of the program for both roadside and natural channels is demonstrated with examples.

The design and analysis of linings for roadside channels and other drainageways is both an art and a science. It is a science because researchers have conducted experiments and developed theoretical constructs of lining behavior under varied geometric and hydraulic conditions. Such efforts have been synthesized by FHWA for guidance in the form of Hydraulic Engineering Circulars 15 (HEC-15) (*1*) and 11 (HEC-11) (*2*).

Lining design and analysis is also an art in which experience and intuition are keys to success. This is true because the "science" is incomplete and, at times, contradictory. The guidance provided in HEC-15 and HEC-11, for example, describes a limited range of conditions for channel design, leaving the designer without formulas or charts for other situations experienced in the field. Sometimes these helpful documents provide contradictory guidance and methodologies that the designer must resolve.

The development of HYCHL, a computer program to assist designers in channel lining analysis and design, involved a synthesis and expansion of the concepts provided in HEC-15 and HEC-11. The program standardizes and facilitates application of design concepts. This paper describes the principal areas in which enhancements have taken place, including Manning's roughness, Shields' parameter, irregular channel shapes, and the use of stability factors.

SCOPE OF HYCHL AND LINING GUIDANCE

HYCHL represents a consolidation of analysis and design techniques presented in HEC-15 (*1*) and HEC-11 (*2*). Although both documents address the analysis of lining stability, each focuses on different classes of problems. HEC-15 focuses on linings in roadside channels, which are characterized by relatively uniform cross sections on a constant slope. Types of lining include riprap, rigid, vegetative, gabion, and temporary. Alternatively, HEC-11 addresses natural channels with irregular cross sections, varying bottom slopes, and generally carrying larger flows. HEC-11 focuses on the design of riprap lining in such cases. Together, HEC-15 and HEC-11 provide a series of analysis and design tools that are present in HYCHL.

HYCHL is a part of the HYDRAIN computer system, but it can be operated separately. Documentation for HYCHL is found in Volume VII (*3*) of the overall HYDRAIN documentation. HYCHL allows the user to use English or SI units of measurement. The program performs all computations in English units because these are the common units for all the reference materials. If a designer prefers metric units, HYCHL performs the necessary conversions.

Rigid, Vegetative, Gabion, and Temporary Linings

HEC-15 outlines procedures for analyzing channel linings based on tractive-force theory. The procedure involves comparing an estimated shear stress resulting from flow in a channel to the maximum permissible shear stress determined for a given lining type. If the shear from flowing water increases to the point at which it is greater than the permissible shear of the lining, failure may occur. An estimate of the maximum discharge that a channel can convey is calculated when the estimated shear is assumed to equal permissible shear.

The analysis of rigid, vegetative, gabion, and temporary linings in HYCHL is applicable to channels of uniform cross section and constant bottom slope. Roadside channels typically exhibit such characteristics. HYCHL offers a variety of design and analysis options, including

1. Rigid or flexible linings,
2. Permanent or temporary linings,
3. Single or composite linings,
4. Straight or curved channel sections,
5. Alternative regular channel shapes, and
6. Constant or variable channel flow.

Depending on the function of a channel, the availability of materials, costs, aesthetics, and desired service life, a designer may choose from a variety of lining types available in HYCHL. Rigid linings in HYCHL include concrete, grouted riprap, stone masonry, soil cement, and asphalt. Flexible linings in HYCHL include those that may be considered permanent and those considered temporary. Permanent flexible linings include vegetation, riprap, and gabions. Temporary linings in-

GKY and Associates, Inc., 5411-E Backlick Road, Springfield, Va. 22151.

clude woven paper, jute mesh, fiberglass roving, straw with net, curled wood mat, synthetic mat, and bare soil (unlined).

HYCHL also provides for the analysis of these lining types when two are specified together as a composite lining. Composite linings are typically designed with a low-flow lining protecting the bottom of a channel, where higher shear stresses occur, and a sideslope lining protecting the channel sides. Composite linings are used when lining side slopes with the same material applied to the bottom is undesirable for reasons of economics, aesthetics, or safety.

The designer of rigid, vegetative, and temporary linings may apply HYCHL to a variety of geometric configurations. HYCHL calculates the shear stresses on linings in straight channel sections as well as the higher stresses found in bend sections. Channel cross sections available in HYCHL for these lining types are trapezoidal, parabolic, triangular, and triangular with rounded bottom.

The performance of rigid, vegetative, gabion, and temporary linings can be evaluated using a constant design flow or a variable inflow. The variable inflow is characterized as a uniform lineal flow that results in an increasing discharge with channel length. Under such conditions, HYCHL gives the designer an estimate of the length of channel for which a given lining may be suitable.

HEC-15 includes limited guidance for the analysis of gabion linings on steep slopes (10 to 25 percent), but provides no guidance on any other conditions. Therefore, calculating shear stress for gabion linings follows the same methodologies as described for riprap in HEC-15, using the median rock size (D_{50}) for the gabion fill material. This assumes that the wire enclosure does not significantly affect the roughness of the lining. Work by Simons et al. (*4*) supports this assumption.

Riprap Linings

HEC-15 and HEC-11 both outline procedures for analyzing riprap-lined channels. These procedures are based on the same logic, that is, the tractive-force theory, but they include additional considerations not necessary for analyzing rigid, vegetative, gabion, and temporary lining types. Although HEC-15 is recommended for design flows less than 50 ft³/sec (1.4 m³/sec) and HEC-11 for flows in excess of 50 ft³/sec, the same basic principles are used in deriving the analysis and design equations in these documents. The tractive-force procedure is applied to develop the riprap analysis and design procedures used in HYCHL (in commenting on an earlier version of HEC-15, Blodgett (*5*) notes that the flow range limitations are related to the data available at the time but may not be justified).

A channel lined with riprap can be analyzed for stability, given the riprap size. Conversely, the riprap size can be determined on the basis of a user-supplied stability factor. Composite channels that have riprap for the low-flow lining or the sideslope lining can be analyzed. HYCHL can also analyze irregular channel shapes lined with riprap only.

In a riprap-lined channel, most hydraulic calculations are based on Manning's equation. An exception occurs when the flow depth is small compared with a characteristic riprap size. In such cases—for example, on steep slopes—the effects of the rock protruding into the flow field cannot be ignored. The Bathurst hydraulic procedure given in HEC-15 is then applied to determine the flow depth and velocity in a given channel.

HYCHL METHODOLOGIES

The analytical methodologies used in HYCHL are deceptively simple. They are deceptive because much judgment may be required to select appropriate parameters or assumptions for a given application. Most of the linings are analyzed following a common procedure. Riprap linings must be considered separately.

Rigid, Vegetative, Gabion, and Temporary Linings

The analysis and design of rigid, vegetative, gabion, and temporary linings in channels of constant cross section and slope, typical of roadside channels, is accomplished by the application of tractive-force theory. The procedure used to analyze temporary linings is identical to that applied for permanent linings. However, because temporary linings are intended to have a shorter service life, the design flow may be lower. The hydraulic characterization of the channel flow and the calculation of the shear stresses are presented for a variety of lining types and channel configurations.

Most roadside channels carry uniform flow that can be represented by Manning's formula. For analysis and design purposes, uniform flow conditions are assumed with the energy slope approximately equal to average bed slope. By making this assumption, flow conditions can be defined by a uniform flow equation such as Manning's equation. Depending on the type of lining, HYCHL determines the appropriate roughness coefficient and then calculates the depth and velocity for a given design flow.

Usually, the analysis of depth/velocity and roughness coefficient must be iterative. Once the depth has been calculated, shear stress for the channel bottom is obtained from the following equation:

$$\tau_c = \gamma d_{\max} S_F \tag{1}$$

where

τ_c = calculated shear stress on the channel bottom [lb/ft² (N/m²)],
γ = specific weight of water [lb/ft³ (N/m³)],
$d_{\max}$ = normal depth [ft (m)], and
S_F = friction slope [ft/ft (m/m)].

Shear stress is the force exerted on the lining by flowing water per unit area of the lining. Each lining has associated with it a permissible shear stress, τ_p. Most of the permissible shear values come from tables or charts in HEC-15 and are considered conservative; that is, they are appropriate for design purposes. For gabions, HYCHL calculates the permissible shear stress as a function of mattress thickness and median rock size.

With the permissible shear and calculated shear estimated, a stability factor is calculated as

$$SF = \frac{\tau_p}{\tau_c} \tag{2}$$

where

SF = stability factor,
τ_p = permissible shear stress [lb/ft^2 (N/m^2)], and
τ_c = calculated shear stress on the channel bottom [lb/ft^2 (N/m^2)].

If the stability factor is less than 1, the lining is considered unstable. In addition to analyzing the channel bottom, HYCHL calculates the stability factor on the side slopes, for composite linings, and in bends. Side slopes and composite linings are evaluated by multiplying τ_c by a side shear factor, K_{side}. K_{side} is a function of the channel geometry. Bends are evaluated analogously, by multiplying τ_c by a bend shear factor, K_B. K_B is a function of the radius of curvature and some characteristic width of the channel. For side shear and bends, HYCHL calculates separate stability factors.

Riprap Linings

Although it is based on the same underlying principles of tractive-force theory, the design of riprap linings has been separated to highlight the design process. Both HEC-15 and HEC-11 address components of riprap lining design under different flow conditions and channel types. HYCHL assists the designer by automatically recognizing the appropriate conditions and using the applicable lining design procedures for riprap-lined channels.

The stability factor was previously defined as the ratio of the riprap material's critical, or permissible, shear stress (τ_p) to the tractive force exerted by the flow (τ_c). τ_c is estimated using Equation 1. The permissible shear stress for riprap is given as

$$\tau_p = F_* (\gamma_s - \gamma) D_{50} \tag{3}$$

where

F_* = Shields' parameter,
γ_s,γ = specific weight of the riprap and water, respectively [lb/ft^3 (N/m^3)], and
D_{50} = median riprap size [ft (m)].

In the case of riprap analysis for the channel bottom, the stability factor is calculated as follows:

$$SF_b = \frac{\tau_p}{\tau_c} = \frac{F_* (\gamma_s - \gamma) D_{50}}{\gamma d_{max} S_F} = \frac{F_* (S_g - 1) D_{50}}{d_{max} S_F} \tag{4}$$

where SF_b is the stability factor for the channel bottom and S_g is the specific gravity of the riprap.

To simplify for design purposes, Manning's equation can be expressed as

$$S_F = \frac{V^2 n^2}{2.22 R^{1.333}} \tag{5}$$

Substituting for slope in Equation 4, the equation for calculating the stability factor for the channel bottom is given as

$$SF_b = \frac{F_* (S_g - 1) D_{50}}{d_{max}} \times \frac{2.22 R^{1.333}}{V^2 n^2} \tag{6}$$

For riprap design of the channel bottom, Equation 6 is solved for D_{50}

$$D_{50,b} = \frac{SF_b d_{max} V^2 n^2}{F_* (S_g - 1) 2.22 R^{1.333}} \tag{7}$$

where $D_{50,b}$ is the design riprap size for the channel bottom in feet.

As is done for the other channel lining types, HYCHL calculates separate stability factors for side slopes and in bends. HYCHL can also evaluate riprap linings on irregular channel cross sections.

ISSUES IN INTEGRATING AND COMPUTERIZING HEC-15 AND HEC-11

The HYCHL program is a tool that applies a consistent methodology to a wide range of conditions. To accomplish this, four major issues were resolved during program development: (a) proper selection of Manning's n for riprap linings, (b) proper selection of Shields' parameter for riprap linings, (c) adaptation of methodologies to channel cross sections other than trapezoidal, and (d) proper use of stability factors.

The issue of the proper selection of Manning's n for riprap lining arises from the use of two methods for estimating roughness in HEC-15—Blodgett (*6*) and Bathurst (*7*)—and three methods for estimating roughness in HEC-11—Blodgett (*6*) (two equations), Jarrett (*8*), and Anderson (*9*). The evaluation was complicated by the fact that Appendix D of HEC-11 recommends the Anderson method be employed to generate a design equation, while Chapter 3 recommends the use of the Blodgett or Jarrett equations when applying the design equation. This generates an inherent inconsistency.

After reviewing the literature, a solution that is technically applicable and generally compatible with existing guidance was developed and incorporated into HYCHL. For riprap design, the default methodology for calculating the roughness coefficient depends on the ratio of the average depth (d_a) to the median riprap size (D_{50}). For d_a/D_{50} less than 2, the Bathurst approach is used to estimate Manning's roughness. For d_a/D_{50} between 2 and 185, inclusive, the following equation from Blodgett and HEC-11 (Equation 2) is used:

$$n = \frac{0.0926 d_a^{1/6}}{0.724 + 1.85 \log \left(\frac{d_a}{D_{50}} \right)} \tag{8}$$

where d_a is the average flow depth in the main channel in feet.

For d_a/D_{50} greater than 185, the following equation, also from Blodgett and HEC-11 (Equation 3), is used:

$$n = 0.019\, d_a^{0.167} \tag{9}$$

For the advanced designer, who may have reason to use another approach, HYCHL allows for default calculations to be overridden. Regardless of the d_a/D_{50} ratio, a designer may select the Blodgett equation (Equation 2, HEC-11), the Anderson equation, or a user-supplied value (Equation 2 in HEC-11 is incomplete, probably because of a typographical error).

With the user-supplied option, the Jarrett equation or other approaches may be applied.

The second major issue involves the selection of a Shields' parameter. This issue was also created by the implicit or explicit use of different values in the guidance documents without clarifying the reasons for their selection in each case. HEC-15 uses values of 0.040 (in deriving Equation 8) and 0.15 (in the discussion of steep slopes in Appendix C). HEC-11 incorporates a value of 0.047 in its design equations.

A review of the literature suggests variation of this parameter with changing hydraulic conditions, as characterized by Reynolds' number. Wang and Shen (*10*) cite experimental data in which Shields' parameter assumes values of 0.15 and above for high ($>10^5$) Reynolds' numbers. Bathurst (*7*) also observed changes in boundary resistance in flow regimes with elevated Reynolds' numbers. Although Bathurst and Wang and Shen approached their investigations from different perspectives, they all observed changes in riprap behavior at high Reynolds' numbers. The solution for HYCHL was selected to be technically defensible and compatible with existing guidance. As with the issue of roughness coefficient, the approach was to use a default value, with an option of designer override. The default Shields' parameter in all cases is 0.047. However, HYCHL also computes Reynolds' number and provides a message when it exceeds 10^5. The designer may then choose to use a larger value; however, only experienced designers should make such an adjustment.

The third issue is one of expanding the guidance provided in HEC-15 and HEC-11 rather than resolving varied interpretations. Specifically, much of the guidance related to side slopes and bends is only directly applicable to trapezoidal channel cross sections. However, HEC-15 also discusses V-shaped, parabolic, and V-shaped–with–rounded-bottom cross sections, whereas HEC-11 focuses on irregular natural cross sections.

The guidance shows how to use the geometry of a trapezoidal channel to evaluate the change of stability of riprap on the side slope, the attenuation of shear stress on the sides, and the bend shear stress—bend shear stress being a function of the radius of curvature of the channel alignment and the bottom width. Application of these concepts to other channel shapes is not apparent in the guidance.

For irregular channel shapes, the solution in HYCHL is to ask the designer to identify the points on the cross section that best represent the channel bottom and that divide the main channel from the overbanks (four points in all). From those data and the cross section itself, HYCHL constructs a geometrically and hydraulically equivalent trapezoid. This trapezoid is then used to complete the stability analyses for side slopes and bends.

For the three other regular shapes, a series of adjustments are made. To analyze sideslope stability of riprap, it is noted that the slope of the sides increases or remains constant as the water level rises. Therefore, the tendency to fail due to the sideslope angle is greatest at the water surface. Therefore, the slope at the surface is used to analyze riprap stability. Although this is a somewhat conservative approach, it is consistently applied and is appropriate for design purposes.

To analyze the attenuation of shear on the side slopes, a review of the Anderson report (*9*), from which the trapezoidal approach was derived, revealed that he had also completed an analysis of V-shaped channels. This information was retrieved and incorporated into HYCHL. It was observed in reviewing Anderson's analysis that the attenuation of shear stress (from the maximum computed as a function of depth) results from the sharp corners in the trapezoidal and V-shaped cross sections that do not allow the full shear stress to develop. Because the parabolic and V-shaped–with–rounded-bottom cross sections do not have such corners, no attenuation is expected; HYCHL reflects this interpretation.

For bends, it is necessary to identify some characteristic width such that the "sharpness" of the bend can be evaluated. For a trapezoidal channel, the bottom width is used. For all other channel cross sections, the characteristic width is calculated as the flow area divided by the maximum depth.

The final major issue in developing HYCHL was an issue of interpretation. Much of the channel lining design and analysis process is based on empirical data and depends significantly on engineering judgment. Therefore, it was undesirable for HYCHL to evaluate a lining and indicate whether or not it is stable. The dividing line is obscure.

To overcome this, the notion of a stability factor—defined as τ_p/τ_c—is used. If the stability factor is less than 1, the lining can be clearly labeled unstable, given the hydraulic conditions used to make the evaluation. However, if the stability factor is equal to or greater than 1, the lining may still not be stable. Uncertainty in the data and the degree to which a situation is simplified for analysis may lead the designer to require a stability factor of 1.6 or higher. The HYCHL document provides guidance in this matter. For uniform roadside channels, a stability factor near 1 may be adequate.

EXAMPLE APPLICATIONS

Two hypothetical examples are included to illustrate the methodologies used in HYCHL. For each example, the problem is described and the resulting output discussed.

Example 1: Composite Linings

This example shows how to analyze a channel with a composite lining. It is taken from Example 13 of HEC-15. A trapezoidal channel on a slope of 0.02 ft/ft has a 3-ft base width and 3:1 (horizontal:vertical) side slopes. The flow is 10 ft^3/sec, the low-flow lining is concrete, and the sideslope lining is vegetative (Class C). The lining transition depth is 0 ft, meaning the low-flow lining only lines the channel bottom. Figure 1 displays the cross section.

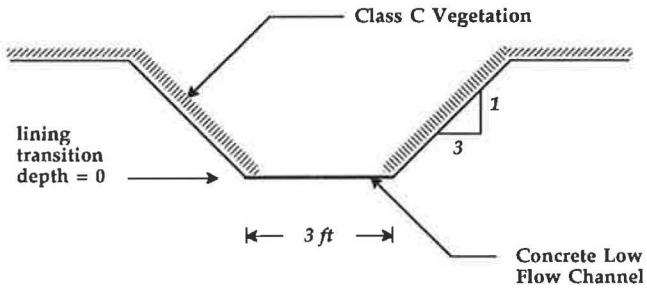

FIGURE 1 Composite lining example.

The output, given in Figure 2, shows that both linings are stable; the vegetative lining has a stability factor of 1.07. It is almost flowing with maximum discharge, which is 12.0 ft³/sec. The depth is 0.87 ft, and the effective Manning's n value is 0.071. The final line shows that K_{SU}—the ratio of side lining shear to bottom lining shear—is 0.86.

Example 2: Irregular Channel Design

This example illustrates the design of a riprap-lined channel for an irregular cross section. Figure 3 shows a sketch of the cross section detailing the main channel and the left and right floodplains. Input includes a field-measured maximum depth of 12.5 ft and a main channel velocity of 7 ft/sec. The design incorporates a stability factor of 1.2 and a Shields' parameter of 0.047.

The x-, y-coordinates describing the cross section are printed along with the x-value of the four coordinates that bound the main channel in the output shown in Figure 4. Because of a high Reynolds' number, a message is printed, and the advanced designer may consider using a higher Shields' param-

```
       ******  HYCHL  ****** (Version 1.1) ******          Date 05-30-91

Commands Read From File: C:\HYCHAN\JB2.CHL

     JOB EXAMPLE 1
     UNI 0
** UNITS PARAMETER = 0  (ENGLISH)
     CHL .02    10
     TRP 3      3
** LEFT SIDE SLOPE    3.0 AND RIGHT SIDE SLOPE    3.0
** THE BASE WIDTH OF THE TRAPEZOID (FT)    3.00
     LRG 1 1
** THE MAXIMUM CHANNEL DEPTH (FT) IS    1.00
     CPS 0
     LVG C
     END
***************END OF COMMAND FILE*************

EXAMPLE 1
------------
INPUT REVIEW
------------
  DESIGN PARAMETERS:
     DESIGN DISCHARGE (CFS):            10.00
     CHANNEL SHAPE:                  TRAPEZOIDAL
     CHANNEL SLOPE (FT/FT):             .020
     LINING TRANSITION HEIGHT (FT):     .00
-----------------------------------------
HYDRAULIC CALCULATIONS USING NORMAL DEPTH
-----------------------------------------

                          DESIGN     MAXIMUM
                          ------     -------
FLOW (CFS)                10.00       12.00
DEPTH (FT)                 .87         .93
AREA (FT^2)               4.86        5.39
WETTED PERIMETER (FT)     8.49        8.89
HYDRAULIC RADIUS (FT)      .57         .61
VELOCITY (FT/SEC)         2.06        2.23
MANNINGS N (LOW FLOW)      .013        .013
MANNINGS N (SIDE SLOPE)    .093        .087
EFFECTIVE MANNINGS N       .071        .068
------------------
STABILITY ANALYSIS
------------------

                    LINING      PERMIS SHR   CALC. SHR  STAB.
   CONDITION        TYPE        (LB/FT^2)    (LB/FT^2)  FACTOR   REMARKS
   ---------        ---------   ----------   ---------  ------   -------
LOW FLOW LINING
  BOTTOM; STRAIGHT  CONCRETE       *******      1.08     ******   STABLE
SIDE SLOPE LINING
  SIDE; STRAIGHT    VEGETATIVE  C    1.00       .93      1.07     STABLE

RATIO OF SIDE SHEAR TO BOTTOM SHEAR =     .86

*** NORMAL END OF HYCHL ***
```

FIGURE 2 Output for Example 1.

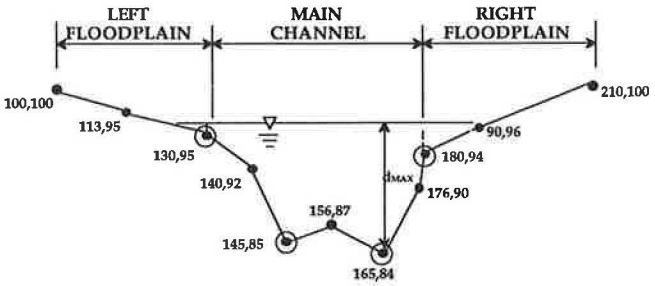

FIGURE 3 Irregular channel example.

```
       ******  HYCHL  ****** (Version 1.1) ******          Date 11-18-91

Commands Read From File: C:\HYCHL\EXAMPLE6.CHL

     JOB EXAMPLE 6
     UNI 0
** UNITS PARAMETER = 0  (ENGLISH)
     CHL -12.5  -7.0
     GR  100    100    113    98     130    95     140    92
** NUMBER  X-COORD(FT)  Y-COORD(FT)
**    1        100.00       100.00
**    2        113.00        98.00
**    3        130.00        95.00
**    4        140.00        92.00
**    5        145.00        85.00
**    6        156.00        87.00
**    7        165.00        84.00
**    8        176.00        90.00
**    9        180.00        94.00
**   10        190.00        96.00
**   11        210.00       100.00
     SA  130    145    165    180
**   LOCATION    X COORD (FT)
    LEFT BANK          130.00
    LEFT BASE          145.00
    RIGHT BASE         165.00
    RIGHT BANK         180.00
     LRR -1.2   2 0 2.65   0.047
** STABILITY FACTOR    1.20
** SPECIFIC GRAVITY    2.65
** SHIELDS PARAMETER    .047
     END
***************END OF COMMAND FILE*************

EXAMPLE 6
------------
INPUT REVIEW
------------
  DESIGN PARAMETERS:
     DESIGN VELOCITY (FT/S):            7.00
     CHANNEL SHAPE:                  IRREGULAR
     MAXIMUM FLOW DEPTH (FT):          12.50
-----------------------------------------------------------
HYDRAULIC CALCULATIONS USING NORMAL DEPTH FOR MAIN CHANNEL
-----------------------------------------------------------

                          DESIGN
                          ------
FLOW (CFS)               2849.00
MAX DEPTH (FT)             12.50
AREA (FT^2)               407.00
WETTED PERIMETER (FT)      57.90
HYDRAULIC RADIUS (FT)       7.03
AVG VELOCITY (FT/SEC)       7.00
MANNINGS N (LOW FLOW)       .050
Dsvg / D50                10.22
EQUIVALENT SLOPE (FT/FT)    .004
REYNOLDS NUMBER (10^5)    70.79
*** WARNING *** REYNOLDS NUMBER IS LARGER THAN 10^5

-------------
RIPRAP DESIGN
-------------

                    LINING     PERMIS SHR   CALC. SHR  STAB.
   CONDITION        TYPE       (LB/FT^2)    (LB/FT^2)  FACTOR   D50(FT)
   ---------        ------     ----------   ---------  ------   -------
  BOTTOM; STRAIGHT  RIPRAP         3.86        3.24      1.20      .80
  SIDE; STRAIGHT    RIPRAP         2.63        2.21      1.20      .99

*** NORMAL END OF HYCHL ***
```

FIGURE 4 Output for Example 2.

eter. In the riprap design section, D_{50} was sized for both the channel bottom and the channel side slope for a stability factor of 1.2. From a practical standpoint, it is likely that the designer would choose to line the sides and bottom with the same riprap size. In this case the D_{50} would have to be greater than or equal to 0.99 ft.

SUMMARY AND CONCLUSIONS

The HYCHL computer program was developed as an implementation of FHWA guidance in designing and analyzing channel linings found in HEC-15 and HEC-11. During the design process, it became clear that inconsistencies within the two documents are present and that their scope is limited to a subset of common problems. Because the objective of HYCHL was not only to be the computer version of HEC-15 and HEC-11 but to be a generally useful tool, it was necessary to resolve the issues and expand the scope of problem types.

A thorough review of the channel-lining design literature was instrumental in making the necessary adjustments. A few features went beyond the literature but resulted in conservative solutions. The major issues discussed in this paper are (a) appropriate selection of Manning's n, (b) appropriate selection of Shields' parameter, (c) evaluation of channel geometrics other than trapezoidal, and (d) proper interpretation of stability.

The result of the implementation effort is a generally useful design and analysis tool that applies to a wide range of channel shapes, linings, and hydraulic conditions. The program can be used independently or within the integrated hydraulic design system, HYDRAIN.

REFERENCES

1. *Design of Roadside Channels with Flexible Linings*. Hydraulic Engineering Circular 15, FHWA-87-7. FHWA, U.S. Department of Transportation, April 1988.
2. *Design of Riprap Revetment*. Hydraulic Engineering Circular 11, FHWA-IP-89-016. FHWA, U.S. Department of Transportation, March 1989.
3. *HYDRAIN-Integrated Drainage Design Computer System, Volume VII, HYCHL-Roadside Channels*. Contract DTFH61-88-C-00083. GKY and Associates, Inc., Springfield, Va., May 1991.
4. D. B. Simons, Y. H. Chen, and L. J. Swenson. *Hydraulic Test To Develop Design Criteria for the Use of Reno Mattresses*. Simons, Li, and Associates; Maccaferri Steel Wire Products, Ltd., 1983.
5. J. C. Blodgett. *Rock Riprap Design for Protection of Stream Channels Near Highway Structures: Volume 2—Evaluation of Riprap Design Procedures*. USGS Water-Resources Investigations Report 86-4128. U.S. Geological Survey, 1986.
6. J. C. Blodgett. *Rock Riprap Design for Protection of Stream Channels Near Highway Structures: Volume 1—Hydraulic Characteristics of Open Channels*. USGS Water-Resources Investigations Report 86-4127. U.S. Geological Survey, 1986.
7. J. C. Bathurst, R. M. Li, and D. B. Simons. Resistance Equation for Large-Scale Roughness. *Journal of the Hydraulics Division*, ASCE, Vol. 107, No. HY12, Dec. 1981, pp. 1593–1613.
8. R. D. Jarrett. Hydraulics of High-Gradient Stream. *Journal of the Hydraulics Division*, ASCE, Vol. 110, No. 11, Nov. 1984.
9. A. G. Anderson, A. A. Painta, and J. T. Davenport. *NCHRP Report 108: Tentative Design for Riprap Lined Channels*. HRB, National Research Council, Washington, D.C., 1970.
10. S. Wang and H. W. Shen. Incipient Sediment Motion and Riprap Design. *Journal of the Hydraulics Division*, ASCE, Vol. 111, No. 3, March 1985.

Shear Stress at Base of Bridge Pier

PEGGY A. JOHNSON AND J. STERLING JONES

The vortex motion around an obstruction in a movable bed is extremely complex. To model pier scour as a function of the size and strength of the vortex at the base of the pier, it may be desirable to characterize the strength of the vortex under various conditions in terms of a measurable quantity. The vortex strength is characterized in terms of stress at the base of a bridge pier as a function of pier width and scour depth. A flume experiment was conducted to determine indirectly the relative magnitudes of shear stress for various pier diameters and scour depths using a sediment that is uniform in size and shape. One advantage of the experimental method is that no instrumentation was required in the scour hole; therefore, there was no interruption of the flow pattern around the pier or within the scour hole. From the data, a relationship between the shear stress and the equilibrium scour depth may be developed.

Bridge pier scour can be modeled using a variety of methods. One approach is to derive a theoretical equation or set of equations to describe the scour process. Because the scour process around a bridge pier is extremely complex, many simplifications and assumptions are required to obtain an analytical model. The maximum scour depth, rather than the scour process, is more commonly modeled empirically as a function of various scour parameters such as pier width and approach flow characteristics. This method shows the effect of individual parameters on the maximum depth of scour.

Another approach to modeling pier scour is to analyze the vortex at the base of the pier. The vortex is believed to be directly responsible for the occurrence of scour holes at the base of bridge piers (*1*). After making assumptions and necessary simplifications, the size and strength of the vortex is modeled to determine the amount of erosion that will be caused by the vortex. To model pier scour as a function of the size and strength of the vortex, it is necessary to understand the effect of pier width, hydrologic conditions, and scour depth on the magnitude of the vortex strength. There are many difficulties in modeling pier scour by this approach; the vortex motion around an obstruction in a movable bed is extremely complex. It may be desirable, therefore, to characterize the strength of the vortex under various conditions in terms of a measurable quantity.

The objective of this study is to characterize the vortex strength in terms of shear stress at the base of a bridge pier as a function of pier width and scour depth. This study should provide information about the magnitude of the shear stress for the purpose of predicting both scour depths and rates.

P. A. Johnson, Department of Civil Engineering, University of Maryland, College Park, Md. 20742. J. S. Jones, Turner-Fairbank Highway Research Center, Federal Highway Administration, McLean, Va. 22101.

PREVIOUS STUDIES

Although a number of studies reported in the literature have been aimed at modeling the vortex at the base of an obstruction, few studies exist in which measurements of velocity or shear stress within the vortex or at the upstream face of the pier are reported. Melville (*2*) indirectly measured velocities in the diving current along the upstream face of a model pier by measuring the velocities at various points around the pier and using trigonometric relationships to obtain the downflow velocities. He found that the magnitude of the vertical velocity in the diving current is a maximum near the surface of the scour hole. As the diving current approaches the base of the scour hole, the vertical velocity decreases. Melville also found that the shear stress within the hole decreases as the hole deepens, indicating that the vortex strength diminishes with depth. He concluded that the downflow velocity is a function of the approach flow velocity and the pier width; however, Melville's experiment was conducted using one pier size, so there were no data with which to correlate the effect of pier size on either the shear stress or the downflow velocity.

Shen et al. (*3*) used potential flow theory to determine the vertical velocity in the diving current near the pier. He found that the maximum vertical velocity is equal to the approach flow velocity and that the shear stress at the bottom of the scour hole is approximately equal to the shear stress of the approach flow at maximum scour condition.

A method of determining the approach velocity at which riprap around a bridge pier will fail was developed by Parola (*4*). In his experiment, Parola set a 4-in. model bridge pier in sand, scoured a hole to a predetermined depth, stabilized both the scour hole and bed surface, then lined the hole with ¼-in. gravel. He then introduced a flow to the flume, gradually lowered the tailgate, and watched for failure (i.e., movement) of the gravel within the hole. When the gravel failed, he measured the upstream flow depths and velocities at various points along a cross section. He repeated the experiment for various scour depths and two pier configurations. He assumed that the effective velocity at the pier at the time of failure of the gravel was equal to the velocity of incipient motion for that particle size. Parola found that the effective velocity at the pier was approximately 1.5 times the approach velocity required to cause failure of the riprap for a circular pier and 1.7 times the approach velocity for a rectangular pier. Shear stress is a function of velocity squared; hence the effective shear stress at the pier is on the order of 2.25 to 2.90 times the shear stress of the approach flow. This indirect approach to "measuring" velocity and shear stress at a pier was the basis for the design of the experiment in this study.

EXPERIMENTAL APPROACH

The experiment to determine indirectly the shear stress within a scour hole at the base of a pier was conducted in the FHWA Hydraulics Laboratory at the Turner-Fairbanks Highway Research Center in McLean, Virginia. The experiment was conducted in a rectangular flume 6 ft wide and 70 ft long in the center of which was a recessed section 8 ft long, 6 ft wide, and 1½ ft deep. Marbles were used instead of gravel (as in Parola's experiment) in an attempt to reduce scatter in the data. Gravel varies significantly in shape and size, thus the particles tend to interlock, causing large variations in the initial movements of the sediment. Marbles were chosen because they are uniform in size and shape.

The experiment was divided into two phases: (a) an unobstructed flow experiment to determine the threshold of movement for the marbles, and (b) an experiment to determine shear stresses within a scour hole for different pier sizes.

Unobstructed Flow

The purpose of this portion of the study was to determine the threshold shear stress that would just cause the marbles to move. To prepare the bed of the flume, one layer of marbles was glued to the bed from the headbox to a distance downstream of the observation area in order to establish the proper flow resistance. At the observation area, a layer of red marbles was glued to a level board placed in the recessed area. On top of the red marbles, a single layer of yellow marbles was placed; these marbles were free to move.

After the flume was prepared, a flow rate of about 6 ft³/sec was supplied to the flume with the tailgate in an upright position such that the flow depth was great enough and the velocity low enough that the marbles would not move in the observation area. The tailgate was then lowered very slowly, by small increments, so that steady, uniform flow could be assumed. The marbles in the observation area were observed closely so that movement could be detected. When a discernible patch of red appeared, the tailgate was held at its position and upstream velocity and flow depth measurements were recorded.

This process was repeated four times. The shear stress necessary to cause movement of the marbles was then computed as a function of the average flow velocity and depth by using the integrated form of the assumed logarithmic velocity distribution:

$$\tau_o = \frac{\rho V^2}{\left[5.75 \log\left(12.27 \frac{y_o}{k_s}\right)\right]^2} \tag{1}$$

where

τ_o = average shear stress on the channel bottom upstream of the pier,
V = average approach velocity,
y_o = flow depth, and
k_s = particle diameter.

For the second portion of the study, the value of τ_o was assumed to be the effective shear stress at the base of a pier, τ_p, at the time of failure of the marbles. The value of τ_p is thus equal to the average of τ_o for the four runs.

Shear Stress Within the Scour Hole

The flume was next prepared to develop a scour hole so that the shear stress within the hole could be determined. A model bridge pier, constructed from 4-in.-diameter PVC pipe, was attached to a square Plexiglas plate and bolted to the floor of the flume in the recessed section. The recessed section was then filled with a medium-grained sand, saturated with water, and leveled across the surface. A flow rate of about 6 ft³/sec was supplied to the flume with the tailgate sufficiently raised so that scour would not occur. The scour hole was then developed by lowering the tailgate and increasing the velocity until the sand just began to move (approximately incipient motion). The flow was maintained at this velocity and depth for about 2 hr to develop a scour hole of maximum depth around the pier. After the 2-hr, the flume and scour hole were drained. The hole was stabilized with an epoxy spray and allowed to dry for about 24 hr. After drying, the sand surface was leveled, and care was taken not to disturb the scour hole. The surface was then cemented so that the bed would remain in place at higher velocities. The bed was again allowed to dry for 24 hr.

To determine indirectly the shear stress at the base of the scour hole, the hole was lined with 5/16-in. marbles. First it was lined with yellow marbles, then with white. When the white marbles began to move, the event was clearly visible as the yellow appeared. Failure of the marbles was then defined as the appearance of a discernible path of yellow. A flow rate of about 6.5 ft³/sec was supplied to the flume with the tailgate raised sufficiently high to prevent movement of the marbles in the scour hole. The tailgate was lowered slowly in intervals such that the assumptions of steady, uniform flow were not violated significantly. When the white marbles began to move and a discernible patch of yellow was detected, the tailgate was stopped and flow measurements were taken. Measurements of the flow depth and velocity were taken in four locations across each of two cross sections upstream of the model pier in the undisturbed flow. Velocity measurements were taken at 20, 40, 60, and 80 percent of the flow depth and at ¼ in. from the channel bottom using a Nixon propeller meter.

After the flow measurements were completed, the experiment was repeated in the same scour hole (which had been relined with marbles), for flow rates of about 7.5 and 9.0 ft³/sec. Flow measurements were again recorded after a yellow patch appeared.

The entire process was repeated for other predetermined scour depths. The scour hole was refilled with sand and a new hole scoured, this time to a shallower depth. The scour hole and bed were fixed as described above, the hole lined with marbles, and the three flow rates supplied to the flume. This process was repeated until the depth of the scour hole was zero, that is, level with the flume bed. After flow measure-

ments were made for the scour depth of zero, the "pier" was removed and the experiment repeated for 6- and 10-in. model piers.

RESULTS

The unobstructed flow experiment resulted in four values of τ_o computed from Equation 1. The average shear stress for the four runs was 0.052 lb/ft^2 with a coefficient of variation of 0.077.

The scour hole experiments resulted in flow measurements for 45 experimental runs. The data, including the pier diameter, flow depth, flow velocity, scour depth, flow rate, and Froude number, are listed in Table 1. The flow velocities and depths represent the values that caused failure (i.e., a discernible patch of yellow) for a particular pier diameter, flow rate, and scour depth.

TABLE 1 EXPERIMENTAL RESULTS

Pier Width (ft)	Flow Depth (ft)	Velocity (ft/s)	Scour Depth (in)	Fr #	Q (cfs)	τ (lb/ft^2)	τ_p/τ_o
0.375	0.854	1.833	0	0.350	9.38	0.036	2.16
0.375	0.708	1.796	0	0.376	7.63	0.037	2.09
0.375	0.638	1.690	0	0.373	6.46	0.034	2.27
0.375	0.850	1.829	0.625	0.350	9.32	0.036	2.16
0.375	0.768	1.701	0.625	0.342	7.83	0.032	2.40
0.375	0.578	1.768	0.625	0.410	6.12	0.039	2.00
0.375	0.818	1.914	1.5	0.373	9.39	0.040	1.95
0.375	0.655	1.961	1.5	0.427	7.70	0.045	1.70
0.375	0.614	1.851	1.5	0.417	6.81	0.041	1.86
0.375	0.713	2.128	2.375	0.444	9.10	0.052	1.49
0.375	0.563	2.275	2.375	0.534	7.68	0.065	1.19
0.375	0.494	2.264	2.375	0.568	6.71	0.067	1.14
0.375	0.714	2.131	3.25	0.445	9.12	0.052	1.49
0.375	0.596	2.141	3.25	0.489	7.66	0.056	1.38
0.375	0.523	2.130	3.25	0.519	6.68	0.058	1.32
0.549	0.926	1.615	0	0.296	8.97	0.027	2.86
0.549	0.808	1.574	0	0.309	7.62	0.027	2.86
0.549	0.722	1.576	0	0.327	6.82	0.028	2.74
0.549	0.904	1.634	1	0.303	8.86	0.028	2.77
0.549	0.682	1.779	1	0.380	7.27	0.037	2.10
0.549	0.620	1.686	1	0.378	6.27	0.034	2.25
0.549	0.790	1.895	2	0.376	8.98	0.039	1.96
0.549	0.674	1.845	2	0.396	7.46	0.040	1.95
0.549	0.546	1.939	2	0.463	6.35	0.048	1.62
0.549	0.854	1.811	3	0.346	9.28	0.035	2.21
0.549	0.686	1.866	3	0.397	7.68	0.040	1.91
0.549	0.618	1.799	3	0.403	6.66	0.039	1.98
0.549	0.812	1.875	4	0.367	9.13	0.038	2.02
0.549	0.676	1.911	4	0.410	7.75	0.042	1.81
0.549	0.592	1.980	4	0.454	7.03	0.048	1.61
0.828	0.934	1.629	4.5	0.297	9.12	0.027	2.82
0.828	0.737	1.773	4.5	0.364	7.84	0.035	2.18
0.828	0.630	1.739	4.5	0.386	6.57	0.036	2.13
0.828	0.814	1.891	3.1	0.370	9.23	0.039	1.99
0.828	0.722	1.794	3.1	0.372	7.77	0.036	2.11
0.828	0.646	1.689	3.1	0.370	6.54	0.034	2.28
0.828	0.817	1.908	2	0.372	9.35	0.039	1.96
0.828	0.786	1.669	2	0.332	7.86	0.031	2.52
0.828	0.648	1.775	2	0.389	6.90	0.037	2.07
0.828	0.944	1.634	1.5	0.296	9.25	0.027	2.81
0.828	0.852	1.515	1.5	0.289	7.74	0.024	3.15
0.828	0.716	1.518	1.5	0.316	6.51	0.026	2.94
0.828	1.058	1.441	0	0.247	9.14	0.020	3.77
0.828	0.914	1.431	0	0.264	7.84	0.021	3.62
0.828	0.726	1.530	0	0.317	6.66	0.026	2.91

Scour Depth

Clearly, for a given pier diameter and flow depth, the flow velocity must increase to cause failure of the marbles as the scour hole deepens. For the 6-in.-diameter pier and a flow depth of approximately 0.7 ft, the approach velocity increases from 1.58 ft/sec, when the scour depth is 0, to 1.77 ft/sec, when the scour depth is 4.5 in.

Assuming that the critical shear stress of 0.052 lb/ft² is the shear stress at the pier when the marbles fail, ratios of τ_p (shear stress at the pier) to τ_a (bed shear stress of the approach flow causing the marbles to fail) may be computed for various scour depths. These values are also given in Table 1. Equation 1 was used to compute values of τ_a. Figure 1 shows the decrease in τ_p/τ_a with increasing scour depth for pier diameters of 4 and 6 in. The scour depth in Figure 1 is normalized by the maximum (equilibrium) scour depth obtained for each of the pier diameters. For the 6-in. pier,

$\tau_p/\tau_a = 2.74$ (at surface)

$\tau_p/\tau_a = 1.81$ (at $d_s = 4.0$ in.)

where d_s is the scour depth. The depth of two layers of marbles within the hole is 1.1 in.; therefore, the shear stress ratios could not be evaluated at the absolute base of the scour hole. If the scour process stops when the shear stress at the base of the hole is equal to the shear stress on the channel bottom, then τ_p/τ_a must approach 1 as the bottom of the scour hole is approached. Knowledge of this effect is useful in modeling a time-dependent function of the scour process, particularly when cohesive materials are a concern.

Pier Width

It is well recognized that bridge pier width has a significant effect on the depth of scour (*5–8*); in general, the wider the pier, the greater the scour depth. To determine the effect of pier width on the shear stress at the pier, three pier diameters were tested. As shown in Figure 2, for a plane bed ($d_s = 0$), τ_p/τ_a increased nonlinearly as the pier diameter was increased. Figure 2 shows that the change in shear stress is greater between the smaller pier widths. The shear stress ratios varied from 2.09 to 2.91; therefore, for an approximate twofold increase in pier diameter, the shear stress ratio increased about 1.4 times. This result is in agreement with other studies, showing the increase in scour depth for larger pier diameters (*8*). Clearly, the increase in pier diameter is responsible for an increase in shear stress at the pier, which, in turn, is responsible for the increase in scour depth. A comparison of the results reported here to those obtained by Parola (*4*) show the results of this study to be within the range of ratios computed from Parola's data.

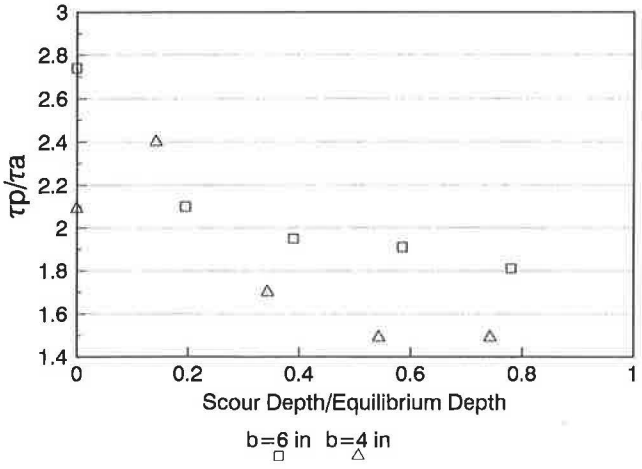

FIGURE 1 Shear stress as function of scour depth (flow depth = 0.7 ft).

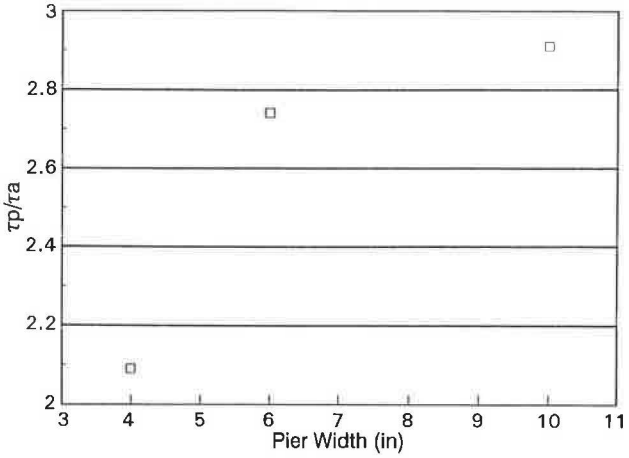

FIGURE 2 Shear stress as function of pier width (flow depth = 0.7 ft, scour depth = 0).

Although the data reported here are in agreement with data from previous studies, caution should be exercised in using them. For a flow depth of 0.7 ft, pier diameters of 4, 6, and 10 in. correspond to flow-depth–to–pier-width ratios, y/b, of 2.1, 1.4, and 0.8, respectively; therefore, these results have most likely included shallow water effects. Melville and Sutherland (*9*) found that the shallow water effect could be overcome or accounted for by the use of a factor (K) ranging from 0 for $y/b = 0$ to 1 for y/b greater than about 3.5, that is, when y/b is greater than about 3.5, shallow water effects are negligible. For y/b less than about 3.5, scour depth increases with flow depth.

Sources of Error

There are several possible sources of error for the shear stress ratios reported here. Determining the critical velocity for marbles was difficult: they tended to roll and bunch up rather than be lifted and moved across the bed surface. Also, the specific gravity (2.445, rather than 2.65) and the shape of the marbles differ from those of 5/16-in. gravel (spherical as opposed to irregular), so established curves of incipient motion, such as Shields' curve, will yield incorrect results. In addition, it was assumed that a single value of the average critical shear stress ($\tau_c = 0.052$ lb/ft²) could be used as the shear stress at the pier at the time of failure. There are two possible sources

of error due to this assumption. First, τ_c was based on an average of four values. The coefficient of variation was quite low, so the average is most likely a reasonable value; however, four data points constitute a rather small sample size, so the actual value of τ_c could vary somewhat from the computed value. Second, τ_c is presented as a deterministic (constant) value. In actuality, there is a random component associated with the critical shear stress, however this was ignored in the analysis of the data.

Another source of error may be due to the subjectivity of the experiment. It was critical that one observer perform all experiments so that failure of the marbles be determined in the same way each time. The observer was required to record flow measurements when a "discernible patch of yellow" was observed. Each observer will interpret this definition of failure differently. By using the same observer each time, this element of subjectivity was greatly reduced. Because relative rather than absolute magnitudes of shear stress were of interest, this source of error was reduced even further.

CONCLUSIONS

A laboratory experiment was conducted to determine the relative magnitudes of shear stress at the base of a bridge pier as a function of pier diameter and scour depth. Marbles, rather than sand or gravel, were used as the bed sediment in the experiment in order to reduce scatter in the data by using a particle that was uniform in size and shape.

The results of this study were based on an experimental method in which the shear stress at the base of the scour hole was measured indirectly. There are advantages and disadvantages in using such a method. One distinct advantage is that no instrumentation was required in the scour hole; therefore, there was no interruption of the flow pattern around the pier or within the scour hole. Another advantage was the low cost of this method compared with that of using expensive instrumentation such as lasers. It is also quite possible that the accuracy obtained from such instrumentation is not required in light of the many other uncertainties in modeling bridge pier scour. For example, the uncertainties in extrapolating laboratory data to a real-world situation and uncertainties in the hydrologic conditions may be great enough to overshadow uncertainties caused by using a less accurate method of determining shear stresses in the laboratory flume.

The main disadvantage of using an indirect method of measuring shear stresses is the high degree of subjectivity in determining at what point the marbles failed; however, the error due to this problem was reduced by using a single observer and by depending on relative magnitudes rather than absolute magnitudes. In addition, the size of the marbles relative to the pier diameter was rather large in this experiment. For the smallest pier used, the pier diameter was only about seven times the diameter of the marbles. This relative size corresponds to that of riprap around a bridge pier. Although this size was adequate for this purpose, caution should be used in extrapolating information about the movement of sand around a bridge pier. The results of the experiment showed that the approach bed shear stress required to move marbles at a 10-in. model pier was about 1.4 times greater than at the 4-in. pier. This increased shear stress is consistent with the greater scour depth at larger piers often noted in scour literature.

The results also showed that the shear stress at the base of the pier decreases as scour depth increases. As the scour depth continues to increase, the shear stress approaches the bed shear stress upstream of the scour hole. The relative magnitude of the shear stress at the base of the scour hole and the bed shear stress is important information for modeling scour as a time-dependent function. This is particularly important for cohesive materials for which the erosion of the material depends highly on the amount of time that it is exposed to a particular shear stress.

On the basis of these results, it can be concluded that the shear stress at the base of a pier increases with increasing bridge pier diameter; however, the increase is not a linear one. The shear stress increases nonlinearly with increasing pier diameter, as does the depth of scour. Once a relationship between the shear stress ratio and the equilibrium depth of scour is established, then the indirect shear stress measurements could become a laboratory expedient for conducting pier scour experiments and could help explain some of the effects of various bed materials.

ACKNOWLEDGMENT

This study was sponsored by FHWA and conducted at the Turner-Fairbank Highway Research Laboratory.

REFERENCES

1. H. W. Shen, Y. Ogawa, and S. S. Karaki. Time Variation of Bed Deformation near Bridge Piers. *Proc., 11th Congress of the International Association for Hydraulic Research*, Leningrad, USSR, 1967, Paper 3.14.
2. B. W. Melville. Local Scour at Bridge Sites. Report 117. School of Engineering, University of Auckland, Australia, 1975.
3. H. W. Shen, V. R. Schneider, and S. Karaki. Local Scour Around Bridge Piers. *Journal of the Hydraulics Division*, ASCE, Vol. 95, No. HY6, 1969, pp. 1919–1939.
4. A. C. Parola. *The Stability of Riprap Used To Protect Bridge Piers*. Ph.D. dissertation. Pennsylvania State University, State College, 1990.
5. H. N. Breusers, G. Nicollet, and H. W. Shen. Local Scour Around Cylindrical Piers. *Journal of Hydraulics Research*, Vol. 15, No. 3, 1977, pp. 211–252.
6. G. R. Hopkins, R. W. Vance, and B. Kasraie. *Scour Around Bridge Piers*. Report FHWA-RD-79-103. FHWA, Washington, D.C., 1980.
7. B. P. Jain and P. N. Modi. Comparative Study of Various Formulae on Scour Around Bridge Piers. *Journal of the Institution of Engineers* (India), Vol. 67, Part CI 3, 1986, pp. 149–159.
8. *Scour at Bridges*. Hydraulic Engineering Circular 18. FHWA, U.S. Department of Transportation, Washington, D.C., 1990.
9. B. W. Melville and A. J. Sutherland. Design Method for Local Scour at Bridge Piers. *Journal of Hydraulics Engineering*, Vol. 114, No. 10, 1988, pp. 1210–1226.

Laboratory Tests of Scour-Monitoring Devices

STEVEN R. ABT, JERRY R. RICHARDSON, SCOTT A. HOGAN, BRIAN L. VAN ZANTEN, AND THOMAS J. SILLER

The recent failure of bridge pier footings and foundations because of scour and erosive processes has resulted in the need to monitor the maximum scour depths. During the past 5 years, more than 30 types of device for measuring scour have been developed for field use. Many of these devices have not been fully tested either in laboratory or field situations. A laboratory testing program was conducted to evaluate the effectiveness and practicability of several scour-monitoring devices. A series of flume tests was performed evaluate driven and falling rod model devices. Sonar measurement devices were tested in a sump and visual accumulation tube to analyze the affects of transducer transmission angle, transducer mounting angle, transducer submergence depth, transducer mounting distance from the pier, and temperature on accuracy and reliability. It was determined that vertically supported falling rods and the scuba mouse were practicable devices when mounted in front of the pier. The sonar device has a high potential for field application, although it is sensitive to water temperature, mounting angle, and transducer placement location in front of the pier.

The recent failure of bridge pier footings and foundations because of long-term degradation, local scour at piers and abutments, and lateral stream migration has highlighted the need to develop a means of monitoring scour depths at and near pier foundations and abutments. Nearly 86 percent of all bridges in the United States span a water body, so durable, accurate, and cost-effective monitoring devices are needed to protect the health and safety of the highway user. Furthermore, because many scour processes are cyclic, accurate measurements of scour during storm events are needed.

During the past 5 years, more than 30 types of scour measurement instruments have been conceptually proposed, planned, or fabricated. Fewer than 20 of these devices have been developed and refined for field use. These scour-monitoring devices include sounding weights, sounding rods, driven rods, ultrasonic sounders, sonar, conductance probes, optical sand-surface meters, and the scuba mouse. Although prototypes of each of these devices are in development or use, many have not been fully tested under either laboratory or field situations.

In an attempt to evaluate the effectiveness of some of the scour-monitoring concepts, a program was formulated to test scale-model and near-prototype scour-monitoring devices. The devices tested and reported in this document were selected through an extensive analysis performed by Resource Consultants, Inc., within the scope of work negotiated in a contract with NCHRP. The selection of devices for measuring scour was based on hydraulic factors, mounting requirements, ability to measure scour depth to ± 1.0 ft, long-term reliability, and cost minimization. It should be recognized that one instrument may not be applicable to all bridges or stream conditions.

S. R. Abt, S. A. Hogan, B. L. Van Zanten, T. J. Siller, Department of Civil Engineering, Colorado State University, Ft. Collins, Colo. 80523. J. R. Richardson, Resources Consultants, Inc., 402 West Mountain Avenue, Ft. Collins, Colo. 80522.

OBJECTIVES

The objectives of the laboratory test program are to

1. Test and evaluate a scale model(s) or prototype measurement instrument or device considered practicable for field consideration.
2. Provide recommended refinements for the redesign or improvement of those instruments that were deemed practicable as a result of the initial testing.
3. Recommend those instruments that appear most practicable for near-prototype and field testing.

This paper will present a description of the laboratory testing program and test results on selected instruments and devices considered practicable.

TEST FACILITIES

The testing program was conducted in the Hydraulics Laboratory at the Engineering Research Center of Colorado State University. The program used three permanent facilities in the laboratory.

Recirculating Flume

Scale-model instruments were tested in an existing recirculating steel flume. The flume—200 ft long, 8 ft wide, and 4 ft deep—can be adjusted to vary the slope from zero to nearly 3 percent. The flume has a discharge capacity of approximately 100 ft^3/sec. Flow through the flume can exceed 10 ft/sec.

The interior of the flume was segmented into three sections: a flow development section, a test section, and a tailwater control and material recovery section. The flow development section extended from the flume headbox and diffuser downstream approximately 100 ft. The test section abutted to the

flow development section and extended downstream approximately 60 ft. A model pier was installed into the test section, simulating placement into a stream channel composed of erodible material. The remaining 40 ft of the flume served as a bed material recovery basin and tailwater control. The flume slope was leveled at approximately 0.5 percent.

The pier is a 1:15 (model:prototype) Froude scale model of the prefailure pier of the New York State Thruway bridge over Schoharie Creek. The model pier is 65.8 in. long and 15.1 in. wide, the footing thickness is 4.0 in., and the pier height is 31.9 in., as illustrated in Figure 1. The pier was mounted such that the base of the footing was elevated approximately 1 ft above the flume bottom and situated parallel to the flume sidewalls.

The bed material was composed of two noncohesive sands with median grain sizes of approximately 2.3 and 4.0 mm. Both bed materials have a coefficient of uniformity of approximately 1.9. The bed materials were loosely placed in the flume to an elevation of 8 in. above the top of the footing.

A driven and sounding rod was used to simulate pier monitoring devices. A circular steel rod 56 in. long and 0.77 in. in diameter was used in all the tests.

Sonar Test Apparatus for Depth

Two sonar devices were tested in the laboratory sump for accuracy and reliability. A prefabricated scour hole was constructed of wood and metal materials. The scour hole was designed for placement at the bottom of the sump such that the back edge (high side) would fit adjacent to the sump wall. The sump is 8 ft deep with a water level that varies from 6 to 7.5 ft deep.

Once the scour hole was placed into the sump and the sump was filled, an angle iron was installed directly above the scour hole such that the angle iron aligned along the centerline of the scour hole. A point gauge with transducer mounting bracket was installed on the angle iron. The mounting bracket was pre-fabricated allowing the transducer face to rotate 0 to 30 degrees. The sonar device(s) were installed into the mounting bracket located at the end of the point gauge. The test apparatus allowed the user to situate the transducer at any depth into the sump and locate the transducer at any position over the scour hole center line.

The two sonar devices tested in the sump were the Eagle Corp. Sonar Model Z-9500 with a transmission angle of 8 degrees and the Lawrence Corp. sonar with a transmission angle of 20 degrees. Both devices are commercially available.

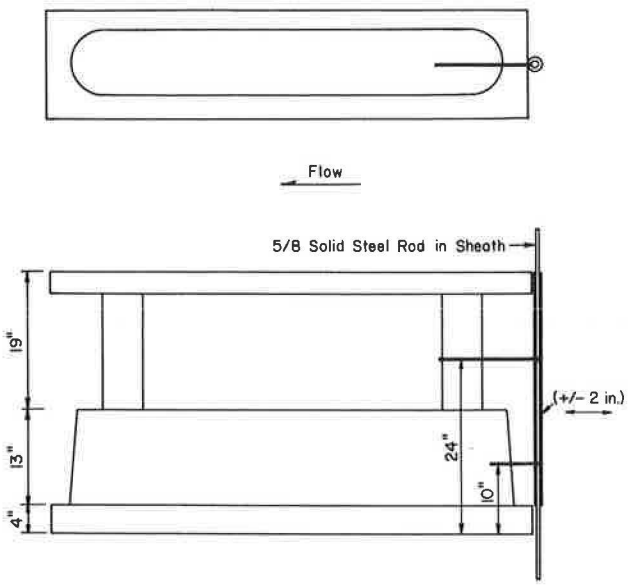

FIGURE 1 Plan (*top*) and profile (*bottom*) of model pier.

Sonar Test Apparatus for Temperature

A Plexiglas visual accumulation tube (VA) was used to determine how temperature may affect the accuracy of the Eagle Corp. Z-9500 sonar instrument. The VA tube is 10 ft high and 16.375 in. in diameter (OD); its walls are 0.25 in. thick. A point gauge with mounting bracket was suspended from the top of the tube. The sonar transducer was installed into the bracket at the base of the point gauge. Water was placed into the tube to a depth of approximately 6.8 ft. The water temperature was varied by adding warmer water or ice as required. A mercury thermometer accurate to ± 1°F was used to monitor the fluid temperature. A point gauge, ±0.05 ft, was used to monitor the water depth.

TEST PROGRAM

The test program was conducted in three phases, each phase was composed of a series of tests oriented toward accomplishing one of the stated objectives. Each test phase will be summarized.

Phase I

The objective of the Phase I tests was to evaluate the general applicability of using vertically supported and near-vertical sounding rods in simulated alluvial bed channels. A series of 10 tests was conducted in the recirculating flume. The test configurations were analyzed using two bed materials. The first set of six test configurations used a 4.0-mm bed material and included a base run without monitoring device, a vertically supported falling rod placed immediately upstream of the pier foundation, a vertically supported driven rod placed immediately upstream of the pier foundation with simulated scuba mouse, a vertically supported falling rod placed through the footing, a vertically supported driven rod placed through the footing, and a vertically supported falling rod with expanded base plate placed immediately upstream of the pier foundation. The second set of four test configurations used a 2.3-mm bed material and included a base run without monitoring device, a vertically supported falling rod with enlarged base plate placed immediately upstream of the pier foundation, a vertically supported driven rod with scuba mouse placed immediately upstream of the pier foundation, and an angled (45 degrees) falling rod with base plate.

Each of the 10 tests was conducted in a similar fashion. After placement of the pier, the test section was filled (approximately 2 ft) with the appropriate bed material. The bed was leveled. Flow was initiated and the flume was slowly filled until the water depth was approximately 0.8 ft deep. The discharge was adjusted until the flow velocity was approximately 2.0 ft/sec. During the run, velocity measurements were obtained at 0.6 times the flow depth measured from the water surface. The run extended for approximately 2 hr. The flow was discontinued and the bed was contoured. The discharge was reinitiated to a flow depth of approximately 1.2 ft and a velocity of approximately 3.0 ft/sec. After a 2-hr test duration and collection of the velocity data, the flume was again shut down and the bed contoured. The discharge was again reestablished at an approximate depth of 1.5 ft and an approximate velocity of 4.0 ft/sec. Upon completion of the run, the bed was contoured and photographically documented. When monitoring devices were installed, data were also collected pertaining to the device scour-depth measurements. Figure 2 presents the point gauge and velocity measurement locations sin the test section.

Phase II

The objective of Phase II was to evaluate the accuracy and reliability of using a sonar monitoring device under a spectrum of operating conditions. Two sonar transducers were tested previously under similar operating conditions. Test parameters included the transducer's mounting angle, mounting distance from the simulated pier (wall), and submergence depth. Transducer mounting angles varied from 0 to 25 degrees, and transducer submergence ranged from 0 to 2.5 ft below the water surface. The transducer was situated adjacent to the pier at Station 0. The transducer was extended from the simulated pier 0.0 to 5.0 ft in intervals of 0.5 ft. A total of 360 data points were collected.

The test procedure was similar for each test series. Once the appropriate transducer was installed into the point gauge mounting bracket and adjusted to the appropriate mounting angle, the sonar device was turned to the on position and calibrated. The transducer face was then submerged and placed adjacent to the simulated pier directly above the centerline of the simulated scour hole. The sonar was allowed to stabilize, and a depth measurement was recorded. The transducer was moved from the pier 0.5 ft along the simulated scour hole centerline, and the sonar measurement was again recorded. Transducer measurements were systematically taken until the transducer extended 5 ft from the simulated pier along the centerline of the scour hole. The transducer was then lowered into the sump, and the sonar measurements were repeated. When all the submergence depths and distance depths were obtained, the entire process was repeated for each of the different mounting angles. The second transducer was installed and a limited data set was recorded.

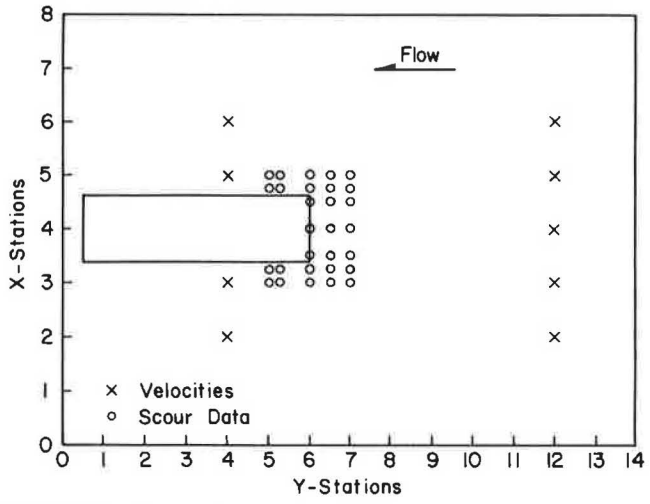

FIGURE 2 Data collection locations in flume test sections.

Phase III

The objective of the Phase III testing program was to determine whether the accuracy of the sonar device is affected by a change in the fluid temperature. Only the Eagle Corp. Model Z-9500 device was tested in this phase. A series of 24 test measurements was obtained. The test parameters included the water temperature and the submergence of the transducer. The water temperature varied from 42°F to 96°F and the transducer submergence varied from 0.0 to 1.5 ft below the water surface.

The test procedure was similar for all sequential measurements. Warm water was initially placed into the VA tube. The transducer was installed into the mounting bracket (0-degree mounting angle) and placed into the VA tube with the transducer face just below the water surface. The sonar device was turned to the "on" position, and the transducer was calibrated. After the water in the tube was stirred and the water temperature measured, the device was allowed to stabilize and a depth measurement was recorded. Then the transducer was lowered into the tube to the appropriate submergence depth and another measurement was recorded. Once all the submergence-related measurements were completed, water was drained from the tube and cooler water was added, thereby lowering the reservoir water temperature. When the temperature reached the desired level, the sonar device was again tested. This process was repeated for each of the temperatures in the test series.

TEST RESULTS

The results of the testing program will be presented in three sections: pier monitoring devices, accuracy of sonar devices, and temperature affects on sonar. Quantitative and qualitative results will be presented.

Pier Monitoring Devices

The pier monitoring devices refer to the vertically supported and near-vertical sounding rods. Ten test series were conducted with the pier monitoring devices in the recirculating flume.

The initial test series conducted was with the pier installed in the 4.0-mm bed material without a monitoring device. Velocities of approximately 2, 3, and 4 ft/sec were routed through the channel; the resulting scour depths were measured and recorded. Each velocity run extended for 2 hr. Figure 3 depicts the scour hole after 6 hr of testing. It is observed that the maximum depth of scour occurred directly beneath the footing along the leading edge. Table 1 presents a summary of the approximate flow rates, velocities, and maximum scour depths (point gauge) observed. The base test served as a standard by which the remaining tests with monitoring devices could be compared.

The second test series simulated a vertically supported falling rod installed immediately upstream of the pier footing as shown in Figure 4. The foot of the rod was placed adjacent to the initial bed elevation. The rod measurement was taken at the end of each test run and was compared to the actual maximum depth of scour. It was observed that the rod drove itself into the bed, resulting in a maximum depth of scour measurement greater than the actual observed depth. It is speculated that the energy imparted into the device from the flow vibrated the rod to a level at which the bed material

FIGURE 3 Scour hole observed without monitoring device.

TABLE 1 SUMMARY OF FLUME TESTING PROGRAM

8' FLUME TESTING SUMMARY						
Test No.	**Configuration**	**Flow Rate (cfs)**	**Flow Depth (ft)**	**Approach Velocity (fps)**	**d_{50} (mm)**	**Maximum Scour Depth (ft)**
1A	No Device - Base Run	15	0.8	2.11	4.0	0.17
1B	No Device - Base Run	28	1.2	2.98	4.0	0.60
1C	No Device - Base Run	45	1.5	3.90	4.0	0.68
2A	Falling Rod - front of footing	15	0.8	2.16	4.0	0.17
2B	Falling Rod - front of footing	28	1.2	2.92	4.0	0.57
2C	Falling Rod - front of footing	45	1.5	3.84	4.0	0.62
3A	Driven Rod - front of footing w/ scuba mouse	15	0.8	2.07	4.0	0.23
3B	Driven Rod - front of footing w/ scuba mouse	28	1.2	3.13	4.0	0.72
3C	Driven Rod - front of footing w/ scuba mouse	45	0.8	3.96	4.0	0.73
4A	Falling Rod - through footing	15	0.8	2.38	4.0	0.47
4B	Falling Rod - through footing	28	1.2	3.11	4.0	0.70
4C	Falling Rod - through footing	45	1.5	3.97	4.0	0.76
5A	Driven Rod - through footing	15	0.8	2.06	4.0	0.20
5B	Driven Rod - through footing	28	1.2	3.17	4.0	0.56
5C	Driven Rod - through footing	45	1.5	3.74	4.0	0.56

(continued on next page)

TABLE 1 (*continued*)

Test No.	Configuration	Flow Rate (cfs)	Flow Depth (ft)	Approach Velocity (fps)	d_{50} (mm)	Maximum Scour Depth (ft)
6A	Falling Rod - front of footing with base plate	15	0.8	2.09	4.0	0.17
6B	Falling Rod - front of footing with base plate	28	1.2	3.13	4.0	0.54
6C	Falling Rod - front of footing with base plate	45	1.5	3.93	4.0	0.57
7A	Falling Rod - front of footing with base plate	15	0.8	2.20	2.3	0.42
7B	Falling Rod - front of footing with base plate	25	1.2	2.57	2.3	0.45
7C	Falling Rod - front of footing with base plate	35	1.4	3.51	2.3	0.67
8A	No Device - base run	15	0.8	2.30	2.3	0.34
8B	No Device - base run	25	1.2	2.51	2.3	0.53
8C	No Device - base run	35	1.4	3.49	2.3	0.53
9A	Driven Rod - front of footing w/ scuba mouse	15	0.8	2.27	2.3	0.37
9B	Driven Rod - front of footing w/ scuba mouse	25	1.2	2.50	2.3	0.45
9C	Driven Rod - front of footing w/ scuba mouse	35	1.4	3.10	2.3	0.62
10A	Falling Angled Rod w/ Base Plate	15	0.8	2.24	2.3	0.47
10B	Falling Angled Rod w/ Base Plate	25	1.2	2.65	2.3	0.67
10C	Falling Angled Rod w/ Base Plate	35	1.4	3.09	2.3	0.69

could firmly support the weight of the rod. The rod was again observed to drive itself into the bed during the 2.0- and 4.0-ft/sec velocity runs. The rod provided a final maximum scour depth of 50 percent greater than the observed measurement. Although the device has merit for further testing, the device should be evaluated for the applicable bed materials in which the device can be confidently used.

In the third test series, a simulated scuba mouse was placed on a vertically supported driven rod. The device is a weighted ring that is free to fall along a guide rod. Conceptually, the ring will remain adjacent to the bed surface as the material erodes near the pier. Figure 5 illustrates the device in the scour hole after the 4.0-ft/sec test run. During the test series, it was observed that the device, as fabricated, tended to bind on the rod because of fine sands. Submergence of the device could bind the ring in place. It is speculated that with the appropriate design, that is, segmenting the ring or leaving adequate clearance between ring and rod, the device has merit for near-prototype testing.

A vertically supported falling rod was installed through the pier footing, as shown in Figure 6, and tested for the three flow conditions. The base of the rod was situated adjacent to the bed directly below the footing. In the initial test flow condition, the scour-hole depth did not extend below the base of the footing, thereby the device did not function. During the second flow condition, the scour hole extended beneath the footing. However, the rod was bound in the footing because of sands and fines that were sucked into the guide channel of the footer. In the third test run, the rod vibrated loose but again became jammed short of the actual scour-hole depth. The use of a vertically supported falling rod installed through the pier footing is not recommended for further testing. The rod tends to bind in the footing channel, it does not measure the maximum depth of scour, and it is considered difficult to retrofit.

A vertically supported driven rod was installed through the pier footing, similarly to the fourth test series. The test was performed to determine the influence of the rod on the maximum depth of scour. The rod did not increase the maximum depth of scour. The device is difficult to maintain and does not measure the maximum depth of scour. The driven rod through the footer is not recommended for further testing.

The sixth test series incorporated the same vertically supported falling device used in the second test series except that a base plate was installed at the bottom of the rod. The base plate diameter was three times the rod diameter. Contrary to the second test series, the rod no longer vibrated into the bed. In fact, the base plate stabilized the bed material under

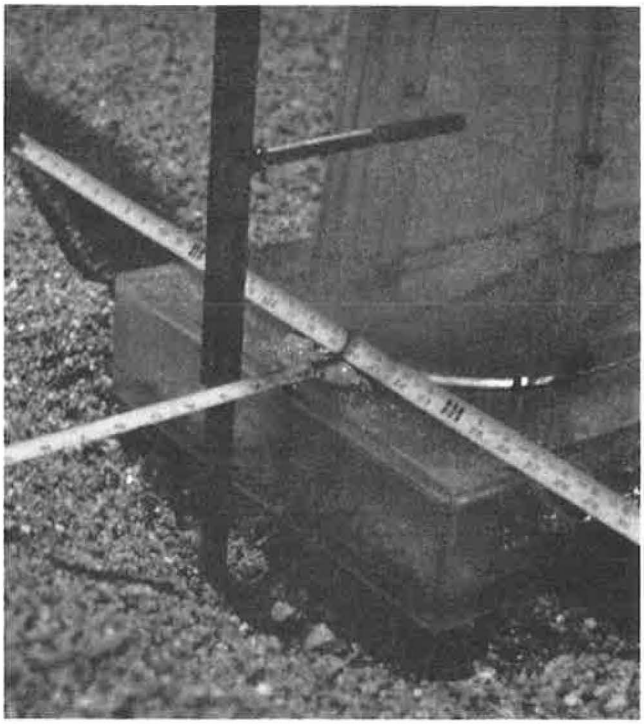

FIGURE 4 Vertically supported falling rod after testing.

the plate, which resulted in slightly shallower scour holes than the point gauge. However, the modified rod showed promise for use in alluvial bed materials because the weight of the rod is spread over a larger area. It is recommended that the vertically supported falling rod with enlarged base plate be tested further.

The bed material, median grain size of 2.3 mm, was placed into the flume. The seventh test series was then conducted in which the vertically supported falling rod with base plate was tested under similar conditions to Test Series 6. The device measured the maximum depth of scour within 0.07 ft of the observed depth, which is the most accurate of all the pier monitoring devices tested. The results are similar to those

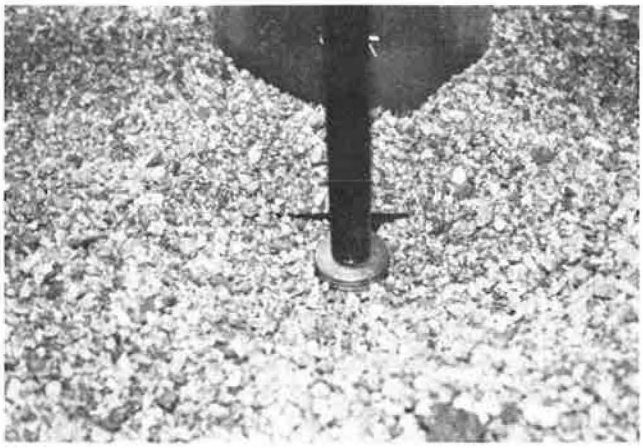

FIGURE 5 Scuba mouse in scour hole after testing.

FIGURE 6 Vertically supported falling rod installed through pier footing.

recorded in Test Series 6. The device is recommended for further evaluation.

Test Series 8 served as a base run (no device) for the 2.3-mm bed material. The maximum scour depths are presented in Table 1.

The scuba mouse device used in Test Series 3 was again tested in Test Series 9. The ring was modified by increasing the clearance between the ring and the driven rod. The scuba mouse device performed very well—it did not bind on the rod. The large surface area of the ring prevented the device from being driven into the bed. The scuba mouse is recommended for further testing at the near-prototype scale.

The 10th test series evaluated the concept of using a falling rod with base plate installed at an angle. The device was placed at a 45-degree angle from the horizontal with the rod aligned parallel with the pier center line. The rod with base plate fell upstream of the pier into the direction of flow as shown in Figure 7. Although the device functioned well during the testing program (similar to the vertically supported falling rod with base plate), the rod base slides away from the location of the maximum depth of scour. The device is not recommended for further testing if configured as presented.

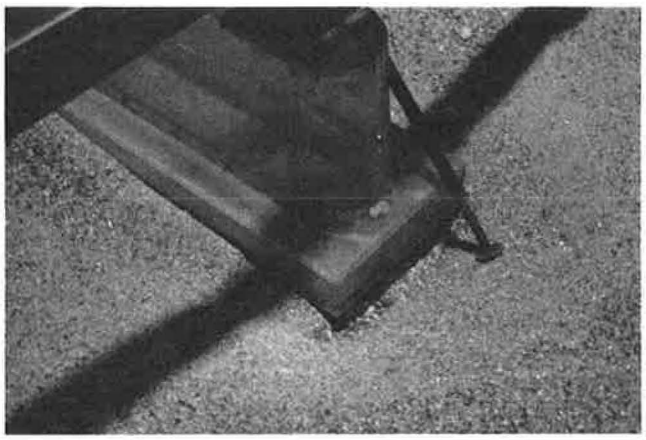

FIGURE 7 Sounding rod with base plate installed at 45 degrees from horizontal.

In addition to the results pertaining to the practicality of the proposed scour-monitoring devices, the investigators were concerned about how the presence of a device affects the maximum depth of scour. A comparison of the maximum scour depths versus the Froude number ($V/\sqrt{gd}$) is presented in Figure 8 for Test Series 1 through 6 (4.0-mm bed material). It is observed in Figure 8 that the maximum depth of scour is similar for all test conditions. Apparently, the presence of the monitoring device does not significantly or consistently affect the maximum depth of scour. As the ratio of the rod diameter to pier width decreases, the effect of the device on enhancing scour will diminish.

Accuracy of Sonar Devices

The sonar device test program evaluated the accuracy of two sonar devices (8- and 20-degree transmission angles). The test parameters included the transducer mounting angle, the distance that the transducer is installed upstream of the pier, and the submergence depth of the transducer. A summary of the differences between sonar and point gauge measurements is given in Tables 2 and 3. The test series A, B, C, D, E, and F represent transducer mounting angles of 0, 5, 10, 15, 20 and 25 degrees, respectively. The entire test program was conducted with the sump water temperature ranging from 50°F to 54°F. The sump water was tranquil.

The sonar devices were evaluated for accuracy as a function of the transducer submergence. The transducers were submerged from 0.0 to 2.5 ft beneath the water surface and were tested directly above the simulated scour hole. The results indicate that the degree of submergence, or distance between transducer and scour hole, directly influences the accuracy of the device in shallow waters. It is observed in Table 2 that as the distance from scour hole to transducer (8-degree device) extended from 3.5 to 6.5 ft, the difference between sonar device and point gauge measurements increased as much as 28 to 152 percent. The average measurement differences appear to become a constant as the water depth exceeds 6.5 ft. Therefore, for a fixed or relatively fixed transducer mounting

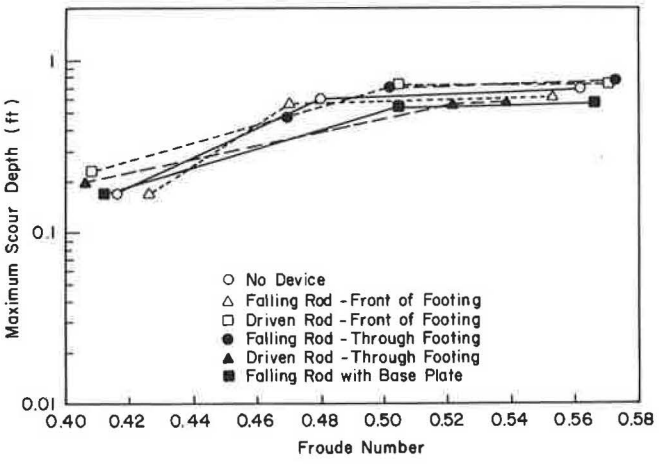

FIGURE 8 Maximum scour depth versus Froude number for Tests 1–6.

TABLE 2 DATA SUMMARY OF SONAR TEST INDEPENDENT OF DISTANCE FROM PIER (8-DEGREE TRANSDUCER)

Test Series Number	Average Differential (ft)	Maximum Differential (ft)	Station
A			
1	0.63	2.20	0.50
2	0.33	0.60	1.00
3	0.32	0.60	1.00
4	0.32	0.75	2.50
5	0.27	0.60	1.00
6	0.25	0.50	0.50
B			
1	0.88	2.70	0.00
2	0.83	2.70	0.00
3	0.53	1.00	0.00,0.50
4	0.46	1.00	0.50
5	0.42	0.90	0.50
6	0.42	0.90	0.50
C			
1	0.84	1.90	0.00
2	0.93	2.00	0.00
3	0.85	2.10	0.00
4	0.66	2.10	0.00
5	0.54	0.95	4.00
6	0.42	0.95	4.00
D			
1	1.12	2.40	0.00
2	1.14	2.00	0.00
3	0.95	2.00	0.00
4	0.97	2.10	0.00
5	0.92	1.80	0.00
6	0.87	1.90	0.00
E			
1	1.18	2.50	0.00
2	1.16	2.50	0.00
3	1.13	2.20	0.00,0.50
4	1.01	2.10	0.00
5	0.99	2.00	0.00,0.50
6	0.96	1.90	0.00
F			
1	1.35	2.70	0.00
2	1.38	2.80	0.00
3	1.25	2.60	0.00
4	1.26	2.50	0.00
5	1.16	2.40	0.00
6	1.05	2.30	0.00

TABLE 3 DATA SUMMARY OF SONAR TEST, INDEPENDENT OF DISTANCE FROM PIER (20-DEGREE TRANSDUCER)

Test Series Number	Average Differential (ft)	Maximum Differential (ft)	Station
A			
1	0.83	2.05	0.00
B			
1	0.71	1.85	0.00
C			
1	0.70	1.85	0.00

location in water 6.5 ft deep or greater, the submergence has little effect on the accuracy of a high-quality sonar device.

An analysis was conducted to determine the pier influence on the accuracy of the sonar device. The sonar transducer was tested as a function of the distance from the pier. The stationing in Tables 2 and 3 refers to the distance, in feet, the transducer was placed upstream of the pier centerline. The accuracy of the sonar device is determined as the difference between sonar and point gauge measurements. The smaller the difference in measurements, the greater the accuracy. The data indicate that the maximum difference, or error, occurs when the transducer is mounted within 1 ft of the pier. Apparently, both the 8- and 20-degree transducers signal reflects from the pier thereby interfering with the instruments ability to measure accurately the depth of the scour hole. The average difference in sonar and point gauge measurements decreases as the distance between pier and transducer increases. The measurement differences become constant at approximately 1.5 ft from the pier. On the basis of the laboratory test results presented, it is recommended that the sonar transducer not be placed within 1.5 ft of the pier.

The data were analyzed to determine the effect of the transducer mounting angle on the accuracy of the sonar device. The data indicate that when the transducer is located 1.5 ft from the pier, the average difference between sonar and point gauge measurements increases as the mounting angle increases. For example, it is observed in Figure 9 that the average difference in measurements, for a transducer located 1.5 ft in front of the pier, extends from 0.22 to 0.84 for mounting angles of 0 to 25 degrees, respectively. The data indicate that the minimum difference in sonar and point gauge measurements occur at mounting angles of 0 and 5 degrees. As the mounting angle increases, the measurement difference increases. Apparently, the transducer is detecting and measuring slope distances not necessarily related to the deepest portion of the scour hole.

The results of the mounting angle analysis indicated that transducer mounting angles of 0 and 5 degrees provide the highest level of resolution and accuracy of the sonar device. It is recommended that an angle slightly greater than 0 degrees be used to ensure that the face of the transducer does not entrap air. Although mounting angles greater than 5 degrees may be used, slope distance adjustments to the measurements must be made.

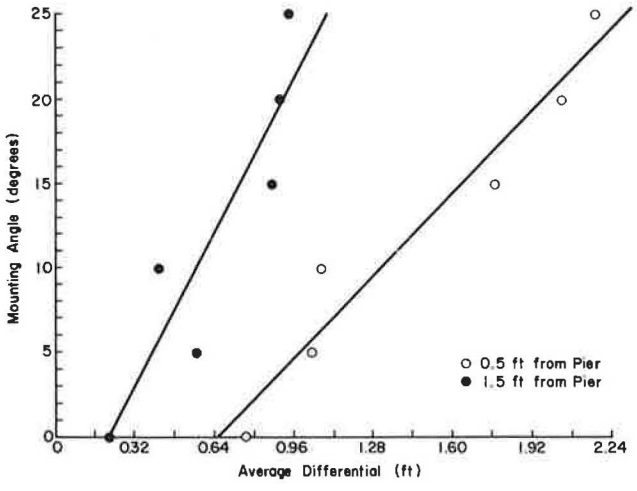

FIGURE 9 Representative comparison of measurement differences versus mounting angle.

A limited comparison was conducted between the 8- and 20-degree sonar instruments. Both devices were tested at 0-, 5-, and 10-degree transducer mounting angles with the transducer located immediately in front of the pier. The accuracy of the devices was similar. Insufficient data were collected to provide a meaningful conclusion.

Temperature Effects on Sonar

The effects of water temperature on the 8-degree sonar transducer device were evaluated. The sonar device was mounted in the VA tube. The water temperatures used to test the sonar device ranged from 42°F to 96°F, as summarized in Table 4. Each sonar device measurement was recorded and compared with the point gauge measured depth for four transducer submergences at each temperature. The difference between each sonar and point gauge measurements as well as the average difference for each water temperature tested are presented in Table 4. It is observed that the accuracy of the device decreased as the temperature of the water decreased. In fact, the depth difference increased by an order of magnitude (0.05 to 0.525 ft) over the 54°F drop in water temperature. Figure 10 presents an indication of the difference in sonar and point gauge measurements as a function of the change in water temperature.

The test results indicate that the sonar device selected for field implementation must be equipped to compensate for temperature stratification in the channel as well as seasonal temperature variations. Therefore, a high-quality instrument is recommended that can adequately compensate for temperature variations.

SUMMARY AND FINDINGS

In an attempt to evaluate the effectiveness and practicability of several scour hole monitoring concepts and instruments, a laboratory testing program was conducted using several model and near-prototype devices. A series of flume tests was conducted in which driven and falling rod model devices were tested and evaluated. Also, sonar measurement devices were tested in a sump and VA tube to determine the potential effects of water temperature and a transducer's transmission angle, mounting angle, submergence depth, and mounting distance from the pier on the accuracy and reliability of the device.

The results of the Phase I flume tests indicate that the vertically supported falling rod has merit for further laboratory and field testing. The blunt-ended rod tended to drive itself into the alluvium because of the vibration from the current. However, when a base plate three times the rod diameter was placed upon the end of the rod, the device appeared to function well in the alluvial bed material.

A scuba mouse was installed on a vertically supported driven rod. The results indicated that if sufficient clearance is pro-

TABLE 4 TEMPERATURE DATA SUMMARY OF SONAR TESTING

Test	Temp. (deg F)	Actual Depth (ft)	Finder Depth (ft)	Change in Depth (ft)	Avg. change in depth (ft)
1	96.0	6.25	6.30	0.05	
		5.75	5.70	0.05	0.050
		5.25	5.20	0.05	
		4.75	4.80	0.05	
2	86.0	6.25	6.30	0.05	
		5.75	5.80	0.05	0.075
		5.25	5.30	0.05	
		4.75	4.90	0.15	
3	78.0	6.25	6.40	0.15	
		5.75	6.10	0.35	0.225
		5.25	5.40	0.15	
		4.75	5.00	0.25	
4	65.0	6.25	6.60	0.35	
		5.75	6.20	0.45	0.425
		5.25	5.70	0.45	
		4.75	5.20	0.45	
5	54.0	6.25	6.60	0.35	
		5.75	6.20	0.45	0.325
		5.25	5.50	0.25	
		4.75	5.00	0.25	
6	42.0	6.25	6.80	0.55	
		5.75	6.20	0.45	0.525
		5.25	5.80	0.55	
		4.75	5.30	0.55	

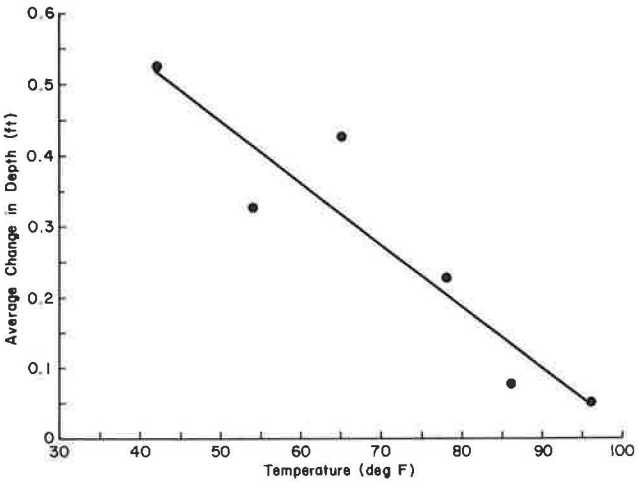

FIGURE 10 Average difference in sonar and point gauge measurements versus water temperature.

vided between the ring and the rod, the device has merit for further laboratory and field testing.

Two concepts were tested with limited success. The vertically supported falling rod was placed immediately upstream of the pier through the footing. The presence of the device did not influence the dimensions of scour. However, the rod did not fall freely because of the bed material binding the device. An angle-supported falling rod was also installed and tested. Because of the rod angle, the device monitored a location upstream of the deepest portion of the scour hole. The measured depth did not correlate well to the maximum depth of scour.

Sonar devices were tested in a laboratory sump and VA tube to determine the applicability of the sonar device for reliable field use. The results indicate that the sonar device should be laboratory- and field-tested further. It was observed that the instrument is sensitive to water temperature, to transducer mounting angle, and to transducer placement location in front of the pier. The instrument is insensitive to the depth of transducer submergence.

Probabilistic Approach to Local Bridge Pier Scour

DONALD E. BARBÉ, JAMES F. CRUISE, AND VIJAY P. SINGH

A method is presented for evaluating the risk of failure of bridge structures due to pier scour during flood events. The method takes into account the hydrodynamics of the flow field in the vicinity of the pier. A newly developed entropy-based velocity distribution is used to define the effective depth of the scour-producing activity in the vortex near the pier. This velocity distribution is integrated to obtain an upper bound on the energy in the vortex, which is then used to estimate the local pier scour. The scour-estimation procedure is used with a flood probability distribution to assign an exceedance probability to estimated scour values. This scour probability distribution can be used along with information about the pier parameters to assign a risk of failure corresponding to any discharge value. The procedure allows for the development of a system of risk assessment priorities to aid in scheduling bridge monitoring and repair.

The undermining of bridge piers by scour resulting from relatively infrequent flood flows has come to be recognized as a major threat to highway safety. In fact, FHWA has urged state highway departments to evaluate the scour potential of their primary bridges. As a part of this procedure, priorities are being set for inspection of sites that demonstrate the most serious potential scour problems. In this paper, a probabilistic method of evaluating bridge sites for possible scour problems is derived and demonstrated using recorded scour data. Using this approach, priority setting for bridge inventories can be based on risk assessments that will identify bridges with a high risk of scour potential.

Research on scour at bridge piers has been proceeding in the United States and elsewhere for more than 50 years. The mechanics by which scour occurs at bridge piers is fairly well understood. However, past research has concentrated on the development of relationships between observed scour (usually in flume experiments) and flow, sediment, and pier variables by regression analyses. Studies of this type abound (*1–4*). This research in general has been summarized by Melville (*5*).

Another technique of scour analysis would be to model the complex hydrodynamic flow system near a bridge pier. Attempts to do so are under way, but successful results have not yet been reported. The technique developed in this study is a combination of the classic regression method and the model approach. It is known that pier scour results from a complex flow pattern in the vicinity of the pier known as the horseshoe vortex. However, in past regression studies, little attention has been given to the dynamics of this system as approach flow conditions are usually employed. In this study, hydraulic variables are selected after consideration is given to the importance of the horseshoe vortex in scour development.

In this approach, the energy in the part of the flow that is physically causing the scour is determined. A probabilistic approach is used to estimate the velocity profile in the scour-producing flow field. This profile is integrated to determine the energy in the flow region, and this energy is used to estimate the resulting scour depth.

The purpose of this project is to produce a methodology for a stochastic risk analysis of scour. The goal is to assign a probability of pier scour corresponding to any river stage observed at a bridge structure. This probability value is then used in conjunction with a flood frequency distribution (probability of the occurrence of different stages) to assign an ultimate risk of bridge pier scour with corresponding confidence limits.

HYDRAULIC CONSIDERATIONS

The hydrodynamic picture of the flow system around bridge piers is very complex. The flow around a single pier is shown schematically in Figure 1. The obstruction of the pier in the flow field causes water to back up on the upstream side of the pier. This small surge is called the bow wave. The pressure differential between the bow wave and the shallower downstream flow causes a strong vertical component in the velocity vector to develop upstream.

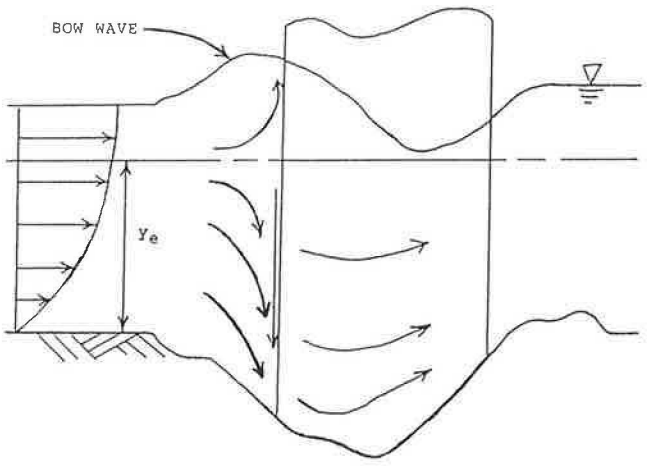

FIGURE 1 Hydrodynamics of flow in vortex.

D. E. Barbé, Department of Civil Engineering, University of New Orleans, Lakefront, New Orleans, La. 70148. J. F. Cruise, V. P. Singh, Department of Civil Engineering, Louisiana State University, Baton Rouge, La. 70803.

Concurrently, an acceleration of the average velocity is caused by the pier constriction and a momentum transfer between the water and the pier surface and channel boundary. The momentum transfer with the pier surface also contributes to the development of the vertical velocity profile. Of course, there is also an energy loss due to friction and boundary drag.

Studies (*6*) have shown that the vertical velocity profile does not extend all the way to the surface but begins at some point below. The region of strong turbulence and vertical velocities around the pier is called the horseshoe vortex. The activity within the horseshoe vortex is the immediate cause of the local scour around the pier.

In this study, a different approach is taken to relate the activity in the vortex to the pier scour. First, a very careful and accurate horizontal velocity profile is derived for the region in the vicinity of the pier, particularly with respect to near bed velocities. Next, the development of vertical velocities is used as an indicator of the energy in the vortex. This zone will define the effective depth of the vortex. The energy in this region is then found by integrating the velocity distribution, and the scour is determined from the energy of the vortex.

The ultimate goal of this analysis is to determine the risk of bridge failure due to pier scour during flood events. To do this, the following steps are necessary: (a) develop a flood probability model; (b) develop an accurate velocity profile in the vicinity of the pier; (c) determine the effective depth of the vortex; (d) determine the energy contained within this depth; (e) determine the relationship between this energy and the local maximum scour; and (f) verify and calibrate field data.

FLOOD PROBABILITY DISTRIBUTION

Work on the development of flood frequency procedures has recently been focused in the area of regional frequency estimation. One of the most popular of these procedures is the index flood method developed by Dalrymple (*7*). In this procedure, an assumed probability distribution is fitted to the observed flood records at each location within a homogeneous region. One standardizes the statistics of the at-site distributions by dividing by the local mean in each case. Regional estimates of the statistics are obtained by averaging the standardized local statistics. The regional distributional parameters are obtained by relating the regional standardized statistics to the distributional parameters. These regional parameters are then used to generate flood magnitudes for the site of interest and are subsequently readjusted to account for differences in scale between watersheds.

This procedure has been developed using the Extreme Value Type 1 (EV1) as the base distribution by Greis and Wood (*8*); it has also been successfully used with the Generalized Extreme Value (GEV) base distribution by Naghavi et al. (*9*). In a study of currently used regional frequency techniques, Potter and Lettenmair (*10*) found the GEV-based procedure to be superior in terms of predictive robustness to any other method tested.

The index method was extended to ungauged watersheds by Naghavi et al. (*9*), who developed relationships between the mean flood in each homogeneous region and the geophysical watershed characteristics within the region. When this technique is used, discharges corresponding to any desired exceedance probability can be estimated for any site at which scour estimates are needed.

DEVELOPMENT OF HORIZONTAL VELOCITY PROFILE

A horizontal velocity profile has been developed by Barbé et al. (*11*), who extended a method previously proposed by Chiu (*12–14*). This method is based on the principle of maximum entropy (*15,16*). Entropy can be used as a measure of the information content imbued in a system.

The Shannon entropy functional (SEF) was the first mathematical representation of entropy for use in information theory (*17,18*). Consider a probability density function $f(x)$ for a continuous random variable x. Then

$$\int_0^\infty f(x)\,dx = 1 \tag{1}$$

and $f(x)$ is positive for all values of x.

SEF is defined as

$$I(f) = -\int_0^\infty f(x)\,\ln[f(x)]\,dx \tag{2}$$

$I(f)$ may be thought of as the expected value or mean of $-\ln[f(x)]$.

The entropy can be maximized by minimizing the a priori assumptions about the system subject to broad physical constraints. For bridge pier scour, the constraints are the laws of conservation of mass, momentum, and energy that must be satisfied by any physical system.

From boundary shear considerations, the classical method of describing the velocity profile is by relating it to the depth. In open channel flow with depth D, the velocity monotonically increases from zero at the bed, because of maximum boundary shear at the bed, to a maximum value at the surface, because of minimum boundary shear when the water-air interface is neglected. Let u be the velocity at a distance y above the channel bed. Then, the probability of the velocity being less than or equal to u is y/D; the cumulative distribution function is

$$F(u) = \frac{y}{D} \tag{3}$$

and the probability density function is

$$f(u) = \frac{1}{D}\frac{dy}{du} \tag{4}$$

By writing the physical constraints in their most general integral form, Barbé (*19*) was able to derive and estimate the solution for velocity profiles corresponding to all of the constraints listed above as well as any combination of them. Let u_D be the maximum velocity that occurs at the surface, and

the constraints used by Barbé et al. (*11*) become

Constraint 1 (from conservation of mass):

$$\int_0^{u_D} uf(u)\,du = u_m \tag{5}$$

where u_m is the mean velocity (depth averaged).

Constraint 2 (from conservation of momentum):

$$\int_0^{u_D} u^2 f(u)\,du = \frac{M}{\rho D} \tag{6}$$

where

M = momentum flux per unit width of channel,
ρ = mass density of water, and
D = depth of flow in the channel.

Constraint 3 (from conservation of energy):

$$\int_0^{u_D} u^3 f(u)\,du = (E - D)\,2gu_m \tag{7}$$

where E is the energy flux per unit width of channel and g is the acceleration due to gravity.

Applying the principle of maximum entropy, the probability density function derived is given as

$$f(u) = \exp\{L_1 - 1 + L_2u + L_3u^2 + L_4u^3\} \tag{8}$$

where L_1, L_2, L_3, and L_4 are parameters of the distribution.

Equation 8 represents the entropy-derived velocity distribution based on the conservation of mass, momentum, and energy. In the vicinity of boundaries, such as channel beds or pier surfaces, it may be difficult to account for energy losses accurately. For this reason, the energy conservation constraint is removed by setting L_4 equal to zero. Then the velocity profiles are obtained by substituting Equation 8 (with $L_4 = 0$) into Equation 4 and obtaining approximate solutions to the resulting integral equations (*11*). The derived profiles were compared to other standard velocity profiles as well as to observed data published by Davoren (*6*) (Figures 2 through 4). These data represent the only currently available observations of velocity and scour measurements taken concurrently in the field during high discharge events. The new three-parameter entropy method using constraints of continuity and momentum results in an excellent description of the entire velocity profile. In particular, note the accurate fit near the channel bed, which validates the selection of constraints. This method was used in this study to obtain the energy in the horseshoe vortex.

The velocity profile used is given by

$$\exp(A)\left\{\exp(L_2u) + L_3\left[\exp(L_2u)\left(u^2 - \frac{2u}{L_2} + \frac{2}{L_2^2}\right)\right]\right\} = \frac{y}{D} + \exp(A)\left\{\frac{1}{L_2} + \frac{2L_3}{L_2^3}\right\} \tag{9}$$

Equation 9 represents a three-parameter velocity profile whose parameters (A,L_2, and L_3) are determined through an approximation technique using only observed mean and maximum (surface) velocities (*11*). In other words, using the principle of maximum entropy, the information content from the conservation of momentum can be added without increasing the number of parameters. The needed parameters remain the obtainable mean and maximum (surface) velocities.

To summarize: the concept of entropy was used to derive a velocity profile subject to the physical laws of conservation of mass and momentum. Thus, no assumptions are necessary

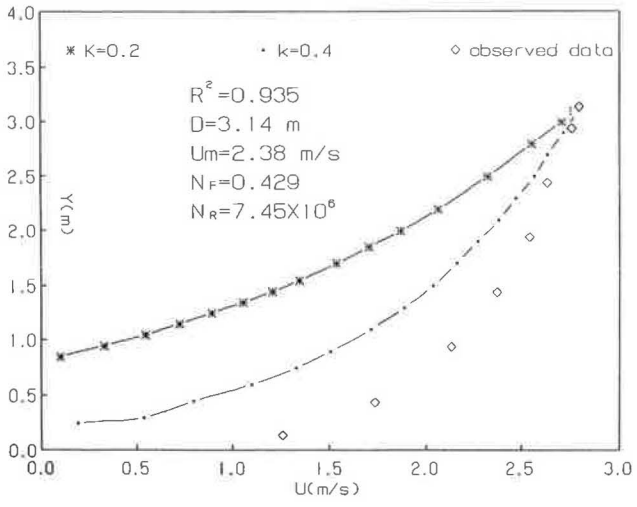

FIGURE 2 Prantl–Von Karman velocity distribution.

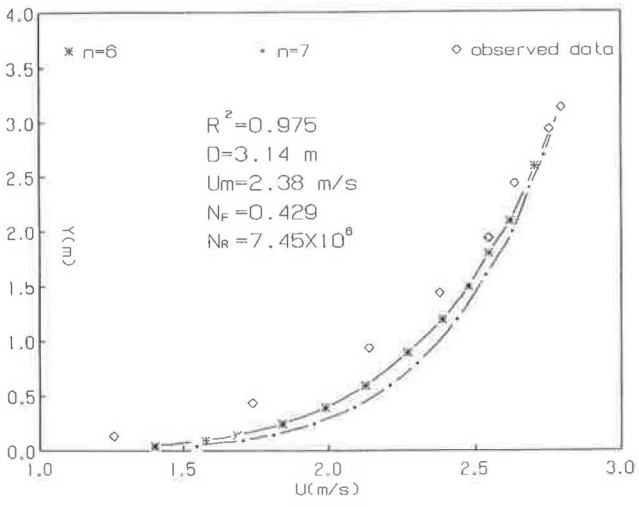

FIGURE 3 Power law velocity distribution.

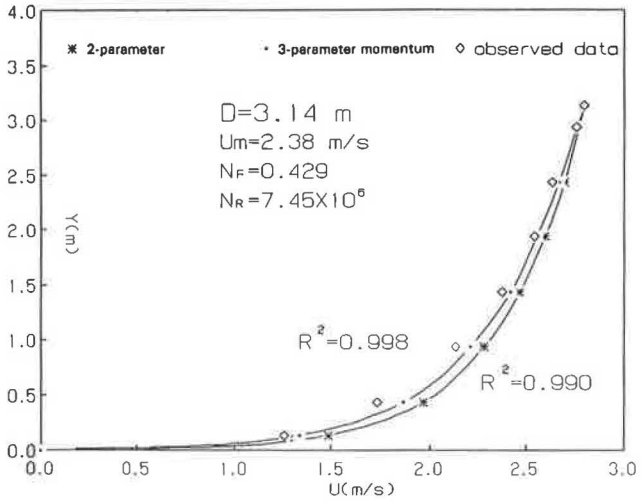

FIGURE 4 Entropy-based velocity distribution.

in deriving this profile. In the event that constraints can be determined representing the conservation of momentum or energy at the pier, then velocity profiles at the pier can be directly determined by this method. In addition, Figures 2 through 4 show that the entropy method resulted in superior fits to observed data, particularly near the bed.

DETERMINATION OF EFFECTIVE DEPTH OF HORSESHOE VORTEX

The effective depth is defined as that part of the approach flow that is deflected downward—that is, the part of the flow that is effective in causing scour (see Figure 1). Barbé (*19*) defined the upper limit of the effective depth as the point at which the vertical velocity component amounted to 3 percent of the horizontal component. However, this definition was based on observations of vertical velocities contained in Davoren's data (*6*).

Alternatively, the point at which vertical velocities become significant can be determined as the point at which the horizontal velocity components diverge significantly from those projected from the entropy distribution if no pier were present. This distribution has been derived by Chiu (*12*) and is currently available. A comprehensive study of the vertical dimensions of the horseshoe vortex was reported by Kothyari et al. (*20*). On the basis of data reported by many previous investigators, a relationship was developed between the effective depth of the vortex and approach flow depth and pier diameter. Their results are published (*21*) in both mathematical and graphical forms and provide a basis for determining the effective depth when observed data are not available.

In this case, based on Davoren's (*6*) observations, Barbé (*19*) developed relationships between the effective depth and the total approach flow depth. The resulting equations produced for the effective depth were

$$y_e = D - 0.6945D^2 + 0.2633D^3 \qquad (0 \le D \le 0.7\,\text{m}) \qquad (10)$$

and

$$y_e = 0.45 + 0.4147(D - 0.7) - 0.1416(D - 0.7)^2 + 0.0193(D - 0.7)^3 \qquad (0.7\,\text{m} \le D \le 3.14\,\text{m}) \qquad (11)$$

where y_e = the effective depth of horizontal flow (in meters) and D = the total approach flow depth (in meters). When compared with the results of Kothyari et al. (*20*), these values appeared to fall in the range of effective depths predicted by their equations.

DETERMINATION OF SCOUR RELATION

Many conventional scour formulas relate conditions in the upstream approach flow to the scour at the bridge pier. The energy in the approach flow field has been shown to be well related to field scour observations (*22*). However, most of these studies used the total depth and velocity head in the upstream section. This formulation neglects energy losses and momentum transfers within the effective depth region in the vicinity of the pier. These losses, as well as the energy lost in the formation of the bow wave, do not translate into the production of scour. A better relation could be expected to exist if only the energy within the effective depth of the vortex were used. This approach was taken in this study: the effective depth was defined as described previously, and the kinetic energy of the vortex turbulence field was derived by integrating the velocity distribution derived from maximum entropy concepts. This energy was then added to the potential energy in the vortex (the effective depth) to obtain an expression of the form

$$d_s = K_1 Y_e + K_2 \frac{\left(\int_0^{y_e} u^3\,dy\right)}{\left(2g\int_0^{y_e} u\,dy\right)} \qquad (12)$$

where

d_s = maximum scour depth,
K_1, K_2 = empirical coefficients,
Y_e = effective depth of downward vertical velocity formation, and
u = velocity in vortex obtained from entropy expression.

Equation 12 is cast in a form commonly encountered among scour formulas. The energy in the effective depth represents an upper bound on energy available to produce scour. The major differences between Equation 12 and conventional energy-based equations are that only the energy within the effective depth is used and the velocity head is based on a velocity profile method that requires no a priori assumptions. The profile can be obtained from observations of only mean and surface velocities and has been shown to be particularly accurate near the channel bed. Also, because the velocity head is based on conservation of mass and momentum, no inconsistencies are introduced into the analysis by neglecting

energy losses in the derivation of the velocity profile. The momentum transfers are accounted for in the effective depth term and the coefficients. The coefficients K_1 and K_2 represent energy loss coefficients due to boundary drag and momentum transfers as horizontal velocities are converted to vertical velocities. The coefficients and the effective depth will be functions of hydraulic and sediment characteristics and bridge geometry. In this way, parameters such as pier width and sediment size will enter the analysis. It is anticipated that flume studies can be used to determine values for these coefficients corresponding to various scenarios. Once the equation has been calibrated to these scenarios, it should function as an effective general scour formula. Equation 12 represents a consistent attempt to relate actual scour-producing energy in the vortex to the resultant scour, based on a minimum of assumptions.

EVALUATION OF NEW SCOUR-ESTIMATION METHOD

A field study of bridge pier scour was performed by Davoren (*6*), who measured vertical and horizontal velocities at the pier as well as real-time scour. The study site consisted of a single 1.5-m-diameter hollow steel cylindrical pier established in the Ohau River downstream of a hydroelectric power station. The study reach had bed sediment with D_{50} = 20 mm and a standard deviation of σ_g = 5.3. Observations were conducted during sustained periods of steady releases from the plant. These conditions represent clear water scour observations.

For demonstration purposes, Equation 12 was evaluated using Davoren's data base (*6*). The constants K_1 and K_2 in the scour equation were determined by a two-parameter least-squares method to fit the data. The coefficients computed were K_1 = 1.793 and K_2 = −2.514; therefore, the new scour equation for Davoren's site is

$$d_s = 1.793\,Y_e - 2.514\frac{\left(\int_0^{ye} u^3\,dy\right)}{\left(2g\int_0^{ye} u\,dy\right)} \qquad r^2 = .924 \qquad (13)$$

These predicted values were compared with Davoren's published observed scour data (*6*). The results are given in Table 1. Runs 1, 3, and 4 were used to calibrate the coefficients K_1 and K_2, and the scour corresponding to Runs 2, 5, and 6 was computed. The table shows that the predicted values compare very well with the observations.

SCOUR RISK ANALYSIS

In applying the procedure, a flood probability distribution is obtained either from observed data or using a regional approach as described previously. A water surface profile method can be used to estimate mean and maximum velocities for any flood magnitude of interest. The entropy method is then used to obtain the velocity profiles. The velocity distribution and the estimated effective depth values are used to obtain the maximum scour-producing energy within the effective depth region. This energy is used to estimate scour depth corresponding to each flood magnitude.

TABLE 1 COMPUTED VERSUS OBSERVED SCOUR

Run	Computed Scour (m)	Observed Scour (m)
1	1.16	1.28
2	1.28	1.20
3	1.01	0.88
4	0.57	0.72
5	0.61	0.59
6	0.25	0.26

EXAMPLE APPLICATION

For example, Davoren (*6*) placed probability estimates on the discharges corresponding to his Runs 1 through 6 using a Gumbel (EV1) distribution based on 55 years of record. These values and the estimated scour values corresponding to each flood magnitude are given in Table 2.

From this table, the scour estimate corresponding to any exceedance probability up to .01 (the 100-year event) can be interpolated. Using this information in conjunction with data about the pier parameters, this bridge could be ranked relative to other bridges for its scheduled monitoring and maintenance.

TABLE 2 PROBABILISTIC ANALYSIS OF DISCHARGES AND SCOUR

Run	Estimated Scour (m)	Discharge (m^3/s)	Exceedance Probability
1	1.16	480	.0303
2	1.28	600	.01
3	1.01	360	.145
4	.57	280	.364
5	.61	180	.833
6	.26	300	.294

CONCLUSIONS

A procedure is presented to aid in the evaluation of scour potential for existing and proposed bridge structures. For existing bridges, hydraulic variables and pier geometry can be used to determine the effective depth of scour-producing activity and the velocity profile in this region. From this information, the energy available to produce scour can be determined. Energy loss coefficients need to be evaluated from either observed data or the results of flume experiments.

For proposed bridge sections, the anticipated hydraulic variables can be determined from backwater models such as WSPRO, and the effective depth can be obtained from the results of Kothyari et al. (*20,21*). It might also help to place experimental piers at the proposed bridge site to collect data to calibrate the equations and determine loss coefficients. In any case, flume studies should be performed to calibrate the proposed procedure to a variety of pier geometries and sediment characteristics. In this way, the procedures can be made general enough to be applicable to any real-world situation in which either existing or proposed bridges must be evaluated for scour vulnerability.

REFERENCES

1. G. R. Hopkins, R. W. Vance, and B. Kesraie. *Scour Around Bridge Piers*. Report FHWA-RD-79-103. FHWA, U.S. Department of Transportation, Washington, D.C., Feb. 1979.
2. H. W. Shen, V. R. Schneider, and S. Karaki. Local Scour Around Bridge Piers. *Journal of the Hydraulics Division*, ASCE, Vol. 95, No. HY6, Nov. 1969, pp. 1919–1940.
3. S. C. Jain. Maximum Clear Water Scour Around Circular Piers. *Journal of the Hydraulics Division*, ASCE, Vol. 7, No. 10, May 1981, pp. 611–626.
4. A. J. Raudkivi. Functional Trends of Scour at Bridge Piers. *Journal of the Hydraulics Division*, ASCE, Vol. 112, No. 1, 1986, pp. 1–13.
5. B. W. Melville. Live-Bed Scour at Bridge Piers. *Journal of Hydraulic Engineering*, Vol. 110, No. 9, 1984, pp. 1234–1247.
6. A. Davoren. *Local Scour Around a Cylindrical Bridge Pier*. Publication 3. Hydrology Center, National Water and Soil Conservation Authority, Ministry of Works and Development, Christchurch, New Zealand, 1985.
7. T. Dalrymple. Flood Frequency Analysis. *Manual of Hydrology, Part 3*. Water Supply Paper 1543-A. U.S. Geological Survey, 1960.
8. P. Greis and E. Wood. Regional Flood Frequency Estimation and Network Design. *Water Resources Research*, Vol. 17, No. 4, 1981, pp. 1167–1177.
9. B. Naghavi, J. Cruise, and S. Ekanayake. *Prediction of Flood Quantiles at Ungaged Watersheds in Louisiana*. Report FHWA-LA-229. Louisiana Transportation Research Center, Baton Rouge, 1990.
10. K. W. Potter and D. P. Lettenmair. A Comparison of Regional Flood Frequency Estimation Methods Using a Resampling Method. *Water Resources Research*, Vol. 26, No. 3, 1990, pp. 415–424.
11. D. E. Barbé, J. F. Cruise, and V. P. Singh. Solution of the Three-Constraint Entropy-Based Velocity Distribution. *Journal of the Hydraulics Division*, ASCE, Vol. 117, No. 10, Oct. 1991, pp. 1389–1396.
12. C. Chiu. Entropy And Probability Concepts In Hydraulics. *Journal of the Hydraulics Division*, ASCE, Vol. 113, No. 5, May 1987, pp. 583–600.
13. C. Chiu. Entropy and 2-D Velocity Distribution in Open Channels. *Journal of the Hydraulics Division*, ASCE, Vol. 114, No. 7, July 1988, pp. 738–756.
14. C. Chiu. Velocity Distribution of Open Channel Flows. *Journal of the Hydraulics Division*, ASCE, Vol. 115, No. 5, May 1989, pp. 576–594.
15. E. T. Jaynes. Information Theory and Statistical Mechanics, I. *Physical Review*, 106, 1957a, pp. 620–630.
16. E. T. Jaynes. Information Theory and Statistical Mechanics, II. *Physical Review*, 108, 1957b, pp. 171–190.
17. C. E. Shannon. The Mathematical Theory of Communications, I and II. *Bell System Technical Journal*, Vol. 27, 1948a, pp. 379–423.
18. C. E. Shannon. The Mathematical Theory of Communications, III and IV. *Bell System Technical Journal*, Vol. 27, 1948b, pp. 623–656.
19. D. E. Barbé. *Analysis of Bridge Scour Using the Principle of Maximum Entropy*. Ph.D. dissertation. Department of Civil Engineering, Louisiana State University, Baton Rouge, 1990.
20. U. C. Kothyari, R. J. Garde, and K. G. Ranga Raju. *Journal of the Hydraulics Division*, ASCE (in press).
21. U. C. Kothyari, R. J. Garde, and K. G. Ranga Raju. *Journal of Hydraulic Research*, International Association for Hydraulics Research (in press).
22. A. P. Strautmann. *Analysis of Scour Problems at Selected Louisiana Bridge Sites*. Thesis. Louisiana State University, Baton Rouge, May 1987.

Stability of Rock Riprap for Protection at Toe of Abutments at Flood Plain

JORGE E. PAGÁN-ORTIZ

The results of research conducted in a hydraulic flume to determine the stability of rock riprap protecting abutments located on flood plains are presented. The observed vulnerable zone for rock riprap failure is presented for two abutment types: vertical-wall and spill-through (H:V = 2:1). Equations and velocity multipliers to assist an engineer in determining the stable rock riprap size are presented for the two abutment types. Conditions found to influence the stability of rock riprap are also presented.

Bridge abutments commonly contract the free flow of water in the channel and flood plains through the bridge opening during high flows. During high flow events, the abutments are subject to strong erosive currents that are forced to pass through the bridge opening. These currents undermine the stream bed at the toe of the abutments and beyond. This phenomen, known as local scour at the abutments, in turn causes acceleration of flow deflected by the abutments. The development of a vortex system induced by the obstruction is the principal mechanism for the development of local scour. The strength of the vorticity generated by the deflection is related to the depth of flow, abutment depth and shape, alignment of the abutment with respect to the flow, size of bed material, rate of bed material transportation, and ice or drift accumulation.

Laboratory measurements indicate that average point velocities away from the abutment area are not influenced by the abutment's presence. Consequently, scour at abutments is considered a local phenomenum that is not significantly related to the overall geometry of the flow (*1*).

A common method for protecting the stream bed from erosive currents is that of placing a rock riprap apron. To determine the size of rock riprap needed to prevent local scouring at abutments, it is necessary to study the stability of the rock as it is exposed to the erosive currents in the channel and flood plain.

LITERATURE REVIEW

The FHWA procedure for determining the rock riprap size to protect abutments from scouring is presented in the Hydraulic Engineering Circular (HEC) 11, entitled *Design of Riprap Revetment* (*2*). The rock riprap size is determined using the following equation:

$$D_{50} = \frac{0.001 * V_a^3}{d_{avg}^{0.05} * K_1^{1.5}} \quad (1)$$

Federal Highway Administration, Bridge Division, Hydraulics and Geotechnical Branch, 400 Seventh Street, S.W., Washington, D.C. 20590.

where

D_{50} = median rock riprap particle size (ft),
V_a = average velocity in the main channel at the constricted section (ft/sec),
d_{avg} = average flow depth in the main flow channel at the constricted section (ft), and
K_1 = bank angle/rock angle factor defined as

$$K_1 = \left(1 - \frac{\sin^2\theta}{\sin^2\phi}\right)^{0.5} \quad (2)$$

where θ is the bank angle with the horizontal, and ϕ is the rock riprap material's angle of repose.

The rock size (D_{50}) computed from Equation 1 must be multiplied by a correction factor C because when the equation was developed, information on velocities in the vicinity of bridge abutments was not available. The factor C is computed as follows:

$$C = C_{sg} * C_{sf} \quad (3)$$

where

$$C_{sg} = \frac{2.12}{(S_s - 1)^{1.5}} \quad (4)$$

and

$$C_{sf} = \left(\frac{SF}{1.2}\right)^{1.5} \quad (5)$$

where

C_{sg} = correction factor for specific gravities other than 2.65,
C_{sf} = correction factor for stability,
SF = stability factor ranging from 1.6 to 2.0 for turbulent flow at the bridge abutment, and
S_s = specific gravity of the rock riprap.

Many researchers have developed equations based on average velocity that relate the critical conditions affecting stability. Isbash (*3*) presented an equation that can be expressed as

$$N_{sc} = E^2 * 2 \quad (6)$$

where N_{sc} is the sediment number representing the ratio of approach flow inertial energy at critical conditions to the

stabilizing potential created by the submerged rock weight (*4*).

For loose stone lying on top of the fill, N_{sc} is expressed as

$$N_{sc} = \frac{V^2}{g * D_{50} * (SG - 1)} \tag{7}$$

where

V = flow velocity that will remove the loose stones (ft/sec),
D_{50} = characteristic median rock size (ft),
SG = specific gravity of the rock,
g = gravitational acceleration (32.2 ft/sec^2), and
E = 0.86 for loose stone lying on top of the fill.

For stones deposited into flowing water that roll (because of the force of water acting over them) until they find a "seat" and a support, E = 1.2.

Rearranging Equation 7 in terms of D_{50} for E = 1.2, we obtain

$$D_{50} = \frac{0.347 * V^2}{g * (SG - 1)} \tag{8}$$

Equation 8 is a rearranged form of the Isbash equation.

Neill established a relation for "first displacement" of uniform graded gravel based on uniform parameters (*5*). The following expresses a conservative design curve:

$$N_{sc} = 2.50 * \left(\frac{D_g}{d}\right)^{-0.20} \tag{9}$$

where D_g is the characteristic rock size on the approach flow bed (in feet) and d is the depth of the approach flow (in feet).

Neill compared his results with those of Mavis, Ho, and Tu; Schaffernak; Meyer-Peter and Müller; and Linnton Hydraulics Laboratory and found good agreement. Parola conducted experiments using Neill's criteria for first displacement and found good agreement too (*4*).

Pagán (*6*) developed the following regression equation for an average sediment number design curve based on Neill's and Parola's experiments for undisturbed flow:

$$N_{sc} = 2.58 * \left(\frac{D_g}{d}\right)^{-0.27} \tag{10}$$

The average design curve represented by Equation 10 will be compared with an average curve to be developed from a series of parameters that characterize the disturbed flow.

Figure 1 shows the sediment number curve, N_{sc}, based on Neill's and Parola's experiments for undisturbed flow—no obstruction to the free flow of water.

FRAMEWORK OF EXPERIMENTS

The parameters that characterize the disturbed flow are

- V_{cc}—average velocity of the contracted flow at observed incipient motion of the rock at the contraction (ft/sec);
- d_{cc}—average depth of the contracted flow at observed incipient motion of rock at the contraction (ft);
- W_a—width of the approach flow (ft);
- W_{t-c}—width of the contraction (ft);
- D_{50}—characteristic median rock size on the contraction flow bed (ft);
- AS—factor associated with the abutment shape;
- K—roughness of the bed upstream;
- K_s—roughness of the bed surrounding the obstruction;

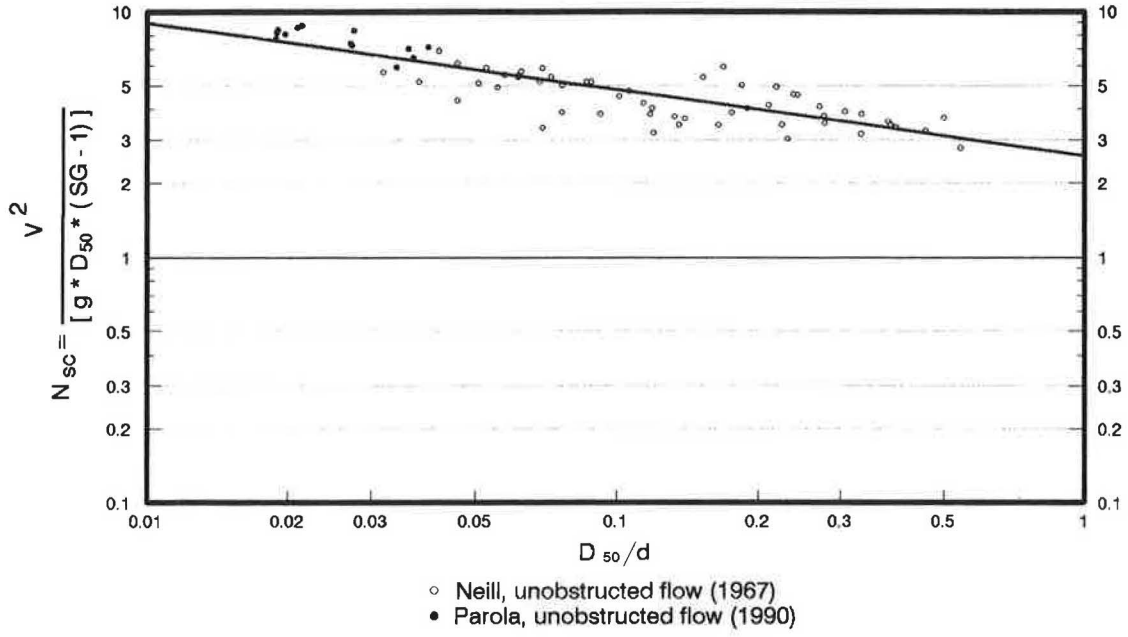

FIGURE 1 Sediment number curve for unobstructed flow.

- g—gravitational acceleration (32.2 ft/sec^2);
- ρ—fluid density (slug/ft^3);
- ρ_s—rock density (slug/ft^3); and
- μ—dynamic viscosity of fluid (slug/ft-sec).

The effect of displacement due to leaching of fines through the armored apron of gravel in the observation area near the toe of the abutment and flood plain was not studied. The size of the bed material (D_{50}) in the obstructed area and the roughness in the vicinity of the obstruction (K_s) are dependent variables. For the purpose of the experiments, K_s was assumed to be adequately represented by D_{50}.

The characteristic parameters can be arranged into a functional equation that describes the critical condition for the initial motion of the rock within the observation area as follows:

$$0 = f(W_a, W_{t-c}, d_{cc}, D_{50}, V_{cc}, AS, K, g, \rho, \rho_s, \mu) \quad (11)$$

The parameter g must appear in combination with ρ and ρ_s as follows:

$$\gamma = g * (\rho_s - \rho) \quad (12)$$

Combining Equations 11 and 12 in a nondimensional form yields

$$N_{sc} = f\left(V_{cc} * \frac{D}{\nu}, \frac{\rho_s}{\rho}, \frac{d_{cc}}{W_{t-c}}, \frac{D_{50}}{d_{cc}}, AS, \frac{W_a}{W_{t-c}}, K\right) \quad (13)$$

where ν equals μ/ρ and D is characteristic rock size (assumed to be adequately represented by D_{50}).

Yalin stated that (ρ_s/ρ) "can be important only with regard to the properties associated with the 'ballistics' of an individual grain. In case of highly turbulent flows needed to cause the initial motion of the rock protection, the influence of the obstruction particle Reynolds' number—effect of viscosity relative to inertia, $V_{cc} * (D/\nu)$—was considered to be negligible because it was greater than 10^3, which is well beyond the range that Shields and other researchers found to be no longer a factor.

Therefore, by applying the preceding considerations and confining the research to subcritical flow, the effect of (ρ_s/ρ) and $[V_{cc} * (D/\nu)]$ can be discounted. Thus, Equation 13 can be reduced as follows:

$$N_{sc} = f\left(\frac{d_{cc}}{W_{t-c}}, \frac{D_{50}}{d_{cc}}, AS, \frac{W_a}{W_{t-c}}, K\right) \quad (14)$$

By using the contracted velocity in N_{sc}, the effect of d_{cc}/W_{t-c}, W_a/W_{t-c}, and K are negligible. Thus, Equation 14 reduces to

$$N_{sc} = f\left(\frac{D_{50}}{d_{cc}}, AS\right) \quad (15)$$

Equation 14 provides the framework used to determine the stability of rock riprap to protect the toe of an abutment at the flood plain. The quantity N_{sc} is defined in Equation 6. The parameter D_{50}/d_{cc} represents the relative roughness of the contracted flow.

Experimental Model

Tow small-scaled abutment models—vertical-wall and spill-through—were used to study the impact of the abutments on time-averaged contraction velocities and the stability of gravel placed around the toe of the abutment and flood plain. The length of the abutment was varied to investigate the effect of the contraction to the flow on the flood plain. For the vertical-wall abutment, the length ranged from 5 to 20 in.; for the spill-through model, the length ranged from 25 to 40 in. The total widths of the vertical-wall and spill-through abutments were 6 and 46 in., respectively. Flow depths ranged from 1.84 to 10.5 in.

Observation Area

An observation area was defined in the hydraulic flume for each abutment model to visualize the failure of gravel for a given flow. These areas are illustrated in Figures 2 and 3.

Gravel Placement

Two sizes of gravel were used in the experiments: D_{50} = 0.30 in. and D_{50} = 0.40 in. The gravel was angular particles that

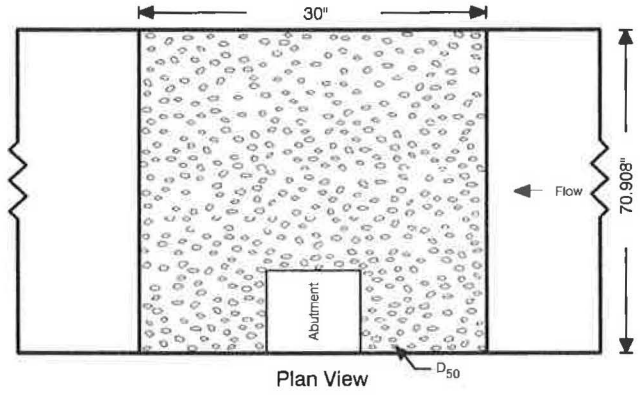

FIGURE 2 Observation area for vertical-wall abutment.

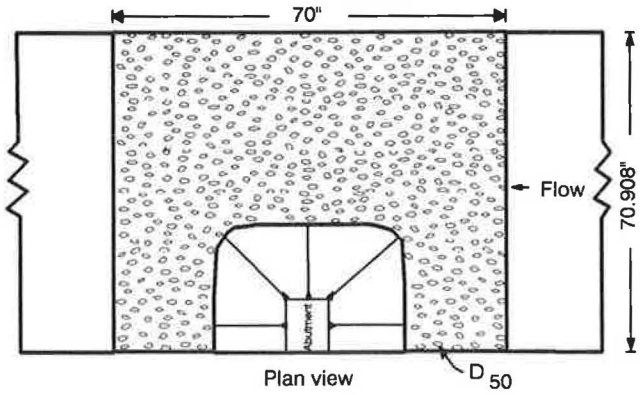

FIGURE 3 Observation area for spill-through abutment.

passed on sieve and were retained on the next standard size so they were intended to be uniform in size. A grain size distribution analysis was run on several samples of the bin of materials used in the experiments. On the basis of these samples, the gravel had a geometric standard deviation of $(D_{84}/D_{16})^{1/2}$ of 1.08 and 1.10 for D_{50} = 0.30 and 0.40 in., respectively.

The gravel was placed in the observation area to a depth of 1.5 in. in three nonuniform layers. The intermediate layer was spray-painted red to help visualize the failure or motion of the upper gravel layer. Figures 4 and 5 illustrate a typical gravel setup for each abutment model. Gradation and layer thickness were not variables in these experiments.

Experimental Procedure

The experimental procedure for each run was as follows:

1. The discharge was set to a constant.
2. The tailgate was raised to develop a velocity past the observation section slightly below the expected incipient velocity of the rock riprap failure.
3. The tailgate was gradually lowered until a discernible patch of surface rock moved in the observation section. This was determined by looking for a visible section of the colored underlying layer of rock.
4. The flow and the tailgate setting were then held constant while a grid of depth and velocity measurements was taken.

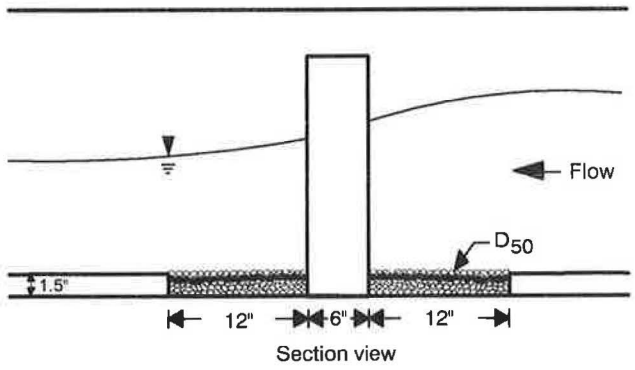

FIGURE 4 Section view of gravel setup for vertical-wall abutment.

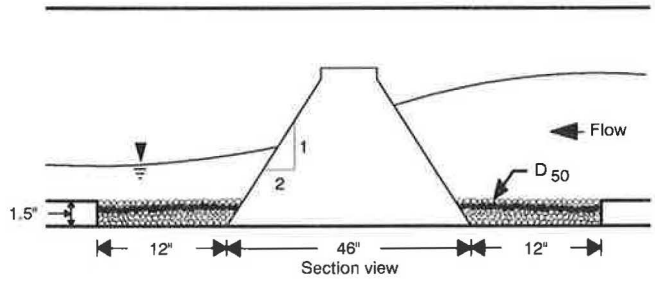

FIGURE 5 Section view of gravel setup for spill-through abutment.

This generally took about 1½ hr. Very few additional particles moved during this data collection period, so it was thought that longer run times would not have changed the results.

Some reviewers implied that longer run times should have been used. The shorter run times were considered appropriate because these were essentially incipient motion experiments rather than depth-of-scour experiments. In hindsight, it would have been useful to run a few experiments at a slightly lower velocity for a long duration (say, 72 hr) to determine whether longer duration tests would have significantly changed the results.

EXPERIMENTAL RESULTS

Independent experiments were conducted with each abutment model to determine the vulnerable zone for the gravel failure within the observation area at different discharges and flow depths. An initial zone of failure thus was identified for each model.

Previous researchers have demonstrated that the scour hole pattern in an unprotected channel and flood plain being obstructed by either a vertical-wall or spill-through abutment normal to the flow occurs at the upstream corner of the abutment (*7*). Pagán (*6*) demonstrated that the failure zone in an armored flood plain surrounding the abutment normal to the flow is a function of the abutment shape.

For the vertical-wall abutment the initial failure zone was consistently observed at the upstream corner of the abutment in the armored flood plain (Figure 6). The zone then expands downstream toward the abutment and away from it with time and increase in discharge.

For the spill-through abutment model, the initial failure zone was consistently observed at the downstream radius of the model just away from its toe (Figure 7). The zone then expands downstream and upstream toward the toe of the abutment and away from it into the flood plain with time and increase in discharge.

Velocity-Based Criteria

Three equally spaced average point velocities were measured within the contraction zone. For the smooth bed experiments

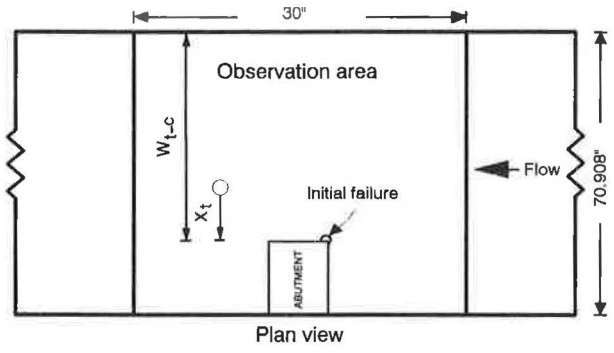

FIGURE 6 Location of initial failure zone for vertical-wall abutment.

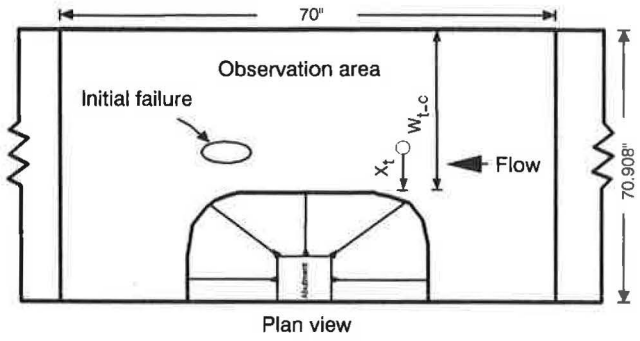

FIGURE 7 Location of initial failure zone for spill-through abutment.

(no gravel placed within the observation area), it was learned that the readings of average point velocities near the face of the abutment parallel to the flow were severely affected by the flow turbulence. Consequently, low velocity readings were measured near the face of the abutment. The same result was obtained in the obstructed flow experiments (gravel placed in the observation area). However, the gravel was failing at the upstream corner of the vertical-wall abutment (Figure 6) and downstream near the toe for the spill-through abutment (Figure 7). Thus, although the flow turbulence affected the velocity readings near the abutment models, that velocity must be much higher that those measured during the experiments to cause the initial motion of the gravel near the toe of the abutment models.

An indirect method to obtain the velocity near the face of the abutment at which the incipient motion of the gravel is observed is to compare the velocity measured with the abutment constricting the free flow, plotting those velocities in terms of the sediment number (N_{sc}), and comparing the plot to that shown in Figure 1.

Vertical-Wall Abutment

The vulnerable zone for incipient motion for this abutment shape was observed at the upstream corner of the abutment (Figure 6). The separation of flow created by the contraction of the abutment shape caused a strong turbulence, particularly for deeper flows. With the flow depth and velocity at the approach and for a computed discharge at the approach representing the design discharge, the velocity and flow depth were computed at the contraction of the abutment in the flood plain using Bernoulli's energy equation without elevation terms and the continuity equation. The energy equation is as follows:

$$\frac{V_{am}^2}{2 * g} + d_a = \frac{V_{cc}^2}{2 * g} + d_{cc} + h_L \tag{16}$$

where

V_{am} = measured average point velocity at the approach (ft/sec),
d_a = average measured depth at the approach (ft),
V_{cc} = computed average point velocity at the contraction for disturbed flow (ft/sec),
d_{cc} = average computed depth at the contraction for obstructed flow (ft), and
h_L = energy losses (assumed to be negligible) (ft).

The continuity equation is

$$Q_{cc} = V_{cc} * W_{t-c} * d_{cc} \tag{17}$$

where Q_{cc} is the computed discharge (in cubic feet per second), and W_{t-c} is the horizontal distance from the toe of the abutment to the channel boundary (in feet).

Using Equation 7, N_{sc} was computed for V_{cc}. The values of N_{sc} were plotted against the D_{50}/d_{cc} ratio. Figure 8 shows a plot of the individual computed sediment number curve for the vertical-wall abutment model for D_{50} = 0.30 and 0.40 in. for obstructed flow.

Figure 8 also shows that the curves for the two gravel sizes, which were derived by regression, were close to one curve and almost parallel to the unobstructed flow curve. The velocity, V_{cc}, is the computed average contracted velocity in the opening for the obstructed flow, but observed failure is for any discernible area of particular movement in that opening.

Figure 9 shows the combined sediment number curve for the two gravel sizes. This plot reveals that the slope of the combined curve follows that of the unobstructed flow curve. For the gravel to fail at the toe of the abutment upstream of the constriction, the local effective velocity must have been close to that which would have caused failure for the unobstructed flow.

Flow at the end of the abutment where the initial failure of rock riprap usually occurs was highly rotational and difficult to quantify with the electromagnetic probe sensor, the instrument available for this study. A so-called local effective velocity was defined as the velocity that would have moved the rock in unobstructed flow.

To determine the stable size of rock riprap, Equation 7 should be rearranged as follows:

$$D_{50} = \frac{V_{cc}^2}{g * N_{sc} * (SG - 1)} \tag{18}$$

By regression analysis of the combined sediment number curve (Figure 9), N_{sc} is obtained as

$$N_{sc} = 0.94 * \left(\frac{D_{50}}{d_{cc}}\right)^{-0.23} \tag{19}$$

Substituting Equation 19 into Equation 18 yields

$$D_{50} = \frac{1.0836 * V_{cc}^{2.598}}{g^{1.299} * d_{cc}^{0.299} * (SG - 1)^{1.299}} \tag{20}$$

Although Equation 20 is not dimensionless as written, it is dimensionally homogeneous—that is, it can be reduced to the same units on both sides. It can be used with either SI or English units as long as consistent units are used in all terms.

Figure 10 presents a plot of V_{cp}/V_{cc} versus X_t/W_{t-c}. At X_t/W_{t-c} = 0, and for 95 percent of the computations, the ratio V_{cp}/V_{cc} fell near 2.0. At X_t/W_{t-c} = 0, and for 5 percent of the computations, the ratio reached 2.304. V_{cp}/V_{cc} repre-

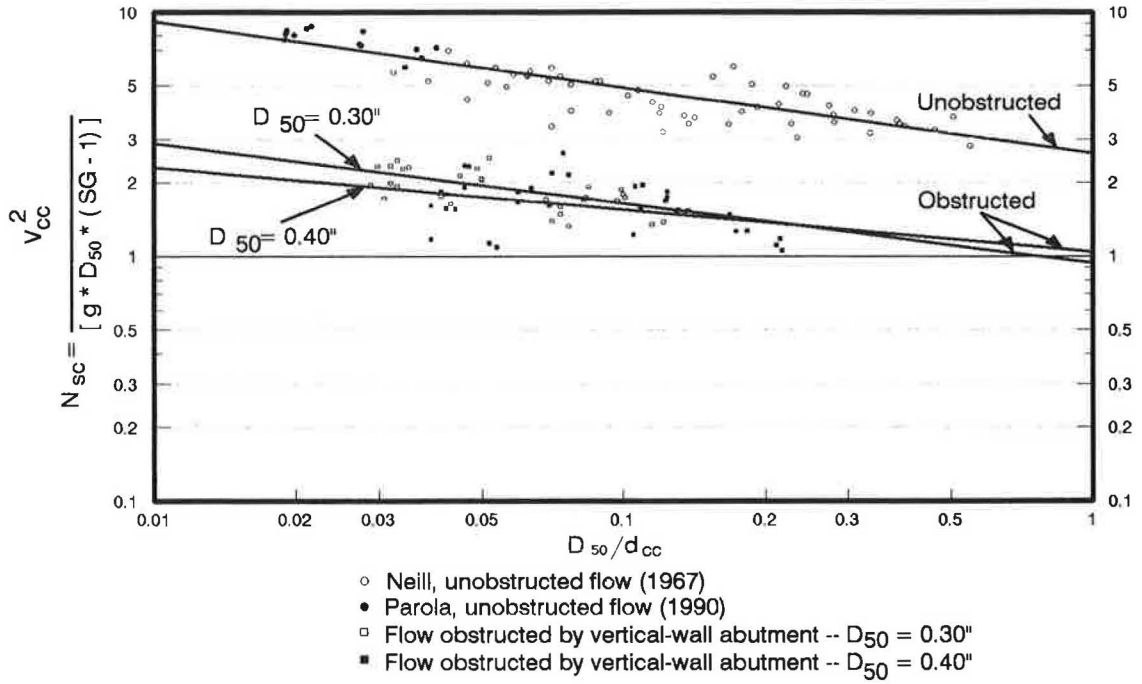

FIGURE 8 Individual sediment number curve for vertical-wall abutment.

sents the effective computed local velocity (near the abutment face at which the rock failed) to the average computed contracted velocity in the flood plain within the contraction. The ratio of V_{cp}/V_{cc} also represents the indirect method—or "simple multiplier"—that should be applied to the average computed contracted velocity in the contraction within the flood plain to obtain the velocity near the abutment face that caused the gravel's incipient motion.

V_{cp} is the computed average point velocity at the contraction for undisturbed flow, in feet per second. V_{cc} is the average computed point velocity, feet per second, at various distances, X_t, from the toe of the abutment for disturbed flow. W_{t-c} is the horizontal distance from the toe of the abutment to the channel boundary, in feet.

The effective velocity had no resemblance to what actually occurred around the abutment, but it was a convenient pa-

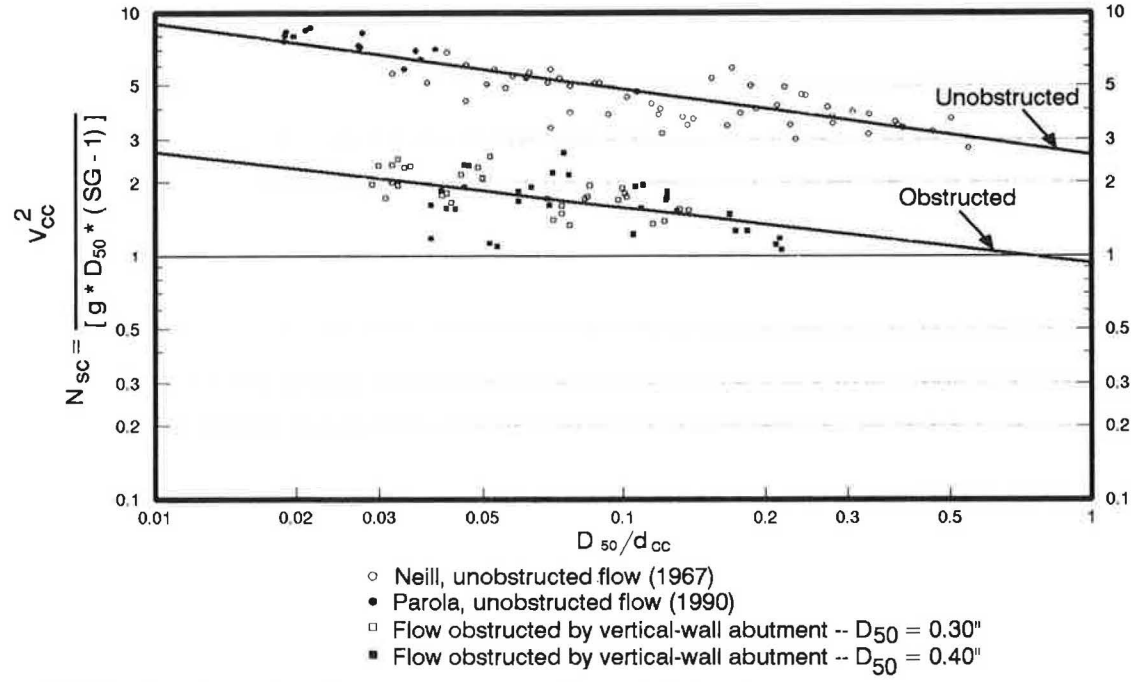

FIGURE 9 Combined sediment number curve for vertical-wall abutment.

rameter to use in developing a simple multiplier (V_{cp}/V_{cc}) for the velocity term in the rearranged Isbash equation—Equation 8. The velocity term within Equation 8 can be multiplied by 2.0 to compute the rock riprap size for the vertical-wall abutment model.

The discharge was increased 1.7 times the discharge that caused the incipient motion of the gravel to observe the extent of the failure zone. The multiplier, 1.7, is suggested on FHWA publication HEC-18 (*8*) to approximate Q_{500} from Q_{100}. This demonstrated that the rock riprap apron should be extended along the entire length of the abutment, both upstream and downstream, and to the parallel face of the abutment to the flow.

Figure 10 also illustrates that the velocity amplification decays rapidly with distance from the toe of the abutment—the effect of the abutment diminished quickly with distance from the abutment. Therefore, it would be reasonable to limit the rock riprap apron to a relative small portion of the constriction. However, additional data analysis is necessary to determine the extent of the rock riprap apron.

Spill-Through Abutment

The observed vulnerable zone for incipient motion for this model was observed downstream of the contraction near the toe of the abutment (Figure 7). The acceleration of flow through the slope of the spill face of the abutment parallel to the flow and the turbulence developed at the vena contracta—the most contracted section of a stream jet—are believed to have influenced the gravel failure at the mentioned zone. With the flow depth and velocity measured at the approach and for a computed discharge at the approach representing the design discharge, the velocity and flow depth were also computed at the contraction of the abutment in the flood plain using Equations 16 and 17.

Using Equation 7, N_{sc} was computed with V_{cc}. The values of N_{sc} were plotted versus the D_{50}/d_{cc} ratio. Figure 11 shows a plot of the individual computed sediment numbers curve for spill-through abutment for D_{50} = 0.30 and 0.40 in. for obstructed flow.

Because of the adverse slope obtained by regression analysis and the insufficient data at D_{50}/d_{cc} ratio smaller than 0.03, an average N_{sc} of 2.09 and 1.67 was taken for D_{50} = 0.30 and 0.40 in., respectively. A combined sediment number curve was obtained by averaging all the computed N_{sc} values for the two gravel sizes used during the experiments (Figure 12). As a result, the average value of N_{sc} was found to be 1.87. Although the scatter of data on the vertical wall and spill-through experiments is similar, the effect of D_{50}/d_{cc} was found to be less significant for the spill-through abutment.

Figure 12 indicates that for the spill-through model, depth is an important factor in determining the stability of the rock riprap when compared with the unobstructed flow curve. This figure also indicates that for the spill-through abutment, the velocity that caused the incipient motion of the gravel in the flood plain near the toe of the abutment should have been at least that for the unobstructed flow.

Therefore, to determine the stable size of rock riprap, Equation 7 should be used as follows:

$$D_{50} = \frac{0.535 * V_{cc}^2}{g * (SG - 1)} \tag{21}$$

Figure 13 presents a plot of V_{cp}/V_{cc} versus X_t/W_{t-c}. The velocity ratio, V_{cp}/V_{cc}, and V_{cc}, V_{cp}, X_t, and W_{t-c} remain as previously defined. At X_t/W_{t-c} = 0, and for 97 percent of the computations, the ratio of V_{cp}/V_{cc} fell near 2.0. At

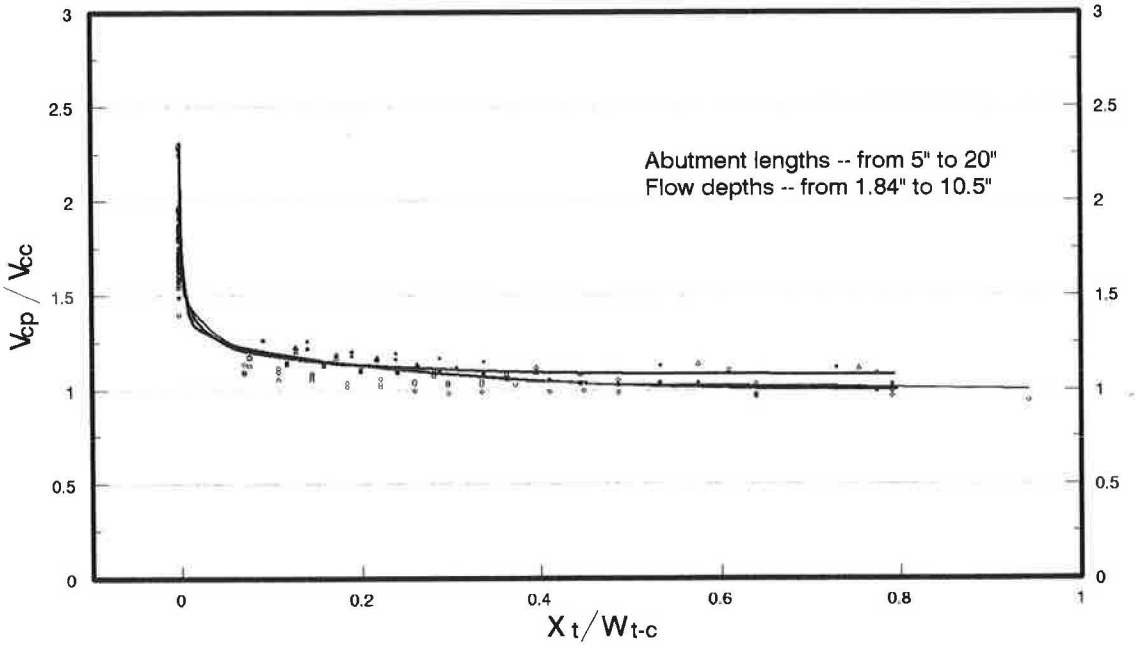

FIGURE 10 Point velocity ratio for vertical-wall abutment.

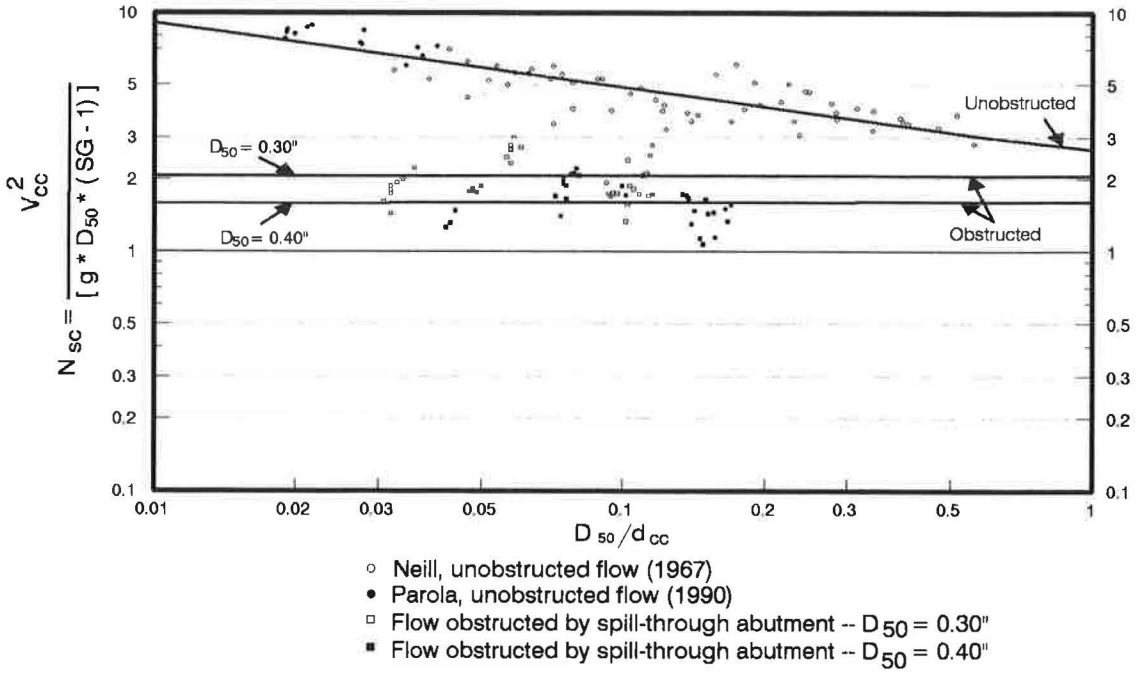

FIGURE 11 Individual sediment number curve for spill-through abutment.

$X_t/W_{t-c} = 0$, and for 3 percent of the computations, the ratio of V_{cp}/V_{cc} reached 2.135.

The ratio of V_{cp}/V_{cc} also represents the indirect method—or "simple multiplier"—that should be applied to the averaged computed contracted velocity in the contraction within the flood plain to obtain the velocity near the abutment face that caused the incipient motion of the gravel.

The local effective velocity had no resemblance to what actually occurred around the abutment, but it was a convenient parameter to use in developing a simple multiplier (V_{cp}/V_{cc}) for the velocity term in the rearranged Isbash equation—Equation 8. Similarly to vertical-wall abutment, the velocity term in the rearranged Isbash equation can be multiplied by 2.0 to compute the rock riprap size for the spill-through abutment.

As with the vertical-wall abutment model, the discharge was also increased by 1.7 times the discharge that caused the incipient motion of the gravel to observe the extent of the

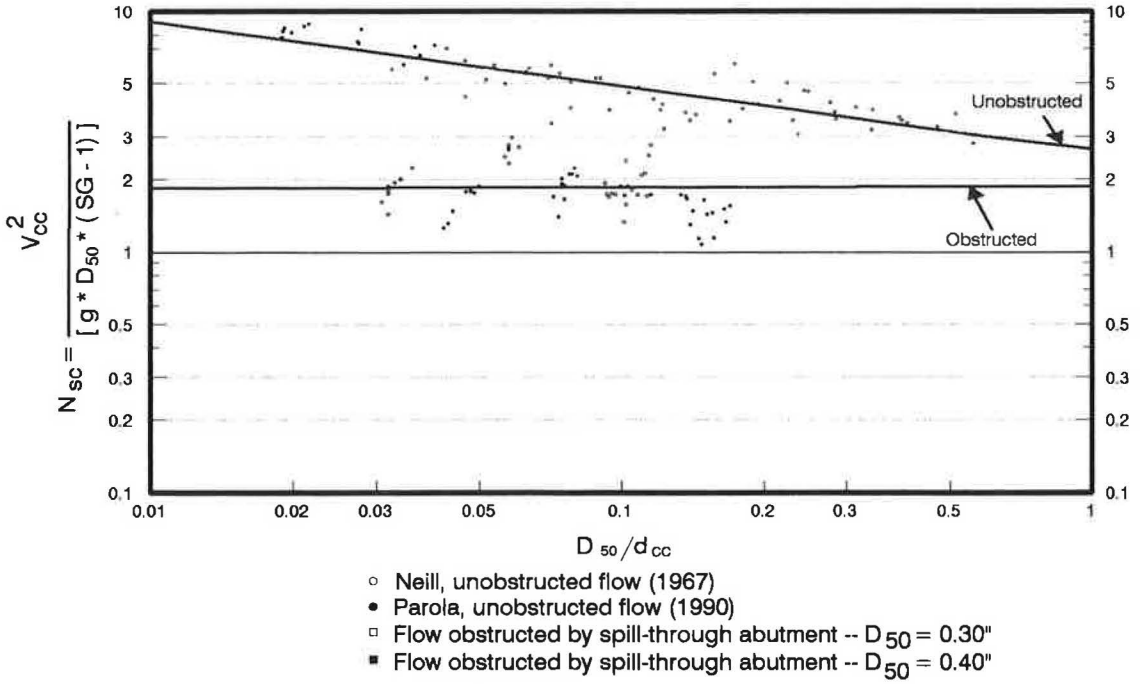

FIGURE 12 Combined sediment number curve for spill-through abutment.

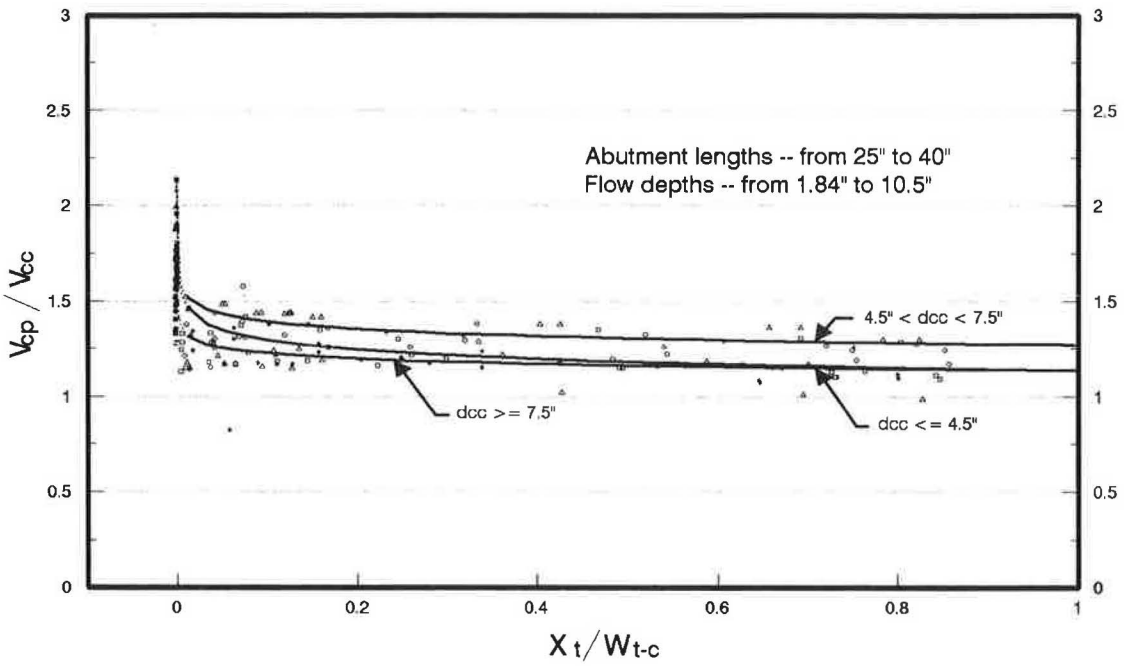

FIGURE 13 Point velocity ratio for spill-through abutment.

failure zone. This demonstrated that the rock riprap apron should be extended along the entire length of the abutment, both upstream and downstream, and to the parallel face of the abutment to the flow.

Figure 13 illustrates that the velocity amplification decays rapidly with distance from the toe of the abutment and that the effect of the abutment diminishes quickly with distance from the abutment. Also, the effect of the abutment occurs in a small portion of the contracted area. Therefore, as with the vertical-wall abutment, it would be reasonable to limit the rock riprap apron to a relatively small portion of the constriction. Again, however, more data analysis is needed to determine the extent of the rock riprap apron for this model.

Some of the preliminary results of this research have been included in HEC-18. It is anticipated that a more complete treatment of this topic will be in updates of HEC-18.

CONCLUSIONS

The location for the most critical failure zone on an abutment encroaching the free flow of water on an armored flood plain depends on the abutment shape. For the vertical-wall abutment model, the critical failure zone occurs at the upstream corner of the abutment and expands downstream toward the abutment and away from the toe with time and increase in discharge. For the spill-through model, the critical failure zone is located downstream of the contraction near the toe and "grows" downstream and upstream of the constriction, expanding to the toe and away from the abutment.

The turbulence of flow and vorticity generated near the face of the abutment are the causes of rock riprap failure. The velocities diminish in intensity and stabilize as distance from the toe of the abutment increases.

Equation 20 can be used to determine a stable rock riprap size to protect the toe of the vertical-wall abutment. Equation 21 can be used for spill-through abutment (note that the use of these equations is limited to abutment encroachments up to 28 percent onto the flood plain for vertical-wall shapes and 56 percent for spill-through shapes—without counting the dimension of the main channel).

The recommended rock riprap thickness should be equivalent to two times D_{50}.

The average velocity in the flood plain within the constricted section should be used in Equations 20 and 21.

The velocity multipliers found in this research for the vertical-wall and spill-through abutments, respectively, can be applied to the velocity term in the Isbash equation for sizing a stable rock riprap size for abutment protection.

Further data analysis is needed to determine the extension of the rock riprap apron for both vertical-wall and spill-through abutments, and further research is needed to investigate the effects of

- A greater encroachment onto the flood plain on the stability of the rock riprap;
- The abutments in a skew to the flow; and
- The main channel in the stability of the rock riprap.

REFERENCES

1. H. K. Liu, F. M. Chang, M. M. Skinner. *Effect of Bridge Constriction on Scour and Backwater*. Feb. 1961.
2. S. A. Brown and E. S. Clyde. *Design of Riprap Revetment*. Hydraulic Engineering Circular 11. FHWA, U.S. Department of Transportation, Washington, D.C., March 1989.
3. S. V. Isbash. Construction of Dams by Depositing Rock in Running Water. *Communication 3, 2nd Congress on Large Dams*, Washington, D.C., 1936.

4. A. Parola, Jr. *The Stability of Riprap Used To Protect Bridge Piers*. Ph.D. dissertation. Pennsylvania State University, State College, May 1990.
5. C. R. Neill and M. S. Yalin. Quantitative Definition of Beginning of Bed Movement. *Journal of the Hydraulics Division*, ASCE, Vol. 95, No. HY1, Jan. 1969.
6. J. E. Pagán-Ortiz. *Stability of Rock Riprap for Protection at the Toe of Abutments Located at the Flood Plain*. M.S. thesis. The George Washington University, Washington, D.C., 1990.
7. *HRB Research Report 13-B: Scour Around Bridges*. HRB, National Research Council, Washington, D.C., 1951.
8. E. V. Richardson, L. J. Harrison, and S. R. Davis. *Evaluating Scour at Bridges*. Hydraulic Engineering Circular 18. FHWA, U.S. Department of Transportation, Washington, D.C., Feb. 1991.

Status of At-Site Flood-Frequency Analysis Among Federal Agencies

WILBERT O. THOMAS, JR.

All federal agencies in the United States currently use Bulletin 17B, *Guidelines for Determining Flood Flow Frequency*, for flood-frequency analyses. The current guidelines, issued in 1982 by the Hydrology Subcommittee of the Interagency Advisory Committee on Water Data, resulted from many years of coordination and discussions among several federal agencies. The evolution of the Bulletin 17B guidelines is briefly summarized, activities of an ongoing Bulletin 17B interagency work group are described, and future directions for flood-frequency analyses among federal agencies are suggested.

The use of Bulletin 17B guidelines is intended to provide a consistent and uniform technique for flood-frequency analyses among the federal agencies. Several engineering and economic reasons dictate the need for a uniform technique. Some of these reasons are as follows:

1. The computation of average annual flood losses for equitable evaluation of flood-control projects.
2. The definition of equitable flood-hazard zones as part of the National Flood Insurance Program.
3. The definition of flood risk required for the economic design of highway drainage structures.

In addition, several federal agencies make estimates of flood magnitude and frequency in fulfilling their agency's mission. A uniform technique facilitates coordination among agencies and permits a more cost-effective use of each agency's budget. Furthermore, a uniform technique minimizes public confusion and discourages litigation that might result from federal agencies' advocating or publishing different flood-frequency estimates for the same location.

Just as important as the engineering and economic motivation is the political motivation for a consistent and uniform technique. In August 1966, the 89th Congress passed House Document 465, entitled *A Unified National Program for Managing Flood Losses*. It recommended the establishment of a panel of the Water Resources Council (WRC) to "present a set of techniques for frequency analyses that are based on the best of known hydrological and statistical procedures." In response to the document, the executive director of WRC assigned the responsibility for developing this set of techniques to the WRC Hydrology Committee. Accordingly, the Hydrology Committee established the Work Group on Flow-Frequency Methods, which comprised members of various federal agencies. The accomplishments of this work group and subsequent work groups are described in the following sections.

U.S. Geological Survey, National Center, Mail Stop 415, Reston, Va. 22092.

HISTORICAL DEVELOPMENT OF FLOOD-FREQUENCY GUIDELINES

In December 1967, the Work Group on Flow-Frequency Methods published Bulletin 15: *A Uniform Technique for Determining Flood Flow Frequencies* (*1*). Benson (*2*) provided additional details on the analysis and decisions that resulted in the publication of Bulletin 15. The recommendation in the bulletin was to fit the Pearson Type III frequency distribution to the logarithms of the annual peak flows using the sample moments (mean, standard deviation, and skew) to estimate the parameters of the distribution. Benson (*2*) and Thomas (*3*) have described the reasons and motivation for this decision.

The publication of Bulletin 15 was a significant event because for the first time a single method for flood-frequency analysis was recommended for use by all federal agencies. However, it soon became evident that the Bulletin 15 technique was not as consistent and was not being as uniformly applied as conceived because of the latitude for nonuniform treatment of outliers, computation of skewness, and treatment of historical information.

In January 1972, the Hydrology Committee of WRC initiated a review of Bulletin 15 and the need for more consistent and uniform guidelines. In March 1976, WRC published Bulletin 17: *Guidelines for Determining Flood Flow Frequency* (*4*). To correct problems noted with Bulletin 15 techniques, Bulletin 17 included the use of a low-outlier test, generalized (regionalized) skew, and a statistical procedure for incorporating historical information in the analysis. The Bulletin 17 techniques continued the practice of fitting the Pearson Type III distribution to the logarithms of annual peak flows by the method of moments.

Soon after Bulletin 17 was published, it was noted that there was a discrepancy about the order of the historical adjustment and the determination of weighted skew. In June 1977, Bulletin 17A was published, which clarified that the historical adjustment was to be applied before the weighting of station and generalized skew (*5*). This clarification is the only significant difference between Bulletins 17 and 17A. A few editorial corrections were also made.

With time, problems with the application of Bulletin 17A techniques began to surface. These problems can be briefly summarized as follows:

1. The low-outlier test did not adequately identify low outliers.
2. Some confusion existed over the estimation and use of generalized skew.

3. There were inconsistencies in the use of the conditional probability adjustment for low outliers.

In September 1981, Bulletin 17B was published (*6*). Several technical changes were made in Bulletin 17B to correct the problems in Bulletin 17A. The significant differences in the two bulletins are

1. Revised guidelines for estimating and using generalized skew;
2. A new procedure for weighting station and generalized skew;
3. A new test for detecting high outliers and a revised test for detecting low outliers; and
4. Revised guidelines for the application the conditional probability adjustment.

In March 1982, Bulletin 17B was reissued under the auspices of the Interagency Advisory Committee on Water Data (IACWD) (*7*). WRC was disbanded in September 1981, and the Hydrology Committee of WRC became the Hydrology Subcommittee of IACWD. Bulletin 17B was reissued because many typographical errors were discovered in the September 1981 version. There are no technical differences in the September 1981 and the March 1982 versions, and the latter version is still being used as the federal agency guidelines for flood-frequency analysis. Thomas provides a more detailed discussion of the evolution of the Bulletin 17B methodology (*3*).

ACTIVITIES OF CURRENT BULLETIN 17B WORK GROUP

In February 1985, the Hydrology Subcommittee of IACWD undertook a study to determine whether the Bulletin 17B guidelines were meeting the needs of the federal agencies and whether the guidelines should be revised or extended. An ad hoc work group was formed by the Hydrology Subcommittee, and a questionnaire was distributed to all federal agencies on IACWD to identify problems and solicit suggestions for improving the Bulletin 17B methodology.

In December 1987, the ad hoc work group submitted a summary report to the Hydrology Subcommittee describing the results of its study. The main conclusions were that the Bulletin 17B techniques are generally sound, that no substantial problems have been identified that cannot be resolved by means included in the guidelines, and that no clearly superior technical alternatives to the Bulletin 17B methodology have emerged. The study did find that problems are sometimes encountered in using Bulletin 17B and recommended that a new work group be formed to develop a series of pamphlets to supplement Bulletin 17B and to provide additional guidance in solving these problems.

The Hydrology Subcommittee study resulted in the following topics suggested for the pamphlet series:

- Generalized (regional) skew,
- Detection and treatment of outliers,
- Mixed population analysis,
- Multistation comparison,
- Watershed changes and time trends,
- Partial duration analysis, and
- Coincident frequency.

From the study, it was clear that users of Bulletin 17B also wanted more examples of applying the various techniques and more diagnostics and interpretation of the analysis results. Users were most concerned about the use of the Bulletin 17B skew map (i.e., definition of generalized skew). The detection and treatment of outliers was the second most important area of concern. The remaining topics were of about equal importance.

In July 1989, a new work group was formed to prepare supplemental guidance to Bulletin 17B in those areas identified by the Hydrology Subcommittee study. In this work group, the U.S. Army Corps of Engineers, the U.S. Bureau of Reclamation, the National Weather Service, the Soil Conservation Service, the Federal Emergency Management Agency, and the U.S. Geological Survey are represented. A member of the Water Resources Branch, Environment Canada, is an observer and adviser to the work group.

On the basis of the topics suggested in the Hydrology Subcommittee study and the needs as perceived by the new work group, the topics identified as important ones to address initially were definition of generalized (regional) skew, detection and treatment of outliers, the effect of watershed changes and time trends, and frequency analysis for regulated watersheds. Progress by 1991 resulted in a draft copy of the report *Evaluating the Effects of Watershed Changes on the Flood-Frequency Curve*, expected to be ready for publication in summer 1992. The report will discuss statistical tests for identifying nonhomogeneity in the annual peak flows resulting from watershed changes and discuss new ways of performing flood-frequency analyses under conditions of watershed change such as urbanization.

It is anticipated that publications of the Bulletin 17B work group will be a combination of lengthy book-type reports and shorter pamphlets. The type of publication will be determined by the nature of the topic and the amount of detail required to discuss it. Current plans are that the work group will prepare supplemental guidance in the four areas noted.

Another related activity of the work group was the support and sponsorship of the development of a hypothesis test to determine if the logarithms or the untransformed values of annual peak flows fit a Pearson Type III distribution. A probability-plot correlation coefficient hypothesis test was developed for the three-parameter Pearson Type III distribution by Vogel and McMartin (*8*). This hypothesis test provides an objective method of evaluating whether the Pearson Type III distribution is an appropriate frequency distribution for flood-frequency analysis in a given region. The applicability of the Pearson Type III distribution should be judged by applying the hypothesis test to several data sets in a region rather than to a single data set.

DIRECTIONS FOR FLOOD-FREQUENCY FUTURE ANALYSIS

Considerable research has been completed in the area of flood-frequency analysis since the 1976 publication of Bulletin 17B. Any attempt to summarize the pertinent research would surely result in omitting some noteworthy contributions. However,

some thoughts and suggestions can be provided on the direction of flood-frequency analysis among federal agencies.

The present Bulletin 17B work group will produce reports and pamphlets in an attempt to enhance and supplement the existing guidelines. This work group does not plan to change or supersede any guidance in the existing guidelines. This means that the base method of flood-frequency analysis for federal agencies will continue to be to fit the Pearson Type III distribution to the logarithms of the annual flood peaks using the sample moments (mean, standard deviation, and skew) to estimate the parameters of the distribution. The supplemental publications will provide needed additional guidance on such topics as how to perform frequency analyses for watersheds undergoing change and for watersheds with major flood-control structures, and how to detect and treat outliers or estimate generalized skew as part of the frequency analysis. This additional guidance is needed, regardless of the base method of frequency analysis.

The study conducted by the Hydrology Subcommittee during 1985–1987 indicated that, for the most part, federal agencies believe that the Bulletin 17B guidelines meet their needs. This, of course, does not mean that Bulletin 17B techniques are superior to all others. The Bulletin 17B method was adopted and developed in the mid-1970s, when access to personal computers was not as prevalent as it is today. The techniques in Bulletin 17B are straightforward, and computations can be performed on a hand-held calculator. This was part of the motivation in adopting the recommended techniques. More complicated and computer-intensive techniques are available today. However, the fact that these techniques are more complicated does not necessarily mean they are superior to the Bulletin 17B methodology. Any study to determine this would take considerable resources that most federal agencies do not have or apparently are not willing to commit.

However, it is the opinion of the author that within the next few years the Bulletin 17B methodology should undergo a major evaluation. Topics to be investigated relate to the appropriate frequency distribution (*9–11*); the appropriate method of parameter estimation (*11–16*); the use of the logarithmic transformation (*17*); and the use and estimation of generalized skew (*18–21*). Recent papers on regional goodness-of-fit tests (*8,11,22–24*) may provide more objective ways of identifying the appropriate frequency distribution.

Appropriate federal agencies need to take an objective look at the considerable research in the last decade to determine whether Bulletin 17B should be revised or replaced. Given the huge expenditures in the construction of flood-control structures, highway drainage structures, and floodplain management, the investment in a comprehensive study of flood-frequency techniques that could take advantage of computational power of today's personal computers appears to be worthwhile.

REFERENCES

1. *A Uniform Technique for Determining Flood Flow Frequencies*. Bulletin 15. U.S. Water Resources Council, Washington, D.C., 1967.
2. M. A. Benson. Uniform Flood-Frequency Estimating Methods for Federal Agencies. *Water Resources Research*, Vol. 4, No. 5, 1968, pp. 891–908.
3. W. O. Thomas, Jr. A Uniform Technique for Flood Frequency Analysis. *Journal of Water Resources Planning and Management*, ASCE, Vol. 111, No. 3, 1985, pp. 321–337.
4. *Guidelines for Determining Flood Flow Frequency*. Bulletin 17. U.S. Water Resources Council, Washington, D.C., 1976.
5. *Guidelines for Determining Flood Flow Frequency*. Bulletin 17A. U.S. Water Resources Council, Washington, D.C., 1977.
6. *Guidelines for Determining Flood Flow Frequency*. Bulletin 17B. U.S. Water Resources Council, Washington, D.C., 1981.
7. Interagency Advisory Committee on Water Data. *Guidelines for Determining Flood Flow Frequency*. Bulletin 17B. Hydrology Subcommittee, Office of Water Data Coordination, U.S. Geological Survey, Reston, Va., 1982.
8. R. M. Vogel and D. E. McMartin. *Probability Plot Goodness-of-Fit and Skewness Estimation Procedures for the Pearson Type III Distribution. Water Resources Research*, Vol. 27, No. 12, 1991, pp. 3149–3158.
9. J. R. Wallis and E. F. Wood. Relative Accuracy of Log Pearson III Procedures. *Journal of Hydraulic Engineering*, ASCE, Vol. 111, No. 7, 1985, pp. 1043–1056.
10. J. M. Landwehr, G. D. Tasker, and R. D. Jarrett. Relative Accuracy of Log Pearson III Procedures (Discussion). *Journal of Hydraulic Engineering*, ASCE, Vol. 113, No. 7, pp. 1206–1210.
11. J. R. M. Hosking. L-Moments: Analysis and Estimation of Distributions Using Linear Combination of Order Statistics. *Journal of Royal Statistical Society*, Vol. 52, No. 1, 1990, pp. 105–124.
12. J. M. Landwehr, N. C. Matalas, and J. R. Wallis. Probability Weighted Moments Compared with Traditional Techniques in Estimating Gumbel Parameters and Quantiles. *Water Resources Research*, Vol. 15, No. 5, 1979, pp. 1055–1064.
13. R. Condie and P. J. Pilon. Fitting the Log-Pearson Type III Distribution to Censored Samples: An Application to Flood Frequency Analysis with Historic Information. *Proc., 6th Canadian Hydrotechnical Conference*, Canadian Society of Civil Engineering, Ottawa, Ontario, 1983, pp. 11–22.
14. J. R. M. Hosking, J. R. Wallis, and E. F. Wood. Estimation of the Generalized Extreme-Value Distribution by the Method of Probability-Weighted Moments. *Technometrics*, Vol. 27, No. 3, 1985, pp. 251–261.
15. J. R. Stedinger and T. A. Cohn. Flood Frequency Analysis with Historical and Paleoflood Information. *Water Resources Research*, Vol. 22, No. 5, 1986, pp. 785–793.
16. P. J. Pilon. *Gamma Type Distribution: Maximum Likelihood Values of the T-Year Event and Their Asymptotic Variance*. Ph.D. dissertation. Department of Civil Engineering, University of Ottawa, Ontario, 1990.
17. J. M. Landwehr, N. C. Matalas, and J. R. Wallis. Some Comparisons of Flood Statistics in Real and Log Space. *Water Resources Research*, Vol. 14, No. 5, 1978, pp. 902–920.
18. R. H. McCuen. Map Skew??? *Journal of Water Resources Planning and Management*, ASCE, Vol. 105, No. WR7, 1979, pp. 269–277.
19. G. Kuczera. Robust Flood Frequency Models. *Water Resources Research*, Vol. 18, No. 2, 1982, pp. 315–324.
20. G. D. Tasker and J. R. Stedinger. Regional Skew with Weighted LS Regression. *Journal of Water Resources Planning and Management*, ASCE, Vol. 112, No. 2, 1986, pp. 225–237.
21. J. U. Chowdhury and J. R. Stedinger. Confidence Interval for Design Floods with Estimated Skew Coefficients: *Journal of Hydraulic Engineering*, ASCE, Vol. 117, No. 7, 1991, pp. 811–831.
22. R. M. Vogel. The Probability Plot Correlation Coefficient Test for Normal, Log-Normal and Gumbel Distributional Hypotheses. *Water Resources Research*, Vol. 22, No. 4, 1986, pp. 587–590.
23. R. M. Vogel and C. N. Kroll. Low-Flow Frequency Analysis Using Probability-Plot Correlation Coefficients. *Journal of Water Resources Planning and Management*, ASCE, Vol. 115, No. 3, 1989, pp. 338–357.
24. J. U. Chowdhury, J. R. Stedinger, and L. Lu. Goodness-of-Fit Tests for Regional GEV Flood Distributions. *Water Resources Research*, Vol. 27, No. 7, 1991, pp. 1765–1776.